Received: 13 April 2024 | Revised: 18 October 2024 | Accepted: 26 October 2024

DOI: 10.1002/ar.25604

SPECIAL ISSUE ARTICLE

The Anatomical Record WILEY

Synapsids and sensitivity: Broad survey of tetrapod trigeminal canal morphology supports an evolutionary trend of increasing facial tactile specialization in the mammal lineage

Juri A. Miyamae[1] | **Julien Benoit**[2] | **Irina Ruf**[3,4,5] | **Zoleka Sibiya**[2,6] | **Bhart-Anjan S. Bhullar**[7,8]

[1]Robotics, University of Michigan, Ann Arbor, Michigan, USA

[2]Evolutionary Studies Institute, University of Witwatersrand, Johannesburg, South Africa

[3]Abteilung Messelforschung und Mammalogie, Senckenberg Forschungsinstitut und Naturmuseum Frankfurt, Frankfurt am Main, Germany

[4]Institut für Geowissenschaften, Goethe-Universität Frankfurt am Main, Frankfurt am Main, Germany

[5]Research Center of Paleontology and Stratigraphy, Jilin University, Changchun, Jilin, China

[6]Council for Geoscience, Silverton, Pretoria, South Africa

[7]Department of Earth and Planetary Sciences, Yale University, New Haven, Connecticut, USA

[8]Yale Peabody Museum, Yale University, New Haven, Connecticut, USA

Correspondence
Juri A. Miyamae, Robotics, University of Michigan, Ann Arbor, MI, USA.
Email: jmiyamae@umich.edu

Funding information
Department of Earth and Planetary Sciences at Yale University; Yale Institute for Biospheric Studies; Robotics at the University of Michigan; DSI-NRF African Origins Platform, Grant/Award Number: AOP210218587003; Genus-Centre of Excellence in Palaeosciences; NSF CAREER, Grant/Award Number: DEB 2046868

Abstract

The trigeminus nerve (cranial nerve V) is a large and significant conduit of sensory information from the face to the brain, with its three branches extending over the head to innervate a wide variety of integumentary sensory receptors, primarily tactile. The paths of the maxillary (V_2) and mandibular (V_3) divisions of the trigeminus frequently transit through dedicated canals within the bones of the upper and lower jaws, thus allowing this neuroanatomy to be captured in the fossil record and be available to interpretations of sensory ability in extinct taxa. Here, we use microCT and synchrotron scans from 38 extant and fossil species spanning a wide phylogenetic sample across tetrapods to investigate whether maxillary and mandibular canal morphology can be informative of sensory biology in the synapsid lineage. We found that in comparison to an amphibian and sauropsid outgroup, synapsids demonstrate a distinctive evolutionary pattern of change from canals that are highly ramified near the rostral tip of the jaws to canals with increasingly simplified morphology. This pattern is especially evident in the maxillary canal, which came to feature a shortened infraorbital canal terminating in a single large infraorbital foramen that serves as the outlet for branches of V_2 that then enter the soft tissues of the face. A comparison with modern analogues supports the hypothesis

that this morphological change correlates to an evolutionary history of synapsid-specific innovations in facial touch. We interpret the highly ramified transitional form found in early nonmammalian synapsids as indicative of enhanced tactile sensitivity of the rostrum via direct or proximal contact, similar to tactile specialists such as probing shorebirds and alligators that possess similar proliferative ramifications of the maxillary and mandibular canals. The transition toward a simplified derived form that emerged among Mid-Triassic prozostrodont cynodonts and is retained among modern mammals is a unique configuration correlated with an equally unique and novel tactile sensory apparatus: mobile mystacial whiskers. Our survey of maxillary and mandibular canals across a phylogenetic and ecological variety of tetrapods highlights the morphological diversity of these structures, but also the need to establish robust form-function relationships for future interpretations of osteological correlates for sensory biology.

KEYWORDS

innervation, integument, paleoneurology, sensory ecology, sensory evolution, whiskers

1 | INTRODUCTION

Reconstructing the sensory world of nonhuman species presents a multi-faceted challenge that is further confounded when those species are long extinct. The tendency of the fossil record to preserve an organism's hard tissues typically precludes direct observation of sensory structures or behavioral responses to sensory stimuli. There are rare instances of extraordinary preservation of brain and neural tissue that allow for anatomical interpretation, such as among Cambrian arthropods (Aria et al., 2023; Strausfeld et al., 2016), the enigmatic and possible basal vertebrate *Tullimonstrum gregarium* from the Carboniferous (Clements et al., 2016), and in some Devonian placoderms (Trinajstic et al., 2007). Vertebrate paleontologists primarily rely on natural endocasts (e.g., Bisconti et al., 2021; Cofran et al., 2023; Dart, 1925) and the development of imaging methods such as serial sectioning (e.g., Stensiö, 1927) or microCT scanning (e.g., Bertrand et al., 2019; Early et al., 2020; Figueroa et al., 2023; Pusch et al., 2019, 2020; Rowe et al., 2011) to visualize the internal spaces formerly occupied by the brain or cranial nerves coursing through the skull to unlock perspectives of how neuroanatomy has changed over evolutionary time—a study formalized as paleoneurology by Tilly Edinger (1897–1967) in the first half of the 20th century (Buchholtz & Seyfarth, 2001).

One particularly productive area of paleoneurology in recent years has been examination of trigeminal canal morphology (e.g., Benoit et al., 2016, 2018, 2020, 2021; Bouabdellah et al., 2022; Pusch et al., 2019, 2020, 2024). In amniotes, the trigeminus (cranial nerve V) is a large cranial nerve featuring three major branches or divisions—the ophthalmic (V_1), maxillary (V_2), and mandibular (V_3)—that spread expansively over the head to innervate the mouth, jaw muscles, and facial integument (Liem et al., 2001; Romer & Parsons, 1986; Williams et al., 1989). In mammals, the trigeminus consists of both afferent sensory nerves supplying the teeth, oronasal cavities, and integumentary layers of the face and portions of the head, as well as efferent motor nerves of several muscles of the head: masseter, temporalis, medial and lateral pterygoideus, mylohyoideus, anterior digastricus, tensor veli palatini, and tensor tympani (Sperber et al., 2000; Williams et al., 1989). The ossified secondary sidewall of the braincase in mammals results in the incorporation of the trigeminal ganglion into the brain cavity (Crompton et al., 2017; Maier, 1993), with each major branch of the nerve exiting through separate openings (Williams et al., 1989). In comparison, the trigeminal ganglion in other tetrapods such as amphibians (Maier, 1993; Norris & Hughes, 1918) and alligators (Lessner & Holliday, 2022) are located outside of the braincase. Despite phylogenetic differences in the placement and morphology of the trigeminal ganglion, the maxillary and/or mandibular branches will re-enter the upper and lower jaws, respectively, where they will travel through dedicated neurovascular canals in the bone (Dyce et al., 2010; Herrick, 1894; Lessner & Holliday, 2022; Watkinson, 1906; Williams et al., 1989), thus allowing this neuroanatomy to be captured in the fossil record and become available for interpretations of facial sensitivity.

Morphological features such as the branching patterns of the trigeminal canals and subsequent number and placement of foramina indicating points where nerve and/or blood vessels exit the bone have been used as osteological correlates for the gross sensory abilities of the facial integument in extinct taxa. For example, such data have been utilized in studies providing arguments for (Carr et al., 2017) and against (Bouabdellah et al., 2022) highly enhanced skin sensitivity in the snouts of tyrannosaurid dinosaurs, as well as supporting the presence of a tactile keratinous beak in early nonmammalian therapsids called anomodonts (Benoit et al., 2018). A particularly compelling use of trigeminal canal morphology has been to infer the emergence of soft tissue characters such as fleshy lips, rhinaria, and mobile mystical whiskers (or vibrissae) within the ancestral synapsid lineage (Benoit et al., 2016, 2020; Brink, 1956; Findlay, 1968; Lingham-Soliar, 2014; Miyamae, 2022; Van Valen, 1960; Watson, 1931). As mystacial whiskers are innervated by the infraorbital branch of V_2 (Dörfl, 1985), hypotheses for the presence of sensory whiskers in stem mammals have centered on the morphology of the maxillary canal and range from correlating a proliferation of foramina as increased innervation and supportive blood supply (Brink, 1956; Findlay, 1968; Van Valen, 1960; Watson, 1931), interpreting the proliferation of foramina as "pits" into which individual whiskers were planted (Lingham-Soliar, 2014; Watson, 1931), and identifying the gradual development of the single infraorbital foramen (IOF) as observed in modern mammals (Benoit et al., 2016, 2020; Miyamae, 2022). However, what remains untested is which of these interpretations are best supported by a form-function comparison based upon a broad sampling across extant vertebrates with understood sensory capabilities.

Our study introduces this comparative assessment of maxillary and mandibular canal morphology across major tetrapod groups. Using microCT and synchrotron scanning, we examined the canals of 38 extant and fossil tetrapod species that represent a non-synapsid outgroup (amphibians and sauropsids) and synapsids (stem and crown mammals). Mystacial whiskers are contingent on at least two distinctively mammalian characters—hair and facial musculature—making them a unique sensory organ capable of actively gathering tactile information that is transmitted via the hair to its innervated base in the integument (Ahl, 1986; Dörfl, 1985; Sarko et al., 2011). We review the morphological diversity of the maxillary and mandibular canals representing different phylogenetic groups and ecologies with the aim of (1) identifying whether whiskers as a unique sensory organ correlates with an equally unique maxillary canal morphology and (2) interpreting the canal morphology of extinct nonmammalian synapsids from comparisons with modern analogues to elucidate the changes in sensory biology that mark the evolutionary path of synapsids.

2 | MATERIALS AND METHODS

The maxillary and mandibular canals of sampled taxa (4 amphibians, 11 sauropsids, 6 nonmammalian synapsids, 17 mammals) were visualized through either microCT or synchrotron scans that were subsequently processed using VGSTUDIO MAX 3.3.2 (Volume Graphics GmbH, Heidelberg, Germany; volumegraphics.com) and Materialize Mimics Version 24.0.0.427 (Materialize NV, Leuven, Belgium; materialise.com). A list of specimens with their microCT or synchrotron scanning parameters are summarized in Table 1. Further details about specimens (e.g., state of preservation, geological age), scanning facilities and scanner models employed, and relevant information about datasets obtained from MorphoSource or DigiMorph online databases are provided in the supplemental materials ("Supporting Materials: Specimen and Scan Information").

The morphology of the segmented maxillary and mandibular canals were described with particular attention to their pathway and patterns of branching, the distribution pattern of branch terminal openings that appear as foramina on the surface of the bone, and the number of these foraminal openings. We identified the trends differentiating canal morphology between non-synapsid outgroups and synapsids taking into consideration evolutionary time, ecology, and the presence of sensory specializations in order to establish form-function relationships.

3 | RESULTS

We describe the gross morphology of the maxillary and mandibular canals of our sample of non-synapsid outgroup taxa and synapsids. Only the left side of the face is described, unless noted as a mirrored figure due to better preservation of the right side (see individual figure captions). For each species, we provide an overall account of the maxillary and mandibular canal morphologies, describe the proximal entry point of the canals into the bone, report the number of foramina on the external surface of the bone that terminate branches deriving from the maxillary or mandibular canals, and indicate the anatomical direction that these foramina open. In order to allow comparison among the sampled taxa, the foramina on the external surface of the bones are numbered sequentially from caudal to rostral without any assumption of homology.

TABLE 1 Specimens used in this study and associated microCT and synchrotron scanning parameters. Resolution is given in isotropic voxel size (x = y = z) unless otherwise indicated.

Group	*Species*	Specimen No.	Scan source	Resolution (mm)	kV	μA
Amphibia, Temnospondyli, Lydekkerinidae	*Lydekkerina huxleyi*[a]	BP/1/4317	Please refer to Data Accessibility	0.0712	100	130
Amphibia, Urodela, Cryptobranchidae	*Cryptobranchus alleganiensis*	UF:HERP:10881	MorphoSource (Media ID 000067236)	0.0422	130	250
Amphibia, Urodela, Ambystomatidae	*Ambystoma tigrinum*	TNHC 17991	DigiMorph	x, y = 0.0215; z = 0.0235	n/a	n/a
Amphibia, Anura, Ranidae	*Lithobates [Rana] capito*	UF:HERP:69063	MorphoSource (Media ID 000065740)	0.0646	100	200
Sauropsida, Neodiapsida	*Orovenator mayorum*[a]	OMNH 74606	MorphoSource (Media ID 000049776)	0.0180	160	200
Sauropsida, Squamata, Teiidae	*Tupinambis teguixin*	FMNH 22416	MorphoSource (Media ID 000097460)	x, y = 0.0654; z = 0.1485	120	200
Sauropsida, Squamata, Dactyloidae	*Anolis cristatellus*	UF:HERP:47686	MorphoSource (Media ID 000021272)	0.0222	100	140
Sauropsida, Squamata, Gekkonidae	*Uroplatus fimbriatus*	UF:HERP:72880	MorphoSource (Media ID 000038134)	0.0414	100	200
Sauropsida, Squamata, Dibamidae	*Dibamus novaeguineae*	UF:HERP:33488	MorphoSource (Media ID 000062342)	0.0081	80	100
Sauropsida, Squamata, Varanidae	*Varanus niloticus*	UF:HERP:83764	MorphoSource (Media ID 000456584)	0.0414	100	200
Sauropsida, Squamata, Boidae	*Eunectes murinus*	UF:HERP:84822	MorphoSource (Media ID 000058657)	0.0735	100	200
Sauropsida, Squamata, Colubridae	*Thamnophis marcianus*	FMNH 26260	DigiMorph	x, y = 0.0264; z = 0.063	n/a	n/a
Sauropsida, Archosauria, Alligatoridae	*Alligator mississippiensis*	TMM M-983	DigiMorph	x, y = 0.25; z = 0.48	n/a	n/a
Sauropsida, Archosauria, Scolopacidae	*Calidris alba*	NHMUK:zoo: S/1994.60.3	MorphoSource (Media ID 000522329)	0.0256	130	150
Sauropsida, Archosauria, Ardeidae	*Bubulcus ibis*	NHMUK:zoo: S/2006.1.20	MorphoSource (Media ID 000522402)	x, y = 0.0611; z = 0.1223	85	846
Synapsida, Eupelycosauria, Ophiacodontidae	*Varanosaurus acutirostris*[a]	FMNH PR 1670	Please refer to Data Accessibility	0.0663	90	90
Synapsida, Therapsida, Therocephalia	*Tetracynodon darti*[a]	UCMP 42869	Please refer to Data Accessibility	0.0337	200	160
Synapsida, Therapsida, Cynodontia	*Thrinaxodon liorhinus*[a]	UCMP 40466	Please refer to Data Accessibility	0.0387	90	93
Synapsida, Cynodontia, Eucynodontia	*Ecteninion lunensis*[a]	PVSJ 422	Please refer to Data Accessibility	x, y = 0.9898; z = 0.1624	180	133
Synapsida, Probainognathia, Prozostrodontia	*Pachygenelus monus*[a]	BP/1/5691	Please refer to Data Accessibility	0.0620	90	140
Synapsida, Probainognathia, Prozostrodontia	*Tritylodon longaevus*[a]	BP/1/4778	Please refer to Data Accessibility	0.0235	164.6	n/a
Synapsida, Mammalia, Ornithorhynchidae	*Ornithorhynchus anatinus*	AMNH:Mammals: M-201312	Please refer to Data Accessibility	0.0367	90	105

TABLE 1 (Continued)

Group	*Species*	Specimen No.	Scan source	Resolution (mm)	kV	μA
Synapsida, Mammalia, Tachyglossidae	*Tachyglossus aculeatus*	YPM MAM 014872	MorphoSource (Media ID 000064578)	0.069	90	110
Synapsida, Mammalia, Symmetrodonta	*Tinodon ferox*[a]	YPM VP 000606	Please refer to Data Accessibility	0.0337	107	80
Synapsida, Mammalia, Didelphidae	*Monodelphis domestica*	Uncatalogued	Please refer to Data Accessibility	1.000	90	110
Synapsida, Mammalia, Dasyuridae	*Dasyurus hallucatus*	TMM M-5921	MorphoSource (Media ID 000116114)	x, y = 0.0349; z = 0.0784	180	133
Synapsida, Mammalia, Macroscelididae	*Elephantulus rupestris*	CAS MAM 30373	Please refer to Data Accessibility	0.0663	106	60
Synapsida, Mammalia, Myrmecophagidae	*Myrmecophaga tridactyla*	AMNH:Mammals: M-133489	MorphoSource (Media ID 000085043)	0.1028	111	168
Synapsida, Mammalia, Muridae	*Mus musculus*	Uncatalogued	Please refer to Data Accessibility	0.0168	100	80
Synapsida, Mammalia, Octodontidae	*Octodon degus*	IIMyC: LMFyC:0102010101	MorphoSource (Media ID 000557434)	22.2613	n/a	n/a
Synapsida, Mammalia, Pteropodidae	*Pteropus scapulatus*	AMNH:Mammals: M-154582	MorphoSource (Media ID 000036605)	0.0300	70	114
Synapsida, Mammalia, Vespertilionidae	*Myotis adversus adversus*	UMZC:Vertebrates: E.5766.B	MorphoSource (Media ID 000420400)	0.0203	110	191
Synapsida, Mammalia, Hominidae	*Pan troglodytes*	AMNH:Mammals: M-167342	MorphoSource (Media ID 000021967)	0.0895	n/a	n/a
Synapsida, Mammalia, Tapiridae	*Tapirus terrestris*	TMM-M16	MorphoSource (Media ID 000100744)	0.2996	210	340
Synapsida, Mammalia, Phocoenidae	*Phocoena phocoena*	MVZ:mammal specimens:172141	MorphoSource (Media ID 000606522)	0.2000	n/a	n/a
Synapsida, Mammalia, Odobenidae	*Odobenus rosmarus*	MVZ:mammal specimens:125566	MorphoSource (Media ID 000590228)	x, y = 0.27; z = 0.45	419	1800
Synapsida, Mammalia, Felidae	*Felis catus*	CET-018	MorphoSource (Media ID 000074882)	0.0642	215	297
Synapsida, Mammalia, Talpidae	*Scalopus aquaticus*	CET-031	MorphoSource (Media ID 000075229)	0.0250	185	159

Note: Institutional abbreviations for specimen numbers: **AMNH**, American Museum of Natural History, New York, NY, USA; **BP**, Evolutionary Studies Institute (formerly Bernard Price), University of Witwatersrand, Johannesburg, South Africa; **CAS**, California Academy of Sciences, San Francisco, CA, USA; **CET**, Laboratory of Claire E. Terhune, Department of Anthropology, University of Arkansas, Fayetteville, AR, USA; **FMNH**, Field Museum of Natural History, Chicago, IL, USA; **IIMyC LMFyC**, Instituto de Investigaciones Marinas y Costeras Laboratorio de Morfología Funcional y Comportmiento, Mar del Plata, Argentina; **MVZ**, Museum of Vertebrate Zoology, University of California, Berkeley, CA, USA; **NHMUK**, Natural History Museum, London, UK; **OMNH**, Sam Noble Oklahoma Museum of Natural History, Norman, OK, USA; **PVSJ**, Museo de Ciencias Naturales, Universidad Nacional de San Juan, San Juan, Argentina; **TMM**, The University of Texas at Austin, Texas Memorial Museum, Austin, TX, USA; **TNHC**, Texas Science and Natural History Museum, The University of Texas at Austin, Austin, TX, USA; **UCMP**, University of California Museum of Paleontology, Berkeley, CA, USA; **UF**, University of Florida, Florida Museum of Natural History, Gainesville, Florida, USA; **UMZC**, Museum of Zoology, University of Cambridge, Cambridge UK; **YPM**, Yale Peabody Museum, New Haven, CT, USA. [Correction added after first online publication on 03 February 2025. The specimen number for *Varanosaurus acutirostris* was changed from "FMNH PR 1760" to "FMNH PR 1670".]
[a]Extinct taxa.

3.1 | Non-synapsid outgroup: Amphibians

3.1.1 | *Lydekkerina huxleyi*

Maxillary canal is long, tubular, and runs anteroposteriorly along the lower margin of the maxilla. Posteriorly, it tapers in line with the posterior branch of the jugal and terminates at the level of the posterior margin of the eye socket (Figure 1a). It broadens anteriorly to form a tubular structure that gives off several side branches toward the supralabial foramina on the external surface of the maxilla. The main canal trunk, found along the posterior lacrimal, has short dorsal branches that point in the posterior

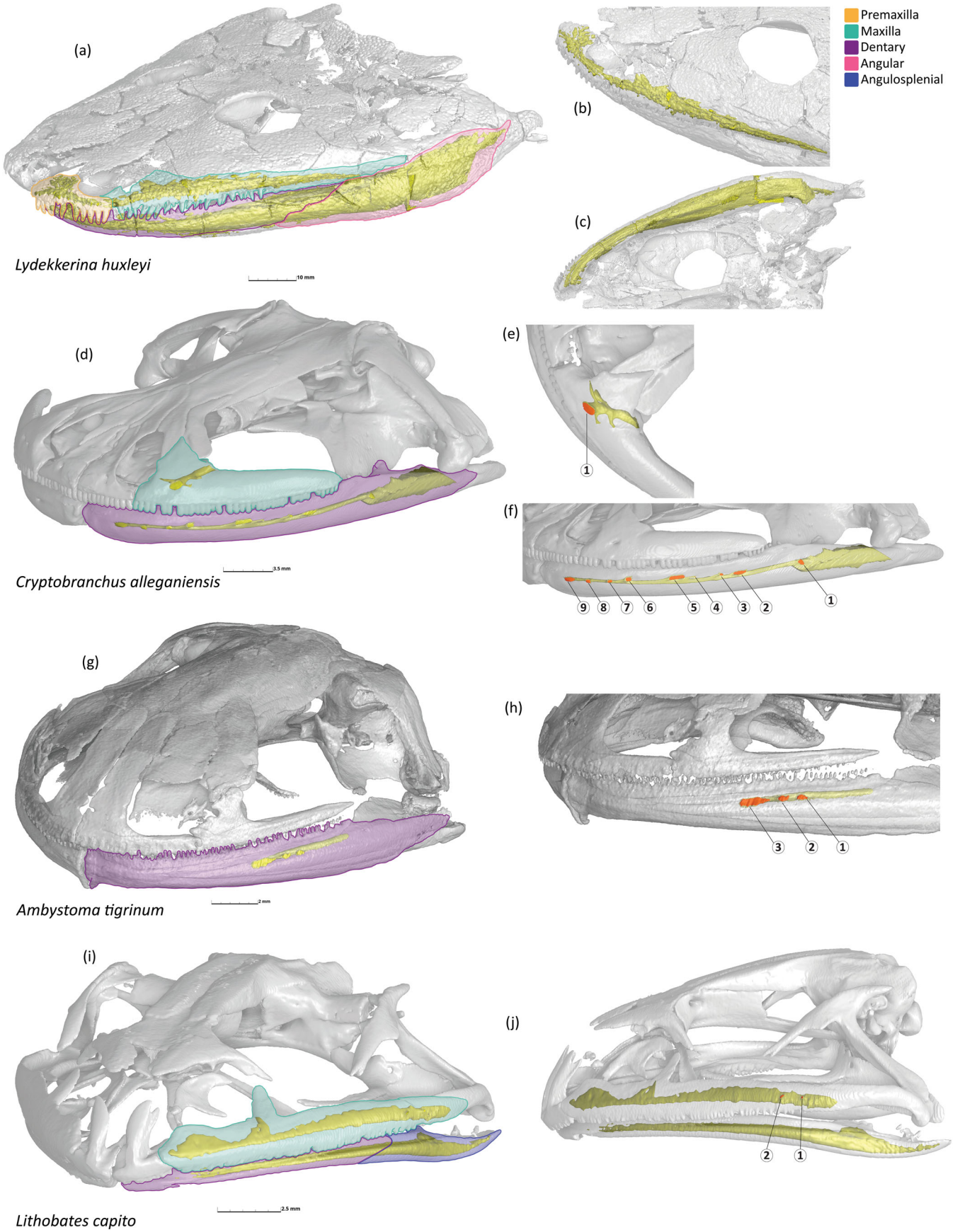

FIGURE 1 Legend on next page.

direction. Near the posterior margin of the nares, there is a broadening of the canal into a conical cavity with branches that extend rostrally into the premaxilla, where the canal terminates in a starburst-shaped cluster of ramifications directed toward the dorsal surface (Figure 1b).

Entry point into the maxilla is not certain, but is likely on the medial surface of the maxilla at the region of the conical cavity, where a sulcus is formed between the maxilla and palatine bones that would allow for the passage of nerves.

Number of maxillary foramina is uncertain because of the broken surface of the skull. We also observed many minute branches diverging from the maxillary canal to the surface of the bone that were not fully captured during segmentation. However, it appears there are small foramina throughout the anteroposterior length of the maxilla, positioned close to the upper toothrow. There is also a concentration of foramina on the dorsorostral surface of the premaxilla.

Mandibular canal is linear and occupies most of the space inside the lower jaw. The canal runs anteroposteriorly along the ventral margin of the lower jaw which is bounded laterally by the dentary, splenial, postsplenial, and angular and bounded medially by the splenial, postsplenial, coronoid series, prearticular, and angular bones (Jeannot et al., 2006) (Figure 1a, splenial and postsplenial not visible in this view). Ramifications tend to be present in the rostral half of the skull and the branches are short and irregularly positioned. There is a concentration of branching at the rostral tip of the jaws near the midline symphysis (Figure 1c).

Entry point is a large, dorsolateral opening located on the medial surface of the angular.

Number of mandibular foramina is uncertain for similar reasons described above for the number of maxillary foramina. However, the mandibular canal appears to have fewer associated foramina overall, with most of the openings concentrated at the rostral tip of the dentary.

3.1.2 | *Cryptobranchus alleganiensis*

Maxillary canal is short and runs linearly through the maxilla in an anteroposterior orientation. There are two laterally directed branches and two medially directed branches (Figure 1d). One of these medial branches terminates in the narial cavity and could be identified as the internal nasal ramus.

Entry point is on the medial surface of the maxilla, at the posterior base of the dorsally ascending process, that is, the pars facialis of the maxilla.

Number of maxillary foramina is 1 and is located on the rostral surface of the maxilla. This large opening is oriented rostrally (Figure 1e).

Mandibular canal extends through nearly the entire length of the lower jaws, which consists of the dentary and, in the posterior region, the space bounded laterally by the dentary and medially by the prearticular. The canal terminates near the midline symphysis. There are several short branches diverging from the canal at fairly regular intervals (Figure 1d).

Entry point is a large, dorsally oriented trough-like opening positioned caudal of the lower tooth row and is bounded by the articular, coronoid, and dentary (per Elwood & Cundall, 1994; the articular is named the angular in Reese, 1906).

Number of mandibular foramina is 9 and are located on the lateral surface of the dentary, just below the base of the lower teeth, and occur at relatively regular intervals (Figure 1f). The foramina follow the semicircular arc of the lower jaws, with foramina 1–5 terminating short, caudally oriented branches. It is likely that one of these openings is an entry point for an alveolar ramus that will join the nerve fibers already traveling through the mandibular canal (McGregor, 1896). Foramen 1 is located beneath the caudal edge of the lower toothrow. Foramina 2–5 are located at the level of the lateral margin of the orbit. Foramina 6–9 are located on the rostral-facing surface of the dentary. These foramina open out in the following orientations: 1—caudal, 2—caudolateral, 3—caudolateral, 4—caudolateral, 5—caudolateral, 6—lateral, 7—lateral, 8—rostral, and 9—rostral.

3.1.3 | *Ambystoma tigrinum*

Maxillary canal is not present (Figure 1g).

FIGURE 1 Amphibian species with maxillary and/or mandibular canals of the left side segmented in yellow. Foramina in red are numbered in an approximately caudal to rostral sequence. Relevant bones are identified and color-coded for each species in the whole skull view on the left. Early Triassic temnospondyl *Lydekkerina huxleyi* (BP/1/4317) is shown in (a) frontal oblique view with relevant bones identified in accordance with Jeannot et al. (2006), (b) in dorsal oblique view showing the maxillary canal, and (c) in ventral oblique view showing the mandibular canal. Aquatic salamander *Cryptobranchus alleganiensis* (UF:HERP:10881) is shown in (d) frontal oblique view, (e) rostrodorsal view of the maxillary canal, and (f) lateral oblique view of the mandibular canal. Terrestrial salamander *Ambystoma tigrinum* (TNHC 17991) is shown in (g) frontal oblique view, and (h) lateral oblique view of the mandibular canal. The frog *Lithobates capito* (UF:HERP 69063) is shown in (i) frontal oblique view with relevant bones identified in accordance with Ecker (1889) and (j) lateral view of the maxillary and mandibular canals.

Mandibular canal is relatively short and linear. The canal extends rostrally through the dentary to the level of the anterior margin of the orbit (Figure 1g).

Entry point is through a ventral-facing sulcus on the medial side of the dentary at the caudal edge of the lower toothrow.

Number of mandibular foramina is 3 and they are evenly spaced on the lateral surface of the dentary (Figure 1h). Foramina 1 and 2 terminate short, stub-like branches. Foramen 3 is the terminus of the mandibular canal. These foramina open out in the following orientations: 1—lateral, 2—lateral, and 3—rostrolateral.

3.1.4 | *Lithobates capito*

Maxillary canal is linear and laterally compressed. It extends through nearly the entire length of the maxilla and terminates at the rostral tip of that bone. There is no significant branching of the canal except for an ascending intrusion into a dorsal process of the maxilla (i.e., pars facialis) at the anterior margin of the orbit (Figure 1i).

Entry point is located at the base of the anterior edge of the pars facialis. Similar to *Lydekkerina*, the entry point for the nerve is quite rostrally positioned compared to the full length of the maxillary canal, which continues to extend caudally from the entry point; therefore, it is not clear whether the nerve has a caudally directed branch or if the minute openings we observed are not nerve foramina, but some other structure or artifact.

Number of maxillary foramina is 2 and they are small openings located on the lateral surface of the lower jaw near the caudal end of the maxillary canal (Figure 1j). Foramen 1 is positioned near the junction between the maxilla and quadratojugal and opens out laterally. Foramen 2 is located a short distance rostrally of foramen 1 and opens out laterally.

Mandibular canal is linear with no evidence of branching. It extends from the angulosplenial rostrally through the dentary to near the midline symphysis (Figure 1j).

Entry point is not detected.

Number of mandibular foramina is 0.

3.2 | Non-synapsid outgroup: Sauropsida

3.2.1 | *Orovenator mayorum*

Maxillary canal extends anteroposteriorly through the bone of the maxilla, traveling parallel to the upper tooth row, and terminating at the rostral tip of the maxilla. The caudal portion of the canal is linear, but expands into a "conical cavity" rostrally (Benoit et al., 2021), in the region where the maxilla shows the greatest dorsal-ventral height (Figure 2a). The branches diverging from the maxillary canal vary in relative length, with the longer ramifications tending to occur caudally and the shorter branches emerging from the conical cavity and rostral half of the canal.

Entry point is a rostral-facing opening on the medial surface of the maxilla, anterior to the rim of the orbit. An anatomical study of the same specimen of *Orovenator* describes a long sulcus leading into the opening of the maxillary canal, indicating that the neurovascular tract was not fully enclosed in bone for much of the caudal end of the maxilla (Ford & Benson, 2019).

Number of maxillary foramina is 25 and they are located on the lateral surface of the maxilla. Foramina 1–13 terminate branches that emerge caudal of the conical cavity and are positioned along the upper toothrow. Foramina 1–5 terminate relatively long branches diverging from the canal and these large openings occur in a single line at regular intervals. Foramina 6–13 terminate branches of long to intermediate length that emerge in multiple directions from the maxillary canal. Foramina 14–22 are associated with branches coming off the conical cavity and are distributed widely over the dorsoventral height of the maxilla. Foramina 23–25 are positioned rostral of the conical cavity. Foramen 25 terminates the maxillary canal as a large opening near the rostral extremity of the maxilla (Figure 2b). These foramina open out in the following orientations: 1—caudal, 2—caudal, 3—caudolateral, 4—caudolateral, 5—lateral, 6—lateral, 7—caudolateral, 8—lateral, 9—lateral, 10—lateral, 11—lateral, 12—ventrolateral, 13—lateral, 14—caudolateral, 15—caudolateral, 16—ventrolateral, 17—ventrolateral, 18—lateral, 19—lateral, 20—rostrolateral, 21—ventrocaudal, 22—dorsorostral, 23—lateral, 24—lateral, and 25—rostrolateral.

Mandibular canal is slender, tubular, and travels anteroposteriorly through the dentary, parallel to the lower toothrow. Most of the branching occurs at the rostral end of the lower jaw and the canal terminates at the midline symphysis (Figure 2a).

Entry point is on the medial surface of the lower jaw, below what is putatively the posterior edge of the bony orbit. The opening is bounded by the dentary and surangular laterally and the prearticular and coronoid bone medially (Ford & Benson, 2019). The entry point appears to be oriented dorsolaterally. Ford and Benson (2019) termed this structure the adductor fossa.

Number of mandibular foramina is 28 and these openings are located on the lateral surface of the dentary; however, the lateral compression of this fossil may have flattened the natural curvature of the lower jaw in life.

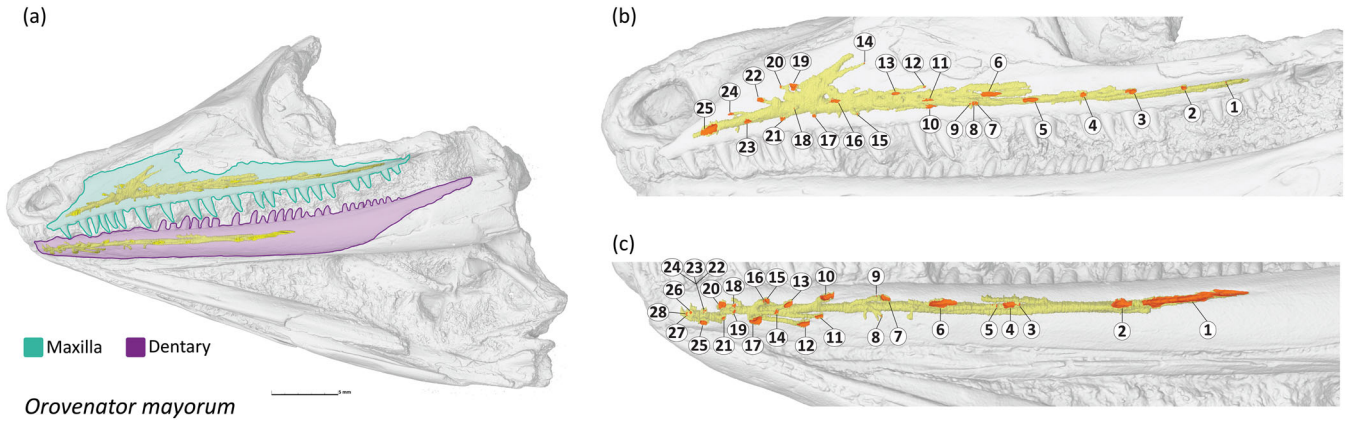

FIGURE 2 Early Permian sauropsid *Orovenator mayorum* (OMNH 74606) is mirrored to display the better-preserved right side. The maxillary and mandibular canals are segmented in yellow. Foramina in red are numbered in an approximately caudal to rostral sequence. Relevant bones are identified and color-coded in the whole skull view on the left. The fossil is shown in (a) lateral view with bone identification guided by Ford and Benson (2019), (b) maxillary canal in lateral oblique view, and (c) mandibular canal in ventral oblique view.

Foramina 1–6 are irregularly spaced and are openings of various sizes, but they appear in a single line parallel with the lower toothrow. Foramen 1 emerges from a long, caudally trailing groove also remarked upon by Ford and Benson (2019). Foramina 7–17 occur near the rostral tip of the jaws and terminate relatively long caudally oriented branches. Foramina 18–28 terminate stubby branches at the rostral extremity of the mandibular canal (Figure 2c). These openings are oriented as follows: 1—ventrocaudal, 2—ventrocaudal, 3—ventrocaudal, 4—ventrocaudal, 5—ventrolateral, 6—ventrolateral, 7—caudolateral, 8—ventral, 9—caudolateral, 10—dorsocaudal, 11—ventrocaudal, 12—ventrocaudal, 13—ventrocaudal, 14—caudolateral, 15—caudolateral, 16—lateral, 17—ventral, 18—caudolateral, 19—caudolateral, 20—ventrocaudal, 21—ventrocaudal, 22—ventrolateral, 23—ventrolateral, 24—ventrolateral, 25—ventral, 26—rostrolateral, 27—rostral, and 28—rostral.

3.2.2 | *Uroplatus fimbriatus*

Maxillary canal appears as a tangled network of branches and cavities, with an expanded region similar to the conical cavity observed in *Orovenator*. The canal extends through the rostral two-thirds of the maxilla, terminating near the caudal border of the nares (Figure 3a). The ramifications diverging from the canal are of various lengths and extend in all directions.

Entry point is within the ventrorostral wall of the orbit, bounded by the maxillary shelf and the prefrontal bone.

Number of maxillary foramina is 17 and they are located on the lateral surface of the maxilla (Figure 3b). Foramina 1–6 terminate caudally oriented branches diverging from the canal behind the expanded cavity. Foramina 7–15 terminate branches associated with the expanded cavity region and are thus spread over a wider dorsoventral area of the maxilla; foramen 7 is an especially large opening. Foramina 16 and 17 terminate branches of the nasal rami rostral to the expanded cavity. Foramina 1, 3, 5, 6, 9, 13, 15, and 16 are positioned in an approximate supralabial row (Figure 3b). Foramina open out in the following orientations: 1—caudal, 2—dorsocaudal, 3—caudal, 4—dorsocaudal, 5—caudal, 6—caudal, 7—lateral, 8—lateral, 9—lateral, 10—dorsal, 11—dorsal, 12—dorsorostral, 13—lateral, 14—lateral, 15—lateral, 16—lateral, and 17—rostral.

Mandibular canal is linear, extends anteroposteriorly through the bones of the lower jaw, and terminates near the midline symphysis (Figure 3a). Branches are short and diverge approximately orthogonal to the canal.

Entry point is located on the medial surface of the lower jaw and positioned near the ventral margin, between the coronoid process and the articular facet. The opening is oriented dorsomedially.

Number of mandibular foramina is 7 and these openings appear at regular intervals in a row along the ventrolateral surface of the rostral half of the dentary (Figure 3c). Foramina open out in the following orientations: 1—lateral, 2—lateral, 3—lateral, 4—lateral, 5—ventrolateral, 6—ventral, and 7—ventral.

3.2.3 | *Dibamus novaeguineae*

Maxillary canal is linear, tubular, and travels anteroposteriorly through the bone of the maxilla parallel to the upper tooth row. The canal extends to the rostral tip of the maxilla (Figure 3d). The branches are short.

Entry point is on the medial side of the maxilla. There is a short sulcus leading into the opening on the maxillary shelf near the junction with the prefrontal.

Number of maxillary foramina is 4 and they emerge at regular intervals in a row on the lateral surface of the maxilla near the upper toothrow (Figure 3e). These openings are oriented as follows: 1—lateral, 2—lateral, 3—rostrolateral, and 4—rostrolateral.

In addition to the maxillary canal, the maxilla and nasal bones bear short, non-contiguous canals (blue canals in Figure 3e) that likely serve as passageways for branches of V_1, but could also accommodate branches of V_2 along the dorsal edge of the maxilla (Rieppel, 1984). There are four separate branches, of which two are simple tubular canals and two are ramified. These branches are rostrolaterally or dorsorostrally oriented and terminate in foramina that are comparable in size to those associated with the maxillary canal.

Mandibular canal is linear, tubular, and extends anteroposteriorly through the dentary and compound bone (i.e., fusion of the surangular, angular, and articular bones per Rieppel, 1984) to near the midline symphysis. The branches diverging from the canal are short.

Entry point is located on the medial surface of the compound bone near the articular facet. The opening is positioned near the dorsal margin and opens out medially. There is a separate smaller opening caudally, but it is uncertain whether this foramen participates in the passage of V_3.

Number of mandibular foramina is 9. Foramina 1–3 are located on the lateral surface of the compound bone. Foramina 4–9 emerge at regular intervals in a row on the lateral surface of the dentary beneath the lower toothrow (Figure 3f). These openings are oriented as follows: 1—dorsal, 2—lateral, 3—lateral, 4—lateral, 5—lateral, 6—lateral, 7—rostrolateral, 8—rostrolateral, and 9—rostral.

3.2.4 | *Tupinambis teguixin*

Maxillary canal is linear, tubular, and extends anteroposteriorly through the maxilla parallel to the upper toothrow until it deflects medially to terminate inside the narial cavity (Figure 3g). Branches diverging from the canal are short and tend to angle rostrolaterally.

Entry point is on the rostral-facing aspect of the orbit, bounded by the maxillary shelf and lacrimal, and ventral to the lacrimal foramen.

Number of maxillary foramina is 8 and these openings appear at regular intervals in a row on the lateral surface of the maxilla near the upper toothrow (Figure 3h). Foramen 1 is considerably larger than the other foramina. These openings are oriented as follows: 1—lateral, 2—lateral, 3—rostrolateral, 4—rostrolateral, 5—rostrolateral, 6—rostrolateral, 7—rostrolateral, and 8—rostrolateral.

Mandibular canal is linear, tubular, and extends anteroposteriorly through the bones of the lower jaw until it terminates near the midline symphysis (Figure 3g).

Entry point is a large opening on the medial surface of the lower jaw, positioned between the coronoid process and articular facet.

Number of mandibular foramina is 6 and they are located on the lateral surface of the lower jaw. Foramen 1 is positioned on the surangular, at the level of the coronoid process. Foramina 2–6 occur in approximately regular intervals on the dentary, beneath the lower toothrow (Figure 3i). These openings are oriented as follows: 1—rostrolateral, 2—caudolateral, 3—lateral, 4—lateral, 5—lateral, and 6—rostrolateral.

3.2.5 | *Anolis cristatellus*

Maxillary canal extends anteroposteriorly through the entire length of the maxilla and terminates in a medially inflected branch that fades into the bone of the premaxilla at the base of the nares. The canal is quite slender caudally, but then expands into a dorsoventrally broadened space that emanates short branches (Figure 3j).

Entry point is on the ventrorostral surface of the orbital wall, is bounded by the lacrimal and maxillary shelf, and is positioned ventral to the larger lacrimal foramen.

Number of maxillary foramina is 12 and they are located on the lateral surface of the maxilla. Foramina 1, 2, 4, 6, 8, 10, and 11 occur at approximately regular intervals in a row along the upper toothrow. Foramina 3, 5, 7, and 9 are positioned dorsally above this supralabial row and are more irregular in distribution. Foramen 12 is a large opening at the lateral edge of the nares (Figure 3k). These openings are oriented as follows: 1—caudolateral, 2—caudolateral, 3—lateral, 4—lateral, 5—lateral, 6—lateral, 7—lateral, 8—lateral, 9—rostrolateral, 10—rostrolateral, 11—rostrolateral, and 12—dorsorostral.

Mandibular canal is linear, extends anteroposteriorly through the bones of the lower jaw, and terminates at the midline symphysis (Figure 3j). Branches are short and diverge orthogonal to the mandibular canal.

Entry point is on the medial surface of the lower jaw, spanning the space between the coronoid process and the articular facet. This large opening is oriented medially.

Number of mandibular foramina is 7 and they are located on the rostral half of the dentary. The openings occur at approximately regular intervals in a single line below the lower toothrow. Foramina 1–6 appear on the

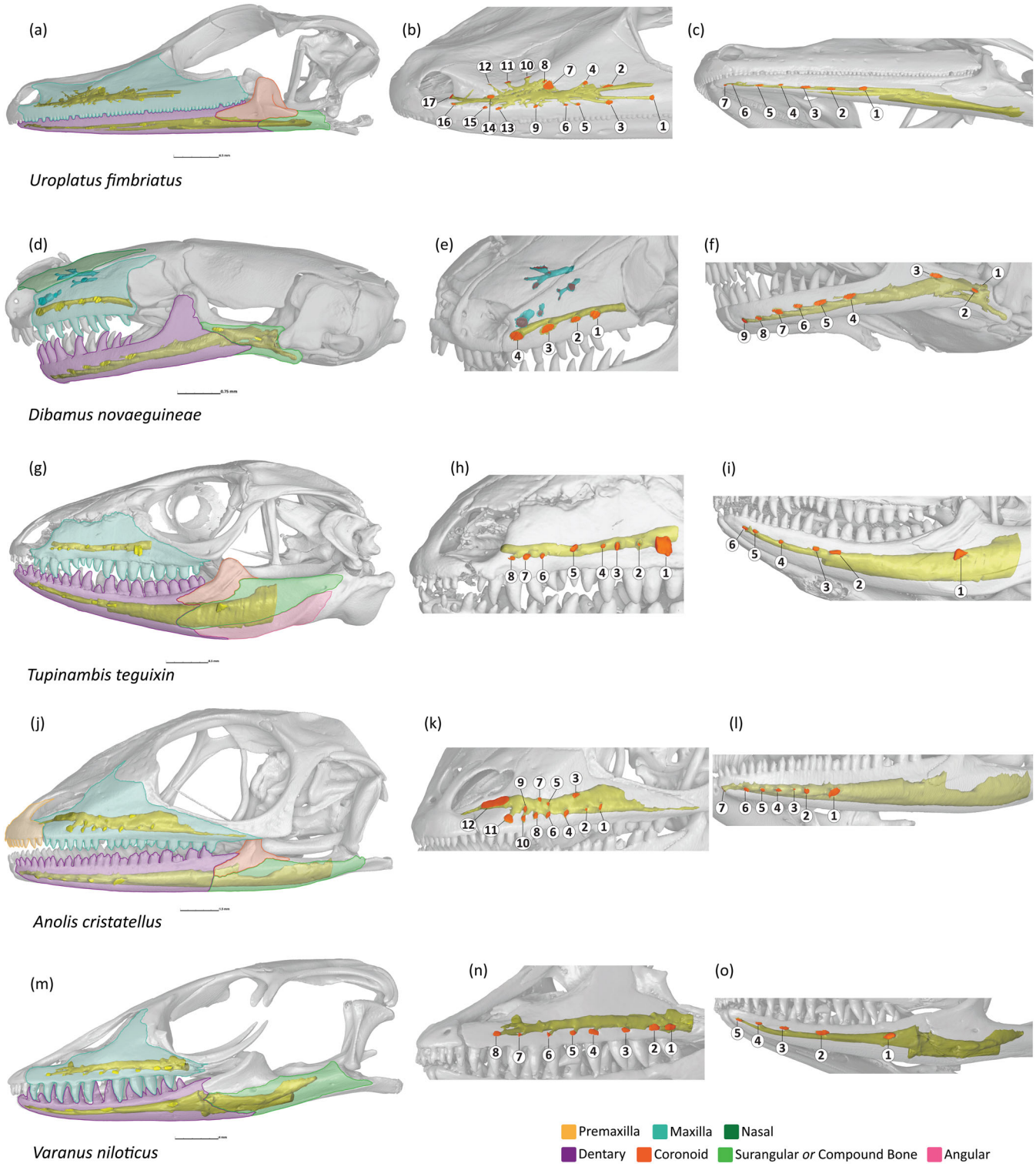

FIGURE 3 Squamate reptiles (lizards) with maxillary and mandibular canals of the left side segmented in yellow. Foramina in red are numbered in an approximately caudal to rostral sequence. Relevant bones are identified and color-coded for each species in the whole skull view on the left. The nocturnal gecko *Uroplatus fimbriatus* (UF:HERP:72880) is shown in (a) lateral view, (b) maxillary canal in lateral oblique view, and (c) mandibular canal in ventral oblique view. The fossorial "blind skink" *Dibamus novaeguineae* (UF:HERP:33488) is shown in (d) lateral view with the compound bone of the lower jaw represented in the same green color as the surangular, (e) maxillary canal and putative V_1 and/or V_2 canals (in blue) in dorsolateral oblique view, and (f) mandibular canal in ventrolateral view. *Tupinambis teguixin* (FMNH 22416) is shown in (g) lateral view, (h) maxillary canal in rostrolateral view, and (i) mandibular canal in ventrolateral oblique view. *Anolis cristatellus* (UF:HERP:47686) is shown in (j) lateral view, (k) maxillary canal in lateral oblique view, and (l) mandibular canal in lateral oblique view. *Varanus niloticus* (UF:HERP:83764) is mirrored to show (m) lateral view, (n) maxillary canal in lateral oblique view, and (o) mandibular canal in lateral oblique view.

lateral surface of the dentary and foramen 7 is at the very tip of the bone, facing toward the symphysis (Figure 3l). These openings are oriented as follows: 1—lateral, 2—caudolateral, 3—caudolateral, 4—lateral, 5—lateral, 6—rostrolateral, and 7—ventromedial.

3.2.6 | *Varanus niloticus*

Maxillary canal is linear, tubular, and extends anteroposteriorly through the maxilla. The canal terminates near the rostral end where it ramifies into a few internal branches, including medially inflected branches into the region of the narial cavity (Figure 3m). The branches are relatively short.

Entry point is on the ventrorostral aspect of the orbital wall. The opening is ventral to the lacrimal foramen and is bounded by the pterygoid and maxilla.

Number of maxillary foramina is 8 and these openings occur at relatively regular intervals in a row above the upper toothrow (Figure 3n). These openings are oriented as follows: 1—lateral, 2—lateral, 3—lateral, 4—rostrolateral, 5—rostrolateral, 6—rostrolateral, 7—rostrolateral, and 8—rostrolateral.

Mandibular canal is linear, tubular, and extends through the bones of the lower jaw to terminate near the midline symphysis (Figure 3m). Branches are short.

Entry point is on the medial surface of the surangular positioned between the coronoid process and articular facet. The opening is large and is oriented medially.

Number of mandibular foramina is 5 and they are located on the lateral surface of the dentary. The openings occur at relatively regular intervals in a line near the lower toothrow (Figure 3o). The foramina are oriented as follows: 1—rostrolateral, 2—lateral, 3—lateral, 4—rostrolateral, and 5—rostral.

3.2.7 | *Eunectes murinus*

Maxillary canal travels through the maxilla in an anteroposterior path parallel to the upper tooth row (Figure 4a). The canal is present only in the rostral half of the maxilla and terminates rostrally with a medially inflected branch that enters the base of the first alveolus. Slender branches diverge laterally and ventrally from the canal likewise appear to be entering into the base of the teeth. The two primary branches emerging from the canal are relatively short and directed rostrolaterally.

Entry point is located on the dorsomedial surface of the maxilla that forms the ventral margin of the bony orbit. There is a potential second point of entry located ventrorostrally of the first described opening and is oriented medially. Both openings are of similar size.

Number of maxillary foramina is 2 and are positioned on the lateral surface of the maxilla. Foramen 1 is positioned above the third alveolus. Foramen 2 is a larger opening positioned above the second alveolus (Figure 4b). Both openings are oriented rostrolaterally.

Mandibular canal is broad, tubular, and extends through the bones of the lower jaws parallel with the lower tooth row. There are several smaller, twisting, medially directed branches that enter areas surrounding the base of the teeth. The canal terminates with a medially inflected branch that extends to the rostral tip of the dentary (Figure 4a).

Entry point is located in a deep, dorsal-facing sulcus formed by the dorsal margin of the surangular (or compound bone). The opening is positioned between the coronoid process and the articular facet.

Number of mandibular foramina is 2. Foramen 1 is a large opening located on the dorsorostral edge of the coronoid process, caudal to the tooth-bearing dentary. Foramen 2 is located on the ventrolateral surface of the dentary, near the midline symphysis at the level of the fifth alveolus (Figure 4c). These openings are oriented as follows: 1—rostromedial and 2—ventrolateral.

3.2.8 | *Thamnophis marcianus*

Maxillary canal is long, thin, and traverses the entire length of the maxilla (Figure 4d). At the caudal end of the maxilla, the canal is broadened into a complex, lattice-like structure that fills the interior space, including the bases and pulp cavities of three separate teeth. The canal then simplifies into a slender linear tube within the portion of the maxilla that forms the ventral rim of the bony orbit. At the rostral tip of the maxilla, the canal once again ramifies into small, laterally directed branches entering the base of the first five teeth.

Entry point is on the medial surface of the maxilla, located on the ventral surface of a flange extending toward the palatine. This relatively small, ventromedially oriented opening is positioned rostral to the anterior edge of the bony orbit.

Number of maxillary foramina is 6. Foramina 1–5 are very small openings associated with the network of ramifications at the caudal end of the maxilla and are irregularly positioned on the lateral surface of the maxilla. These openings may serve as entry points for branches of the superior alveolar nerve—small ramifications of V_2 that enter the maxilla to innervate the teeth (Auen & Langebartel, 1977). Foramen 6 is located beneath the

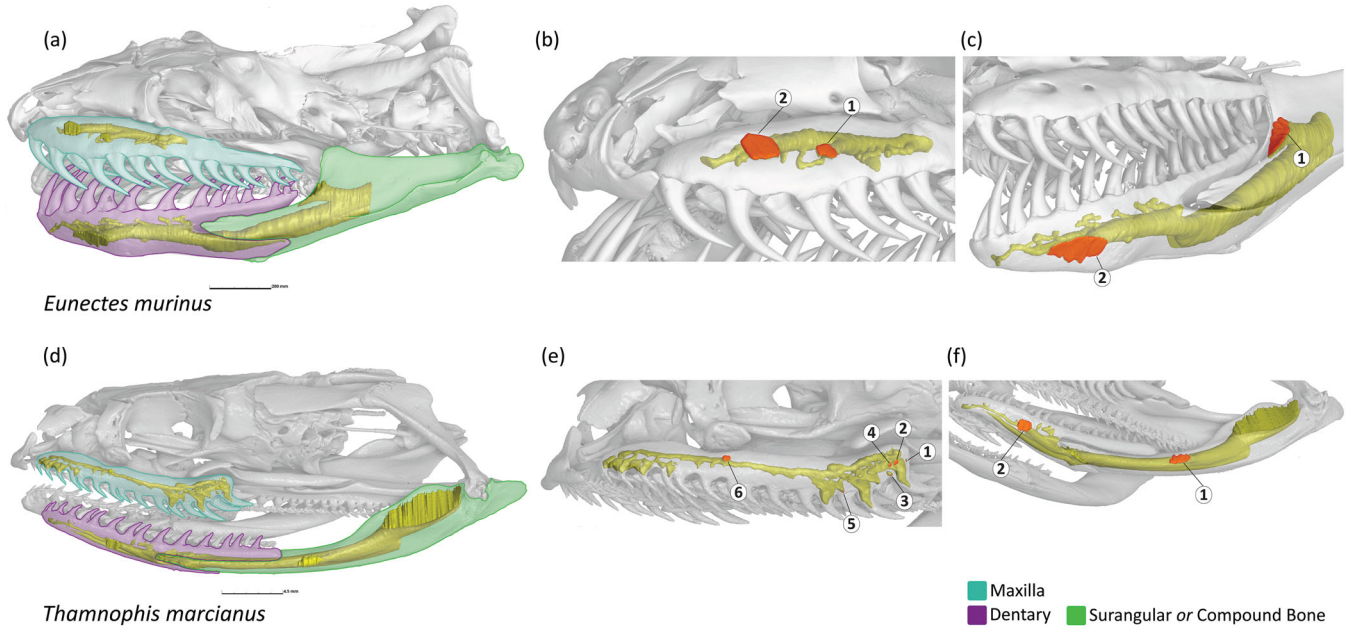

FIGURE 4 Squamate reptiles (snakes) with maxillary and mandibular canals of the left side segmented in yellow. Foramina in red are numbered in an approximately caudal to rostral sequence. Relevant bones are identified and color-coded for each species in the whole skull view on the left. The semiaquatic, infrared sensing boid *Eunectes murinus* (UF:HERP:84822) is shown in (a) lateral oblique view, (b) maxillary canal in lateral oblique view, and (c) mandibular canal in ventrolateral oblique view. The terrestrial colubrid *Thamnophis marcianus* (FMNH 26260) is shown in (d) lateral view, (e) maxillary canal in lateral oblique view, and (f) mandibular canal in ventrolateral oblique view.

anterior edge of the bony orbit on the lateral surface of the maxilla and is the largest of the foramina (Figure 4e). These openings are oriented as follows: 1—caudal, 2—lateral, 3—ventrocaudal, 4—lateral, 5—ventrolateral, and 6—lateral.

Mandibular canal is tubular and passes anteroposteriorly through the bones of the lower jaw where it terminates inside the dentary at the midline symphysis (Figure 4d). In this specimen, there is a clear distinction between the mandibular canal and the ventromedially positioned space for Meckel's cartilage.

Entry point is the large opening at the caudal end of the surangular (i.e., compound bone) just before the jaw articulation and is oriented dorsolaterally.

Number of mandibular foramina is 2. Foramen 1 occurs on the lateral surface of the surangular, close to the junction with the dentary. Foramen 2 is located on the lateral surface of the dentary, approximately at the level of the anterior edge of the orbit (Figure 4f). These openings are oriented as follows: 1—dorsolateral and 2—rostral.

3.2.9 | *Alligator mississippiensis*

Maxillary canal is an extensive web-like network of ramifications extending through both the maxilla and premaxilla, where the canal terminates at the rostral tip of the premaxilla. The size and distribution of the branches is irregular (Figure 5a).

Entry point is ventral to the anterior margin of the bony orbit, on the medial surface of the junction between the maxilla and jugal.

Number of maxillary foramina is many. At least 50+ foramina are visible in our segmentation, but the observation of minute branches connecting to the bone surface and the pitted surface of the facial bones would suggest a far greater number of exit points that may not have been detected due to the resolution of the microCT scan used in this study. The foramina vary in size and have an irregular distribution over the dorsolateral surface of the upper jaw, though most of the openings occur close to the upper toothrow (Figure 5b).

Mandibular canal is wide, occupying a substantial space within the lower jaw as it travels rostrally to the midline symphysis (Figure 5a). A three-dimensional model of the jaw muscles of *A. mississippiensis* based on microCT scans of contrast-stained soft tissue shows that the massive internal space of the lower jaw in the region of the mandibular fenestra is occupied by the intramandibularis muscle and, to a lesser extent, the adductor mandibulae posterior muscle. V_3 was observed running rostrally along the dorsal edge of the

intramandibularis muscle within the mandibular canal (Holliday et al., 2013).

Entry point is a large opening positioned opposite (i.e., medial) to the mandibular fenestra and opens out medially.

Number of mandibular foramina is many, similar to the maxillary canal. At least 40+ foramina are visible in our segmentation. The foramina have an irregular distribution over the lateral surface of the dentary and angular bones, with the tendency to occur near the lower tooth row on the dentary and along the ventral margin of the angular (Figure 5c).

3.2.10 | *Bubulcus ibis*

Maxillary canal does not pass through the highly reduced maxilla, but rather occupies almost the entire interior space of the beak (premaxilla) rostral to the narial opening (Figure 5d). The division of the canal into distinct right and left sides is not clearly distinguishable. The canal terminates at the very rostral tip of the beak. The occupant of the maxillary canal in *Bubulcus* is uncertain. A microCT study of the soft tissue anatomy in the rock dove (*Columba livia*) shows the reduction of V_2 and its termination within the ventral aspect of the orbit, well before any contact with the upper jawbones. Instead, V_1 is observed traversing through the narial cavity to enter into the premaxilla (Jones et al., 2019). In contrast, a classical anatomical study of the domestic turkey (*Meleagris gallopavo domesticus*) depicts V_2 anastomosing with the nasal branches of V_1 and entering into the premaxilla (Ghetie et al., 1976).

Entry point is located with the large openings occupying the midline of the rostral edge of the narial opening.

Number of maxillary foramina is undetermined. There are some irregular openings found in the lateral surface of premaxilla: a cluster close to the caudal end of the canal and a few openings at the rostral tip. It is unclear if the caudal cluster are true foramina or represent a region where the bone has eroded away to expose the canal space. The three or four rostral openings are most likely to be true foramina given their morphology (Figure 5e).

Mandibular canal is laterally compressed, linear, and extends through the entire length of the dentary (Figure 5d). There are a few outpocketings of the canal that may be considered extremely short branches near the rostral tip.

Entry point is on the medial surface of the dentary, at approximately halfway down its length and rostral to the narial cavity. It is a large, elongated opening oriented medially.

Number of mandibular foramina is 1. Foramen 1 is a small opening on the lateral surface near the tip of the dentary that opens out laterally (Figure 5f).

3.2.11 | *Calidris alba*

Maxillary canal is limited to the tip of the premaxilla rostral of the extremely elongated narial cavity (Figure 5g). Consequently, the canal is very short, but it occupies nearly all the internal space of the premaxilla with a dense proliferation of short branches. The identity of the nerves traversing this canal is similar to that discussed above for *Bubulcus*.

Entry point is located at the midline of the rostral edge of the narial cavity.

Number of maxillary foramina is many. There are at least 40+ foramina visible at the rostral tip of the dentary from our segmentation, but the number of exit points is likely to be higher given the extremely pitted surface of the bone. There are some large openings in the rostral half of the canal, including a sulcus-like opening dorsally. Smaller foramina occur as a dense cluster on the dorsolateral surface of the extreme tip of the premaxilla and these openings are oriented in all directions (Figure 5h).

Mandibular canal is linear and extends through the entire length of the dentary. Most of the canal is laterally compressed, but widens into a bulb-shaped expansion at the rostral tip (Figure 5g). Branches are extremely short and limited to the rostral end of the dentary.

Entry point is on the medial surface of the dentary, approximately halfway down its length. It is a medium-sized, somewhat oval-shaped opening oriented medially.

Number of mandibular foramina is many. There are at least 60+ foramina visible from our segmentation, but as with the maxillary foramen, the number of nerve exit points is likely to be much higher. There are a few putative foramina present on the lateral surface of the dentary before the mandibular canal expands. The greatest density of foramina appears on the ventrolateral surface of the extreme rostral tip of the dentary. These foramina appear to be organized in an almost grid-like pattern and are thus oriented in all directions. The thinning of the bone in this region exposes the mandibular canal dorsally and ventrally (Figure 5i).

3.3 | Nonmammalian synapsids

3.3.1 | *Varanosaurus acutirostris*

Maxillary canal is primarily linear and travels through the entire length of the maxilla parallel to the upper tooth row. Foramina are present in the approximate rostral two-thirds of the long snout and terminate short branches diverging from the maxillary canal at irregular intervals along the tooth row (Figure 6a). The identification of foramina was challenged by the fractured surface of the fossil.

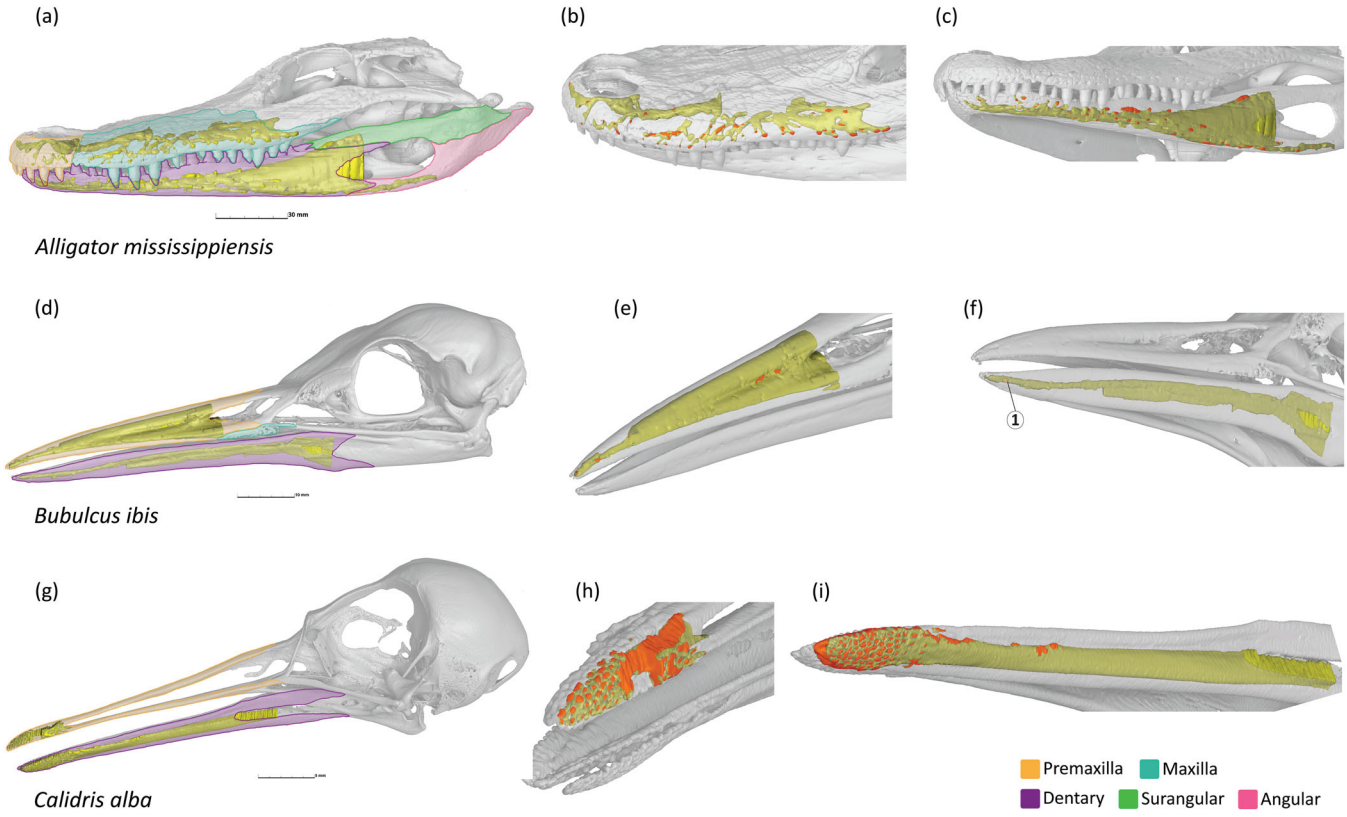

FIGURE 5 Archosaurian reptiles with maxillary and mandibular canals of the left side segmented in yellow. Foramina are in red. Relevant bones are identified and color-coded for each species in the whole skull view on the left. The semiaquatic tactile specialist *Alligator mississippiensis* (TMM M-983) is mirrored to show (a) lateral view, (b) maxillary canal in dorsal oblique view, and (c) mandibular canal in ventrolateral oblique view. The diurnal visual hunter *Bulbulcus ibis* (NHMUK:zoo:S/2006.1.20) shown in (d) lateral oblique view, (e) maxillary canal in lateral oblique view, and (f) mandibular canal in ventrolateral oblique view. The probing shorebird *Calidris alba* (NHMHK:zoo:S/1994.60.3) shown in (g) lateral oblique view, (h) maxillary canal in dorsal oblique view, and (i) mandibular canal in ventrolateral oblique view.

Entry point cannot be clearly determined due to preservation, but the canal in the maxilla becomes visible just caudal to the upper toothrow.

Number of maxillary foramina is 8 and they all occur on the lateral surface of the maxilla, close to the upper toothrow. Branches of the caudal alveolar ramus terminate in foramina 1–3. Branches of the external nasal ramus terminate in foramina 4 and 5. Branches of the internal nasal ramus terminate in foramina 6–8. (Figure 6b). These foramina open out in the following orientations: 1—caudal, 2—rostrolateral, 3—caudal, 4—lateral, 5—lateral, 6—lateral, 7—lateral, and 8—lateral.

Although there is no continuity observed between the maxillary canal and the canals perforating the premaxilla, the latter is densely covered with forward-facing foramina interpreted as exits for the nasopalatine branches of V_2 (Benoit et al., 2018).

Mandibular canal is also primarily linear and travels anteriorly through the dentary near the lower toothrow. The diverging branches are short and irregularly spaced. The canal extends to the rostral tip of the midline symphysis, where there is a concentrated cluster of foramina (Figure 6a).

Entry point is on the medial surface of the dentary, just caudal to the lower toothrow.

Number of mandibular foramina is 14. Foramina 1–8 are distributed at irregular intervals along the lateral surface of the dentary, but foramina 9–13 are clustered at the forward-facing rostral extremity of the lower jaw. (Figure 6c). These foramina open out in the following orientations: 1—caudal, 2—caudal, 3—ventrocaudal, 4—lateral, 5—lateral, 6—ventrolateral, 7—lateral, 8—lateral, 9—caudolateral, 10—ventrolateral, 11—ventral, 12—dorsolateral, 12—ventrorostral, and 14—ventrorostral.

3.3.2 | *Tetracynodon darti*

Maxillary canal consists of a proximal section that travels parallel to the upper toothrow, has the appearance

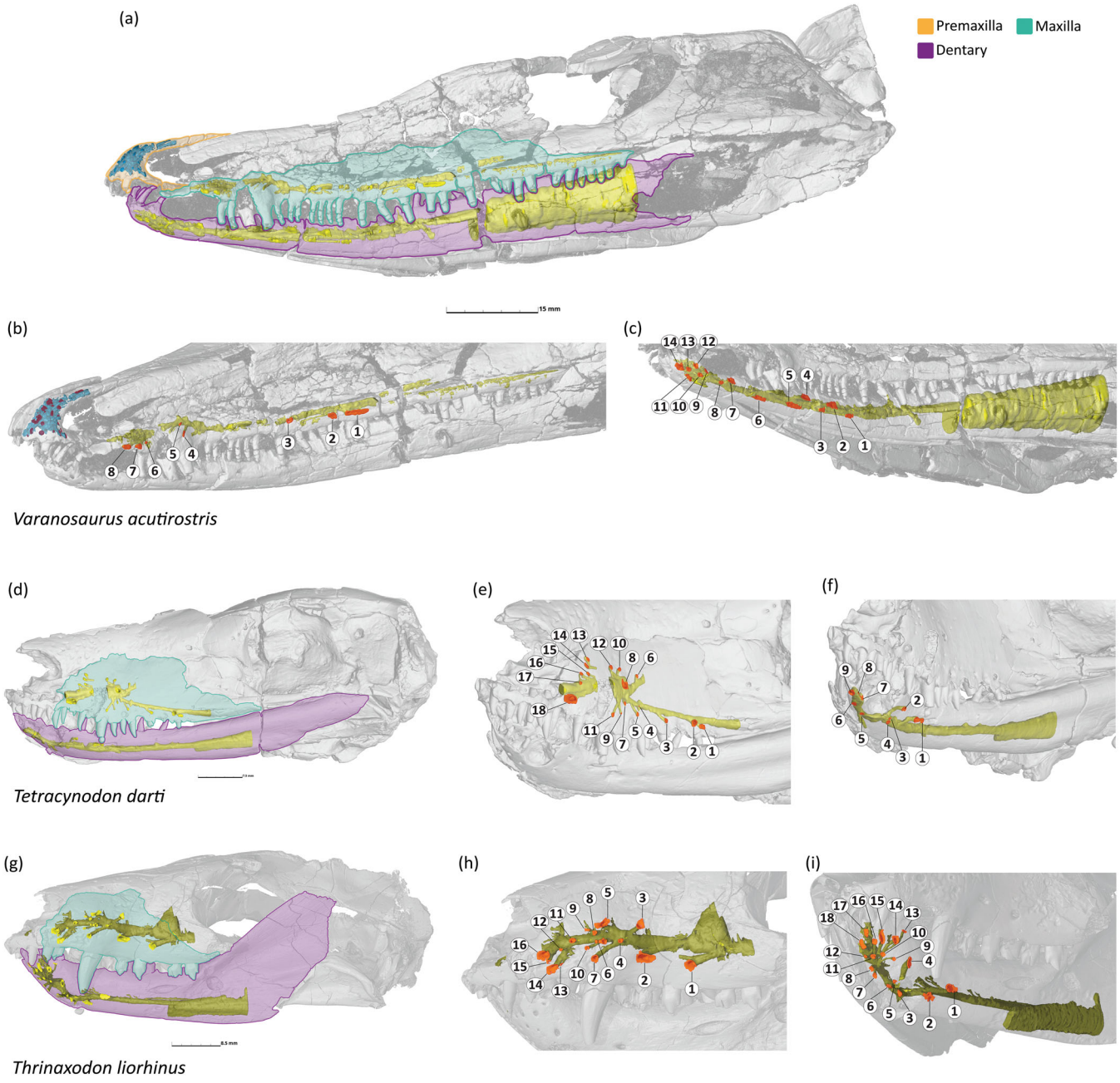

FIGURE 6 Nonmammalian synapsids with maxillary and mandibular canals of the left side segmented in yellow. Foramina in red are numbered in an approximately caudal to rostral sequence. Relevant bones are identified and color-coded for each species in the whole skull view on the left. The Early Permian ophiacodont *Varanosaurus acutirostris* (FMNH PR 1670) is mirrored to show (a) lateral view with bone identification guided by Berman et al. (1995) [Correction added after first online publication on 03 February 2025. The specimen number for Varanosaurus acutirostris was changed from "FMNH PR 1760" to "FMNH PR 1670".], (b) maxillary canal and putative V_2 nasopalatine branch canals (in blue) in lateral oblique view, and (c) mandibular canal in ventrolateral view. The Early Triassic therocephalian *Tetracynodon darti* (UCMP 42869) is shown in (d) lateral view, (e) maxillary canal in rostrolateral view, and (f) mandibular canal in rostroventral view. The Early Triassic cynodont *Thrinaxodon liorhinus* (UCMP 40466) is mirrored to show (g) lateral view, (h) maxillary canal in lateral view, and (i) mandibular canal in rostroventral view.

of a slender and linear tube, and produces short ramifications that terminate in foramina near the toothrow. The canal then shows an abrupt expansion into a wide cavity or sinus region similar to the "conical cavity" observed in *Orovenator* (Figure 6d); though it should be noted that a portion of this area has not been preserved in *Tetracynodon*. Numerous longer branches emerge from this large cavity region. The rostral tip of the upper jaw has not been preserved, so it is uncertain how far the maxillary canal may have extended anteriorly.

Entry point is obscured because lateral compression of the fossil has crushed the area where we expect to see the entry of the canal into the bone of the maxilla; however, the canal becomes visible caudal to the upper toothrow.

Number of maxillary foramina is 18 and they all occur on the lateral surface of the maxilla. Foramina associated with the caudal, middle, and rostral alveolar rami are positioned close to the upper toothrow; however, foramina associated with the external and internal nasal rami are distributed more dorsally to cover a larger surface of the maxilla. Branches of the caudal alveolar ramus terminate in foramina 1–3. Branches of the middle alveolar ramus (aka medium alveolar ramus) terminate in foramina 4, 5, and 7. Branches of the rostral alveolar ramus terminate in foramina 9 and 11. Branches of the external nasal ramus terminate in foramina 6, 8, 10, and 12. Branches of the internal nasal ramus terminate in foramina 13–17. The superior labial ramus likely terminates with foramen 18, which has a notably larger opening compared to other foramina and is located near the toothrow (Figure 6e). These foramina open out in the following orientations: 1—lateral, 2—lateral, 3—caudolateral, 4—caudolateral, 5—ventrocaudal, 6—dorsolateral, 7—ventrolateral, 8—lateral, 9—ventrocaudal, 10—dorsolateral, 11—ventrolateral, 12—dorsolateral, 13—dorsolateral, 14—rostral, 15—rostral, 16—rostral, 17—lateral, and 18—rostroventral.

Mandibular canal is linear and travels through the dentary parallel to the lower toothrow and extends to the midline symphysis of the jaw. There are several short branches occurring in the rostral half of the canal (Figure 6d).

Entry point of the canal into the bone of the dentary is not preserved in this specimen, but the mandibular canal becomes visible at the level of the anterior edge of the orbit, caudal to the start of the toothrows.

Number of mandibular foramina is 9. Foramina 1–4 are located on the lateral surface of the dentary. The opening to foramen 1 is accompanied by a caudally oriented trailing groove. Foramina 3 and 4 are clustered closer to the ventral margin of the dentary. Foramina 5–9 are found on the forward-facing surface of the dentary near the midline symphysis (Figure 6f). These foramina open out in the following orientations: 1—caudolateral, 2—lateral, 3—ventrolateral, 4—lateral, 5—ventral, 6—ventral, 7—lateral, 8—lateral, and 9—ventral.

3.3.3 | *Thrinaxodon liorhinus*

Maxillary canal is broad, tubular, and travels anteriorly through the maxilla to the rostral tip. The ramifications diverging from the canal are relatively long and are especially proliferative in the region rostral to the large upper caniniform tooth (Figure 6g). The rostral end of the upper jaw has not been preserved, so the morphology of the canal in this region is unknown.

Entry point into the maxilla is on the ventral aspect of the medial orbital wall near the junction with the lacrimal bone.

Number of maxillary foramina is 16 and they are all located on the lateral surface of the maxilla. The caudal alveolar ramus terminates in foramen 1. The middle alveolar ramus terminates in foramen 2. Both foramina 1 and 2 are large openings located near the upper toothrow. Branches of the rostral alveolar ramus terminate in foramina 4, 7, and possibly 10. Branches of the external nasal ramus terminate in foramina 3, 5, 8, and 9. The internal nasal ramus terminates in foramen 11. Foramina from these two aforementioned branches are distributed more dorsally on the surface of the maxilla. Branches of the superior labial ramus terminate in foramina 13–16; foramina 14 and 16 are notably large openings in this grouping (Figure 6h). The identification of these branches is based on Benoit et al. (2020). These foramina open out in the following orientations: 1—rostrolateral, 2—lateral, 3—dorsocaudal, 4—lateral, 5—dorsal, 6—dorsocaudal, 7—lateral, 8—rostrolateral, 9—rostrolateral, 10—lateral, 11—rostrolateral, 12—ventrorostral, 13—rostrolateral, 14—rostroventral, 15—rostrolateral, and 16—rostrolateral.

Mandibular canal is primarily linear, passing through the dentary parallel to the lower toothrow and ramifying short branches. The canal extends to the rostral tip of the lower jaws where there is extensive branching in a starburst-like pattern clustered near the midline symphysis (Figure 6g).

Entry point is on the medial surface of the dentary near the ventral margin and just caudal to the lower toothrow.

Number of mandibular foramina is 18, with foramina 1–6 located on the lateral surface of the dentary and the remaining foramina 6–17 concentrated on the forward-facing rostral end of the lower jaws (Figure 6i). These foramina open out in the following orientations: 1—lateral, 2—lateral, 3—lateral, 4—dorsolateral, 5—ventral, 6—lateral, 7—ventrorostral, 8—ventrorostral, 9—dorsolateral, 10—dorsorostral, 11—dorsorostral, 12—rostral, 13—dorsolateral, 14—lateral, 15—dorsorostral, 16—dorsorostral, 17—rostral, and 18—rostral.

3.3.4 | *Ecteninion lunensis*

Maxillary canal is comparatively simplified relative to previously described nonmammalian synapsids *Varanosaurus*, *Tetracynodon*, and *Thrinaxodon*. The canal

travels anteriorly through the maxilla, extending to the rostral end of the upper jaws (Figure 7a).

Entry point into the maxilla is on the ventral aspect of the medial wall of the orbit, near the junction with the lacrimal bone.

Number of maxillary foramina is 6. Foramen 1 is the termination of the middle alveolar ramus and is a large opening positioned above the third and fourth postcanine teeth. Foramen 2 is the termination of the rostral alveolar ramus and is another large opening that is positioned above the first postcanine tooth. The external nasal ramus is a long, slender branch diverging from the alveolar rami and terminates in foramen 3. Branches of the internal nasal ramus terminate in foramina 4 and 5. The superior labial ramus terminates in foramen 6. Foramina associated with the nasal and labial rami are positioned more dorsally on the rostral half of the maxilla (Figure 7b). The identification of these branches is based on Benoit et al. (2020). These openings are oriented as follows: 1—ventrorostral, 2—ventrorostral, 3—lateral, 4—lateral, 5—rostral, and 6—rostrolateral.

Mandibular canal is primarily a linear, slender tube passing anteriorly through the dentary bone toward the midline symphysis. The canal runs along the ventral margin of the dentary for most of its course, but then inflects dorsomedially to terminate in branches at the midline symphysis (Figure 7a).

Entry point is on the medial surface of the dentary, near the ventral margin and caudal to the remains of the coronoid process.

Number of mandibular foramina is 6. Foramina 1–2 are relatively large openings on the lateral surface of the dentary and positioned below the lower postcanine teeth. Foramina 3–6 are smaller openings clustered near the forward-facing region of the midline symphysis (Figure 7c). These foramina open out in the following orientations: 1—rostrolateral, 2—rostrolateral, 3—dorsolateral, 4—dorsorostral, 5—rostral, and 6—rostral.

3.3.5 | *Pachygenelus monus*

Maxillary canal is simplified into a single linear canal traveling through the maxilla with no observed ramifications. The canal does not extend to the rostral tip of the jaw as in the previously described nonmammalian synapsids. Instead, the canal terminates in a single large opening approximately two-thirds down the length of the maxilla (Figure 7d).

Entry point into the maxilla is on the ventral aspect of the medial wall of the orbit, near the junction with the lacrimal bone.

Number of maxillary foramina is 1, is found on the lateral surface of the maxilla, and opens out rostrally (Figure 7e). Benoit et al. (2020) reported the presence of two foramina in *Pachygenelus* (BP/1/5110), one terminating a short infraorbital canal and the other a long rostral alveolar ramus. The single foramen described here accords with the termination of the rostral alveolar ramus given its large size and position near the upper canine. The infraorbital canal was not clearly discernible in the specimen used for this study.

Mandibular canal is a simplified linear canal traveling through the dentary approximately parallel to the toothrow and extending anteriorly to the rostral tip of the lower jaw (Figure 7d).

Entry point is on the medial surface of the dentary, caudal to the lower toothrow and approximately at the level of the anterior edge of the coronoid process.

Number of mandibular foramina is 2 and they are both positioned on the lateral surface of the dentary. Foramen 1 terminates a short ramification that is located at the level of the first and second postcanine teeth. Foramen 2 terminates the mandibular canal and is located at the level of the lower canine tooth (Figure 7f). These openings are oriented as follows: 1—lateral and 2—rostrolateral.

3.3.6 | *Tritylodon longaevus*

Maxillary canal travels a linear path anteriorly through the maxilla and then appears to fade within the bone of the maxilla at the level of the diastema (Figure 7g).

Entry point into the maxilla is on the caudal medial wall of the orbit, at approximately the level of the last postcanine tooth.

Number of maxillary foramina is 3 and they are all located on the lateral surface of the maxilla, caudal to the diastema (Figure 7h). Foramen 1 is the zygomaticofacial foramen and occurs at the maxillary-lacrimal suture. This foramen terminates the relatively long zygomaticofacial canal, which has a separate entry into the maxilla via the orbital zygomaticofacial foramen, but fuses with the maxillary canal (Benoit et al., 2020). The short infraorbital canal terminates in foramen 2, that is, the infraorbital foramen (IOF). Foramen 3 terminates the short rostral alveolar ramus. The identification of these foramina is based on Benoit et al. (2020). These openings are oriented as follows: 1—rostral, 2—rostrolateral, and 3—rostrolateral.

Mandibular canal is not available for this specimen.

3.4 | Mammalia

3.4.1 | *Ornithorhynchus anatinus*

Maxillary canal is extensive and occupies a substantial portion of the maxilla. The canal itself is predominantly linear with short ramifications that reach the rostral tip

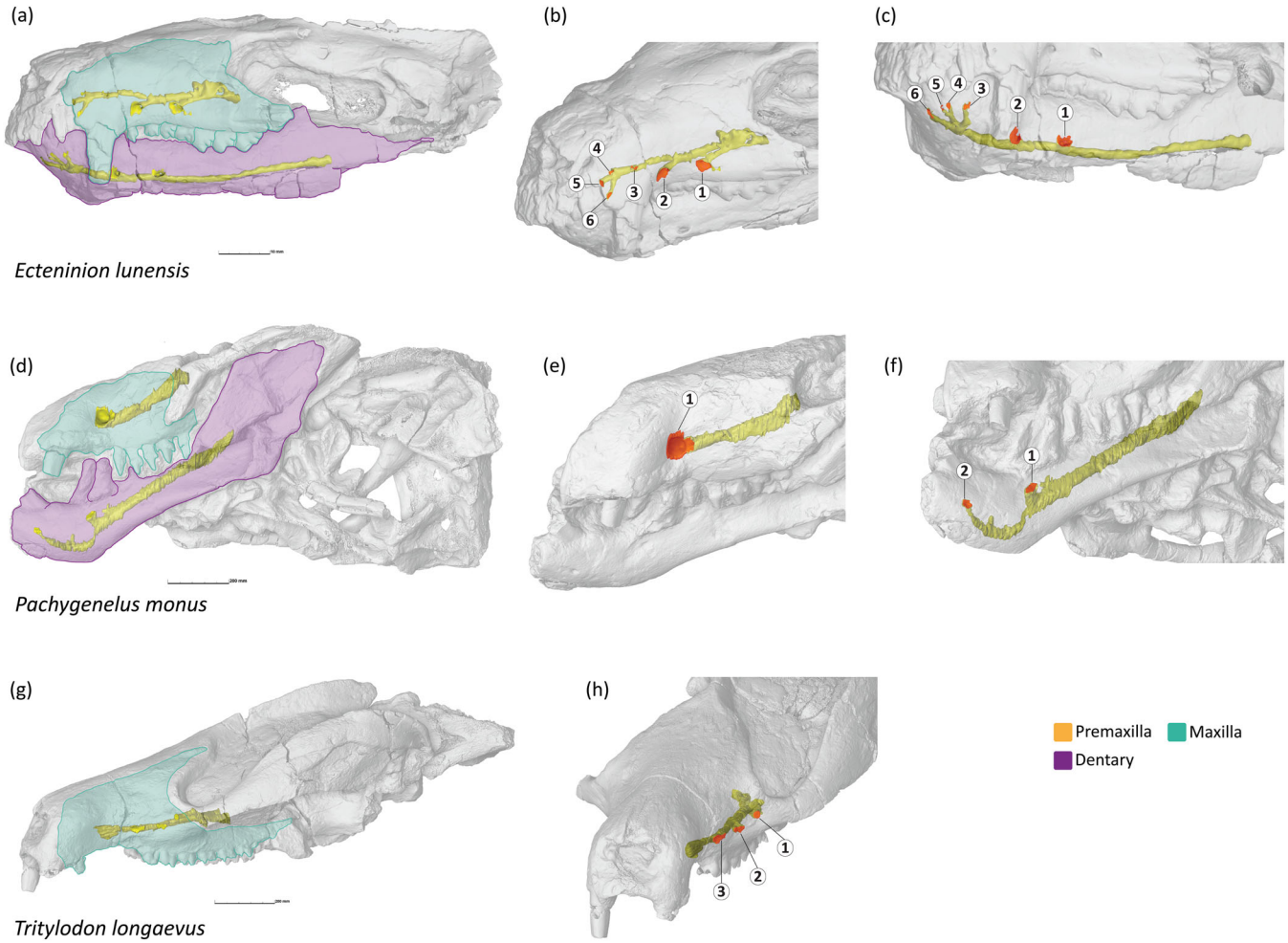

FIGURE 7 Nonmammalian synapsids, continued. Maxillary and mandibular canals of the left side segmented in yellow. Foramina in red are numbered in an approximately caudal to rostral sequence. Relevant bones are identified and color-coded for each species in the whole skull view on the left. The Late Triassic eucynodont *Ecteninion lunensis* (PVSJ 422) is shown in (a) lateral view with bone identification guided by Martinez et al. (1996), (b) maxillary canal in dorsolateral oblique view, and (c) mandibular canal in ventrolateral oblique view. The Early Jurassic probainognathian *Pachygenelus monus* (BP/1/5691) is mirrored to show (d) lateral view, (e) maxillary canal in lateral view, and (f) mandibular canal in lateral oblique view. The Early Jurassic tritylodontid *Tritylodon longaevus* (BP/1/4778) is mirrored to show (g) lateral view of cranium without lower jaw and (h) maxillary canal in rostrodorsal oblique view.

of the maxilla at the junction with the premaxilla (Figure 8a).

Entry point into the maxilla is located on the ventral aspect of the rostral-facing surface of the orbital wall, approximately at the level of the first deciduous molariform tooth in this juvenile specimen (or keratinous grinding pads in the adult).

Number of maxillary foramina is 3. Foramen 1 is a large opening positioned on the lateral edge of the maxilla, and accompanied by a prominent process marking the lateral rim of the canal. Foramen 2 is a large opening positioned on the ventral or palatal aspect of the maxilla approximately at the same level as foramen 1. Foramen 3 is likewise a large opening and is located near the rostral tip of the maxilla, close to the junction with the premaxilla (Figure 8b). Previous anatomical studies identify foramen 1 as equivalent to the IOF (*foramen infraorbitale*), foramen 2 as equivalent to the foramen terminating the middle alveolar ramus (*foramen infraorbitale inferius*), and foramen 3 as equivalent to the foramen terminating the superior or rostral alveolar ramus (*foramen infraorbitale anterius*) (Kesteven & Furst, 1929; Manger & Pettigrew, 1996). These openings are oriented as follows: 1—rostral, 2—ventrorostral, and 3—rostral.

A prominent foramen on the dorsal surface of the nasal bone serves as the exit for the frontal nerve of the ophthalmic division (V_1) of the trigeminus (Manger & Pettigrew, 1996).

Mandibular canal is an extensive, linear canal coursing through the dentary bone to the rostral tip of

the lower jaw (Figure 8a). The ramifications are short and barely seem to angle off from the main axis of the mandibular canal.

Entry point is on the medial surface of the dentary at the level of the coronoid process. The dorsomedial edge of the mandibular foramen is marked by a prominent process, i.e., the lingula.

Number of mandibular foramina is 3. Foramen 1 is a large opening on the lateral surface of the dentary and located at the level of the rostral edge of the lower deciduous molariform teeth (or keratinous grinding pads in the adult). Both foramina 2 and 3 are located at the rostral extremity of the mandible; however, foramen 2 opens on the dorsal surface of the dentary and foramen 3 on the ventral surface (Figure 8c). The anatomical description by Manger and Pettigrew (1996) identifies foramen 1 as the opening for the incisive branch of V_3, foramen 2 as the opening for the internal mental branch, and foramen 3 as the opening for the external mental branch. These foramina open out in the following orientations: 1—rostral, 2—dorsorostral, and 3—ventrorostral.

3.4.2 | *Tachyglossus aculeatus*

Maxillary canal is linear, tubular, and ramifies into four major parts: a slender dorsal branch, a large middle branch that ends at the rostral tip of the maxilla, a series of short ventral branches, and an internal nasal branch that diverges medially to terminate with an opening inside the nasal cavity (Figure 8d).

Entry point is on the ventrorostral aspect of the orbital wall and is bounded by the maxilla and palatine bone.

Number of maxillary foramina is 9. Foramina 1–7 are clustered across the lateral surface of the maxilla and occupy its rostral half. Foramina 2 and 7 diverge from the middle branch. Foramina 1, 3, 4, and 5 are associated with the dorsal branch. Foramina 6 terminates the ventral branch. Foramina 8 and 9 are larger openings at the very tip of the maxilla at its suture with the premaxilla (Figure 8e). The foramina open out in the following orientations: 1—lateral, 2—rostrolateral, 3—lateral, 4—rostrolateral, 5—lateral, 6—ventrolateral, 7—lateral, 8—ventral, and 9—dorsorostral. While assigning homologous identities to these structures is difficult given the elongation of the maxilla and the lack of teeth, what we have designated foramen 8 has been variously identified as the *foramen infraorbitale* (Andres et al., 1991) or the maxillofacial foramen (Manger et al., 1997).

Mandibular canal is linear and extends near to the rostral extremity of the lower jaw, where it forks into two short branches that terminate inside the dentary (Figure 8d).

Entry point is on the medial surface of the dentary, very near the ventral margin approximately at the level of the low coronoid process.

Number of mandibular foramina is 1 and is located on the anterior third of the dentary (Figure 8f). The foramen is at the end of a short canal and opens out dorsolaterally.

3.4.3 | *Tinodon ferox*

Maxillary canal is not available for this specimen.

Mandibular canal is preserved as a largely complete right jaw fragment with the rostral and caudal extremities lost. The canal is linear and travels through the length of the dentary close to the ventral margin following the gentle curvature of the lower jaw (Figure 9a).

Entry point of the mandibular canal is not preserved, but the canal itself becomes visible at the level of the anterior edge of the coronoid process.

Number of mandibular foramina is 2 and they are located on the lateral surface of the dentary. Foramen 1 is positioned between p1 and p2 and opens out dorsolaterally. Foramen 2 is positioned below the lower canine tooth alveolus and opens out dorsorostrally.

3.4.4 | *Monodelphis domestica*

Maxillary canal diverges into two main branches. The infraorbital canal is large, linear, and relatively short. Medial to the infraorbital canal is the long and slender rostral alveolar canal that extends rostrally through the maxilla, deflecting around the root of the upper canine, and sloping ventrally to terminate in the premaxilla within the alveolar space of I3 and I4 (Figure 9b). However, this morphology is contrary to what was reported in Benoit et al. (2020) for *M. domestica*, where the rostral alveolar canal is directed to the root of the canine tooth. It is uncertain whether individual variation in the configuration of the rostral alveolar canal is common in this taxon. The rostral alveolar canal in *Dasyurus hallucatus* (described below) similarly enters the base of the first and second upper incisors instead of being directed into the canine, suggesting that the path of this canal may be less restricted in marsupials.

Entry point is within the rostrally facing wall of the orbit, near the ventral junction with the lacrimal which is approximately at the level of M2.

Number of maxillary foramina is 1, which is located on the lateral surface of the maxilla at the level of P3. This is the IOF that terminates the infraorbital canal. The

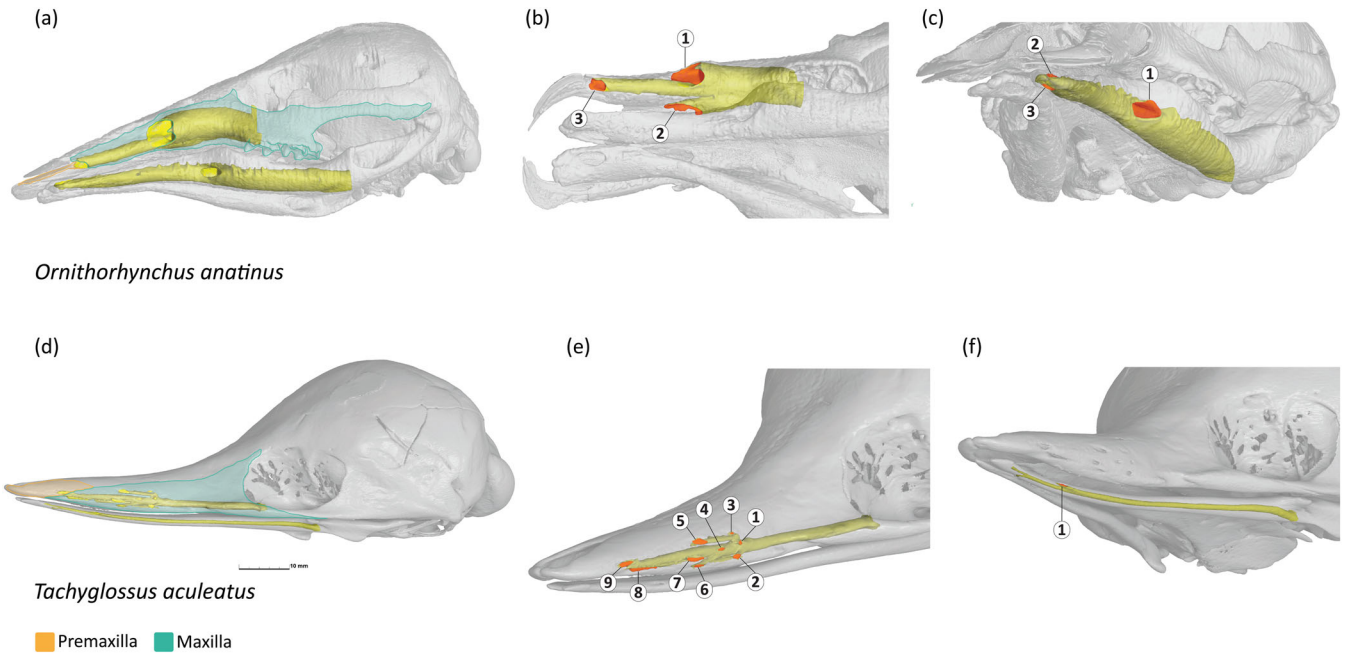

FIGURE 8 Monotremes with maxillary and mandibular canals of the left side segmented in yellow. Foramina in red are numbered in an approximately caudal to rostral sequence. Relevant bones are identified and color-coded for each species in the whole skull view on the left. The semiaquatic and electroreceptive *Ornithorhynchus anatinus* (AMNH:Mammals:M-201312) is shown in (a) lateral view with no scale bar available, (b) maxillary canal in ventrolateral oblique view, and (c) mandibular canal in rostroventral view. The terrestrial and electroreceptive *Tachyglossus aculeatus* (YPM MAM 014872) is shown in (d) lateral view, (e) maxillary canal in rostrolateral view, and (f) mandibular canal in ventrolateral view.

foramen is laterally compressed and opens out rostrally (Figure 9c).

Mandibular canal travels anteriorly through the dentary close to the ventral margin due to the presence of large roots of the premolar and molar teeth (Figure 9b). The ramifications leading to foramina are short. The canal extends to the rostral tip of the lower jaw, fading away inside the dentary near i1.

Entry point is on the medial surface of the dentary, caudal to the lower toothrow and approximately at the level of the midpoint of the coronoid process.

Number of mandibular foramina is *2* and they are found on the lateral surface of the dentary. Foramen 1 is positioned below m3 and opens out laterally. Foramen 2 is positioned below p1 and opens out rostrally (Figure 9d). Both represent mental foramina.

3.4.5 | *Dasyurus hallucatus*

Maxillary canal consists of three main branches. The infraorbital canal is wide, linear, and relatively short. Emerging medially from the infraorbital canal are two slender branches with small, irregular ramifications (Figure 9e). One branch supplies the region at the base of the upper premolars. The second branch is likely the rostral alveolar canal and it extends to the rostral tip of the upper jaw to supply the incisors as well as the surface of the premaxilla.

Entry point of the canal is located on the rostroventral wall of the orbit, near the junction with the lacrimal and jugal.

Number of maxillary foramina is 2. Foramen 1 terminates the infraorbital canal. This single large opening is the IOF and is positioned on the lateral surface of the maxilla at the level of M1 and opens out rostrally. Foramen 2 is a small opening on the dorsal surface of the premaxilla that terminates a branch of the rostral alveolar canal and opens out laterally (Figure 9f).

Mandibular canal is extensive, filling up much of the internal space of the dentary as it follows the ventral margin of the dentary rostrally to the level of the first premolar. There are also several prominent dorsally projecting branches entering into the base of the premolar and molar teeth (Figure 9e).

Entry point is on the medial surface of the dentary, near the ventral margin at approximately the level of the midpoint of the coronoid process.

Number of mandibular foramina is 3 and they are all located on the lateral surface of the mandible. Foramen 1 is positioned beneath m1 and opens out rostrolaterally. Foramen 2 is positioned beneath p1/p2 and opens out

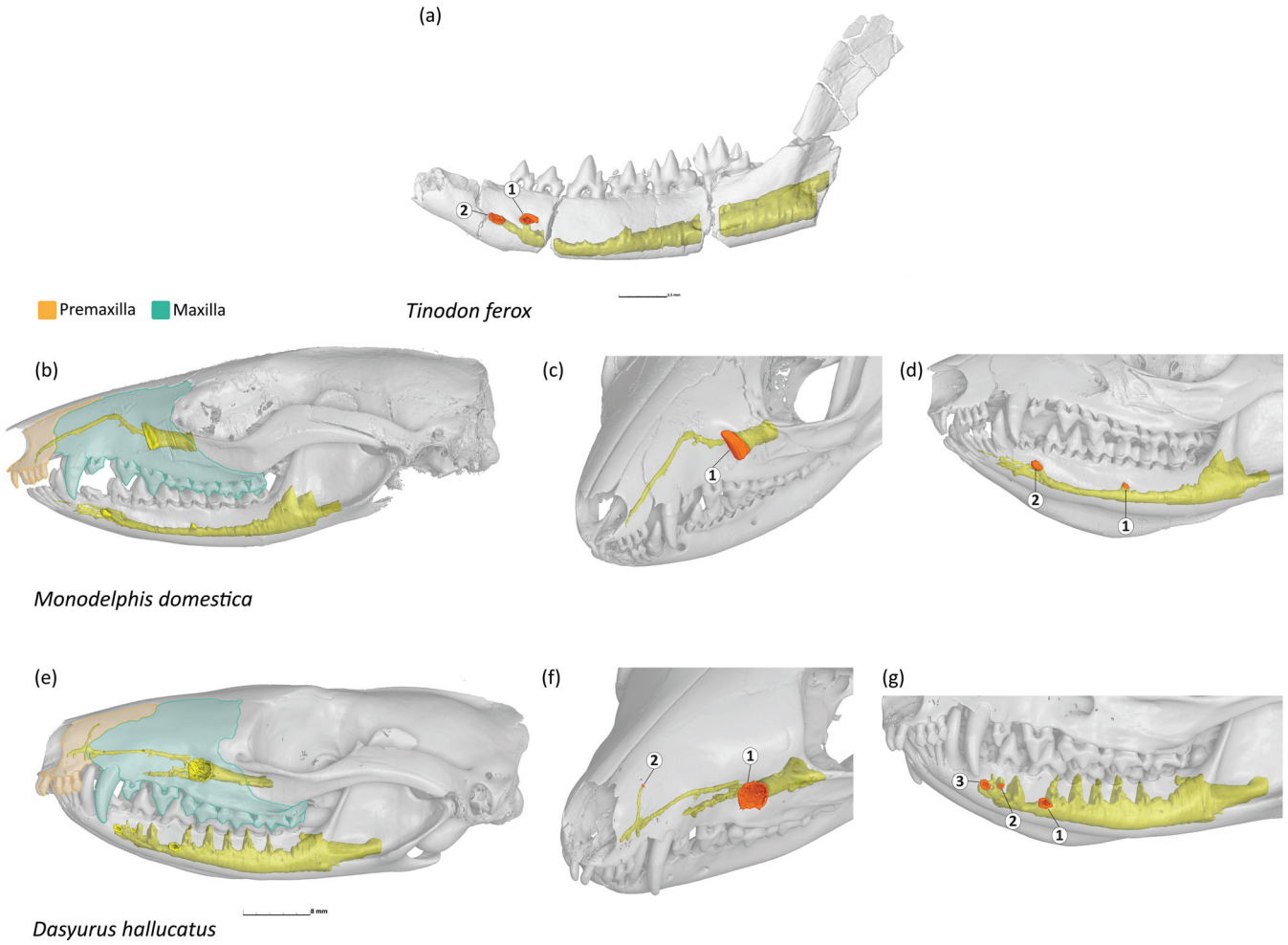

FIGURE 9 Stem therian and metatherians (marsupials). Maxillary and mandibular canals of the left side segmented in yellow. Foramina in red are numbered in an approximately caudal to rostral sequence. Relevant bones are identified and color-coded for each species in the whole skull view on the left. The Late Jurassic symmetrodont *Tinodon ferox* (YPM VP 000606) is mirrored to show (a) the mandibular canal in lateral view of the dentary only. The didelphid marsupial *Monodelphis domestica* (no catalogue number) is shown in (b) lateral view with relevant bones identified and color-coded, no scale bar available, (c) maxillary canal in dorsorostral oblique view, and (d) mandibular canal in ventrorostral oblique view. The dasyurid marsupial *Dasyurus hallucatus* (TMM M-5921) is shown in (e) lateral view with relevant bones identified and color-coded, (f) maxillary canal in dorsorostral oblique view, and (g) mandibular canal in ventrolateral oblique view.

laterally. Foramen 3 is positioned beneath p1 and opens out rostrally (Figure 9g). All three openings can be regarded as mental foramina.

3.4.6 | *Elephantulus rupestris*

Maxillary canal consists of two branches, the short infraorbital canal and the long, slender rostral alveolar canal that extends to the rostral tip of the maxilla at the junction with the premaxilla at the level of I3/C (Figure 10a).

Entry point is located on the rostroventral aspect of the orbital wall, ventral to the smaller lacrimal foramen.

Number of maxillary foramina is 1 which is positioned just rostral to the orbit, approximately above P4. This is the large, rostrally oriented IOF (Figure 10b).

Mandibular canal follows the curvature of the jaw anteriorly along its ventral margin to the rostral tip near the midline mandibular symphysis, where the canal fades into the dentary bone near i3. There are several excursions of the canal into the alveolar space for sending nerves and blood vessels to the tooth roots. The branches are very short (Figure 10a).

Entry point is on the medial surface and near the ventral margin of the dentary, positioned approximately at the level between the coronoid and articular processes.

Number of mandibular foramina is 3 and these mental foramina are positioned on the lateral surface of the dentary. Foramen 1 is located between p4 and m1 and opens out ventrolaterally. Foramen 2 is located beneath p2 and opens out laterally. Foramen 3 is the largest of the three foramina, is located between the canine and p1, and opens out rostrolaterally (Figure 10c).

3.4.7 | *Myrmecophagus tridactyla*

Maxillary canal consists of three parts, the infraorbital canal, a dorsally directed cluster of net-like branches, and a medially directed cluster of net-like branches. None of these components extend very far rostrally despite the highly elongated maxilla and terminate at approximately the same level about one-quarter down the length of the snout (Figure 10d).

Entry point is located on the ventral surface of the cranium, at the base of the zygomatic arch near the junction with the jugal.

Number of maxillary foramina is 1 which is located on the ventrolateral surface of the maxilla. The opening is elongated and opens out ventrorostrally (Figure 10e). There appear to be two other foramina on the lateral surface of the maxilla, positioned approximately halfway down the length of the rostrum; however, we were unable to detect any continuity of these openings with the maxillary canal.

Mandibular canal is linear and extends through the dentary to near the rostral end. However, there are several dorsal projections of the canal reaching into the alveolar space (Figure 10f). These projections, or "dorsal canaliculi," have been identified as retained neurovascular pathways that ancestrally innervated the teeth, despite tooth loss in anteaters (Ferreira-Cardoso et al., 2019).

Entry point is on the medial surface of the dentary, approximately at the level of the low protuberance of the coronoid process.

Number of mandibular foramina is 2 and they are on the lateral surface of the dentary near the rostral tip. Foramina 1 opens out laterally. Foramina 2 is larger, elongated in shape, and opens out laterally (Figure 10f). Both represent mental foramina.

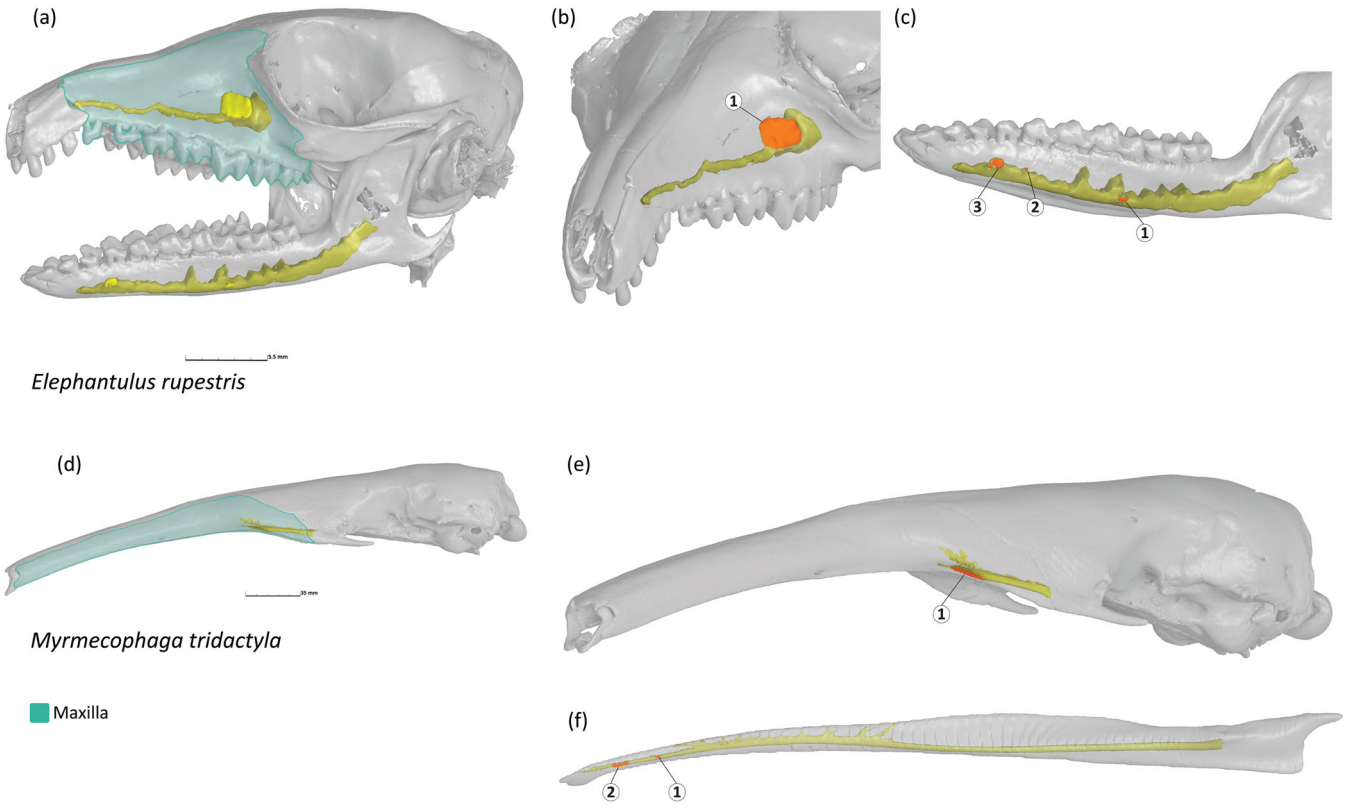

FIGURE 10 Afrothere and xenarthran with maxillary and mandibular canals of the left side segmented in yellow. Foramina in red are numbered in an approximately caudal to rostral sequence. Relevant bones are identified and color-coded for each species in the whole skull view on the left. The afrothere *Elephantulus rupestris* (CAS MAM 30373) is shown in (a) lateral view, (b) maxillary canal in dorsorostral oblique view, and (c) mandibular canal in lateral oblique view. The edentulous xenarthran *Myrmecophaga tridactyla* (AMNH:Mammals:M-133489) shown in (d) lateral view, (e) maxillary canal in lateral oblique view, and (f) mandibular canal in lateral view.

3.4.8 | *Mus musculus*

Maxillary canal consists only of the infraorbital canal, which is very short in length and terminates at the base of the zygomatic arch. No other branches were observed (Figure 11a).

Entry point is a large opening on the rostral-facing aspect of the orbital wall, at approximately the level of M1.

Number of maxillary foramina is 1. This enlarged, keyhole-shaped opening is the IOF and it opens out rostrally (Figure 11b). Examination of the soft tissues in this scan show that the infraorbital nerve tract of the maxillary branch of the trigeminal nerve and accompanying blood vessels occupy the ventral portion of the foramen, which is flattened by the lateral wall of the zygomatic plate. The infraorbital zygomaticomandibularis muscle, also variously named as different divisions of the masseter muscle (Druzinsky et al., 2011), is a jaw adductor that passes through the more rounded dorsal portion of the foramen in typical configuration for myomorphic rodents such as *Mus* (Baverstock et al., 2013; Ginot et al., 2018).

Mandibular canal is slender and travels anteriorly through the dentary by curving around the posteriorly extended root of the lower incisor, passing between this tooth root ventrally and the molar tooth roots dorsally, and terminating just at the base of m1 (Figure 11a).

Entry point is on the medial surface of the dentary, close to the apex of the incisor root and at the level of the articular process.

Number of mandibular foramina is 2 and they are located close together on the dorsolateral surface of the diastema (Figure 11c). They both open out rostrolaterally and represent mental foramina.

3.4.9 | *Octodon degus*

Maxillary canal consists of a short infraorbital canal that terminates at the base of the zygomatic arch. The canal is very wide and circular in shape (Figure 11d).

Entry point is on the rostral-facing aspect of the orbital wall. However, the large size of the opening has overwhelmed and reduced the bony component of the orbital wall.

Number of maxillary foramina is 1. This extremely enlarged, circular opening is the IOF and is oriented rostrally (Figure 11e). As in *Mus*, the infraorbital zygomaticomandibularis muscle passes through the infraorbital canal. In hystricomorph rodents like *Octodon*, this muscle is larger and inserts far more rostrally on the lateral side of the rostrum compared to myomorph and sciuromorph rodent groups (Cox & Jeffery, 2011).

Mandibular canal presents as a complex lattice of passages navigating around the massive tooth roots of the molars and the incisor that dominate the interior space of the mandible. The canal fades out within the space of the diastema, just caudal to the alveolar rim of the lower incisor (Figure 11d).

Entry point is on the medial surface of the dentary, near the dorsal margin between the coronoid and articular processes.

Number of mandibular foramina is 2. However, this is difficult to determine since these mental foramina are extremely small. Foramina 1 is located just rostral of the masseteric fossa at the level of m2 and opens out laterally. Foramina 2 is located on the ventral surface at the level of m1 and opens out ventrally (Figure 11f).

3.4.10 | *Pteropus scapulatus*

Maxillary canal consists of the short, linear infraorbital canal that extends rostrally to the base of the zygomatic arch and ventral margin of the orbit.

Entry point is on the ventrorostral aspect of the orbital wall.

Number of maxillary foramina is 1 and is found on the lateral surface of the maxilla (Figure 12b). This large, rostrally oriented opening is the IOF.

Mandibular canal is mostly linear, extending along the ventral margin of the dentary and terminating at the midline symphysis. There are multiple projections ascending into the alveolar space of the lower tooth roots (Figure 12c).

Entry point is on the medial surface of the dentary, positioned between the broad rounded angle of the dentary (partially broken in this specimen) and the articular process.

Number of mandibular foramina is 2. Foramen 1 is located on the lateral surface of the dentary between the level of the lower canine and p1 and opens out dorsolaterally. Foramen 2 is located on the forward-facing surface of the mandibular symphysis below i1 and opens out dorsorostrally (Figure 12c). Both openings are mental foramina.

3.4.11 | *Myotis adversus adversus*

Maxillary canal consists of the relatively short and broad infraorbital canal terminating rostral to the orbit and a medially directed lattice-like network of canals surrounding the roots of the upper toothrow that terminates at the rostral end of the maxilla.

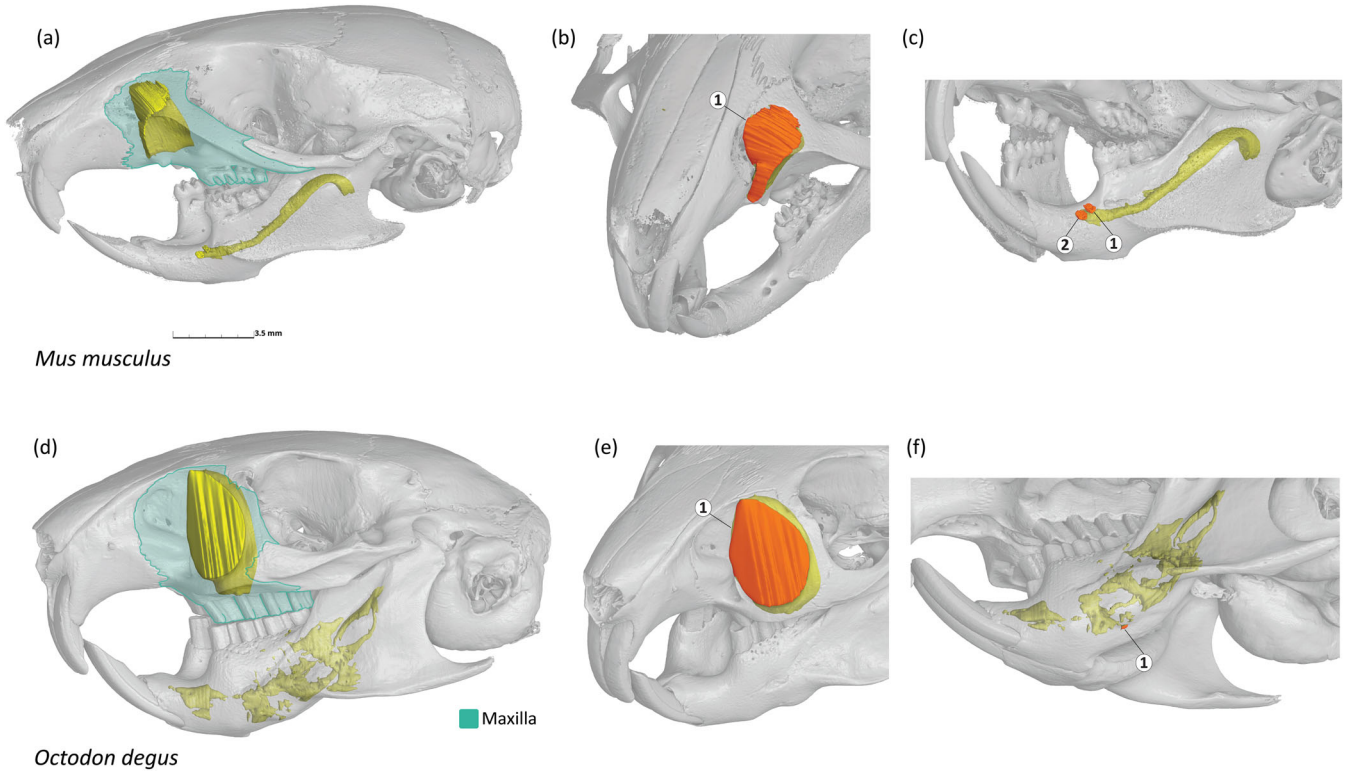

FIGURE 11 Rodents with maxillary and mandibular canals of the left side segmented in yellow. Foramina in red are numbered in an approximately caudal to rostral sequence. Relevant bones are identified and color-coded for each species in the whole skull view on the left. The myomorph *Mus musculus* (no catalogue number) is shown in (a) lateral view, (b) maxillary canal in dorsorostral oblique view, and (c) mandibular canal in rostrolateral view. The hystricomorph *Octodon degus* (IIMyC:LMFyC:0102010101) is shown in (d) lateral view with no scale bar available, (3) maxillary canal in dorsorostral oblique view, and (f) mandibular canal in ventrorostral oblique view.

Entry point is on the rostral aspect of the orbital wall, positioned at the level of M2.

Number of maxillary foramina is 3. Foramen 1 is the IOF and is a large, rostrolaterally oriented opening at the level of P3 (Figure 12e). Foramen 2 is a very small, dorsally oriented opening positioned dorsorostral of the IOF. Foramen 3 is another very small opening and is located on the rostral surface of the prominent bulge of the maxilla overlying the canine tooth root; the foramen opens out rostrally.

Mandibular canal is primarily linear, following the curvature of the dentary, and terminating at the midline symphysis. There are multiple projections ascending into the alveolar space of the lower teeth.

Entry point is a large opening on the medial surface of the ramus of the dentary, positioned between the articular and angular processes.

Number of mandibular foramina is 2 and represent mental foramina. Foramen 1 is a large opening on the lateral surface of the dentary positioned beneath the canine and opens out laterally. Foramen 2 is positioned on the forward-facing surface of the mandibular symphysis beneath i1 and opens out rostrally (Figure 12f).

3.4.12 | *Pan troglodytes*

Maxillary canal consists of a relatively short infraorbital canal that diverges into two short branches that terminate below the orbit (Figure 13a).

Entry point is on the rostral aspect of the orbital wall and is accompanied by a long trailing infraorbital sulcus that extends caudally across the floor of the orbit.

Number of maxillary foramina is 2 and they are both located on the forward-facing surface of the maxilla, approximately at the level of M1. Foramen 1 is positioned dorsal of foramen 2 and opens out dorsorostrally. Foramen 2 is the larger opening and is oriented rostrally (Figure 13b). According to Msuya and Harrison (1994) the number of infraorbital foramina in *P. troglodytes* varies from 1 to 3.

Mandibular canal is broad and follows the curvature of the dentary, extending to the root of the lower canine

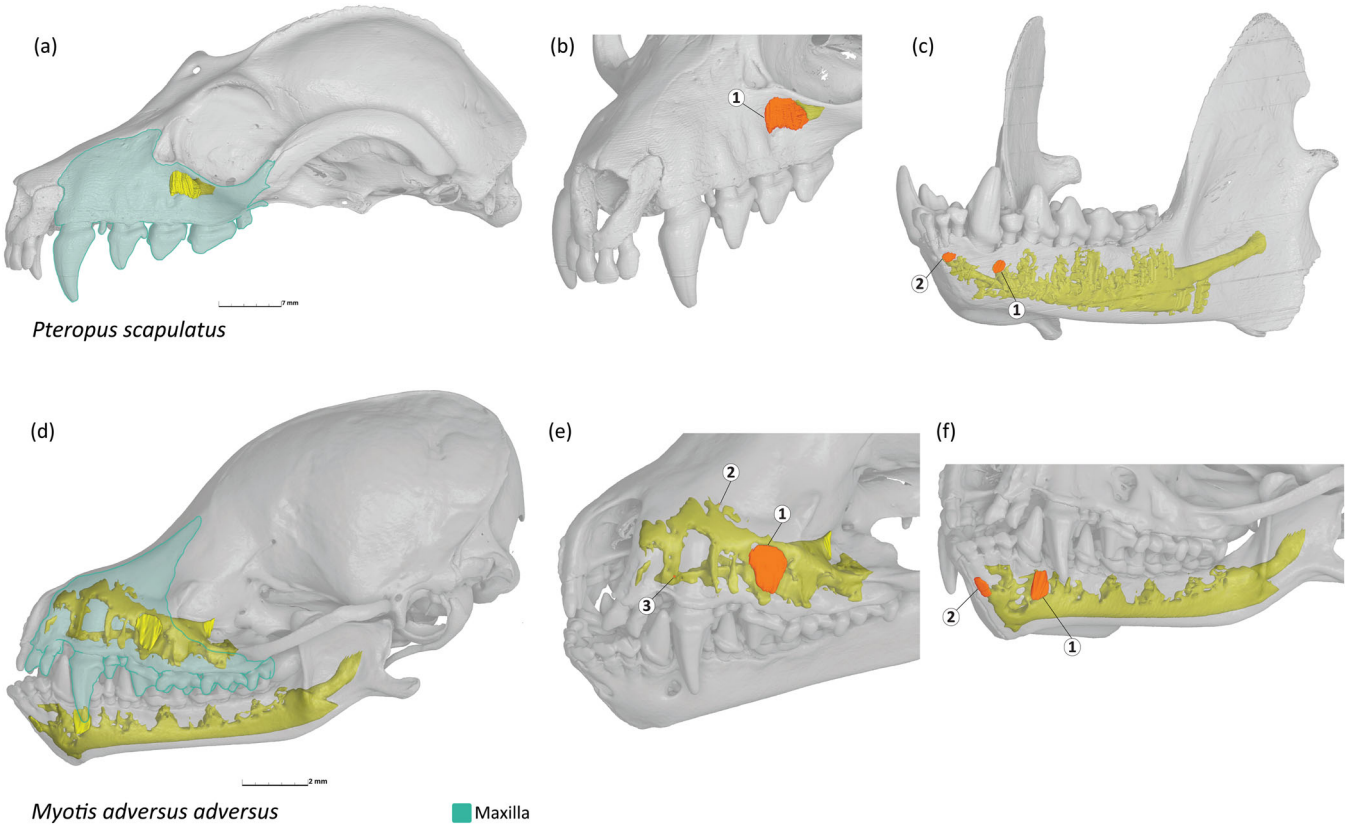

FIGURE 12 Bats with maxillary and mandibular canals of the left side segmented in yellow. Foramina in red are numbered in an approximately caudal to rostral sequence. Relevant bones are identified and color-coded for each species in the whole skull view on the left. The megabat *Pteropus scapulatus* (AMNH: Mammals: M-154582) is shown in (a) lateral view of cranium only, (b) maxillary canal in rostrolateral view, and (c) mandibular canal in rostrolateral view. The echolocating microbat *Myotis adversus adversus* (UMZC: Vertebrates: E.5766.B) is shown in (d) lateral view, (e) maxillary canal in rostrolateral view, and (f) mandibular canal in ventrorostral view.

(Figure 13a). The bone of the dentary has an extremely cancellous interior structure, which made it difficult to identify the precise path of the mandibular canal.

Entry point is on the medial surface of the dentary ramus, approximately at the level of the coronoid process.

Number of mandibular foramina is 1. This mental foramen is located on the lateral surface of the dentary beneath p1 and p2. The opening is large and oriented laterally (Figure 13c).

3.4.13 | *Tapirus terrestris*

Maxillary canal is formed by the broad but relatively short infraorbital canal and the well-developed rostral alveolar branch that continues rostrally until it terminates in short branches at the tip of the premaxilla above the incisors (Figure 14a).

Entry point is on the anterior surface within the bony orbit, located above P4 and M1.

Number of maxillary foramina is 2. Foramen 1 is the large, rostrally facing IOF which is located above P2 and P3. Foramen 2 terminates a short branch of the rostral alveolar canal as a small, rostrally facing opening positioned above I3 (Figure 14b).

Mandibular canal has a large diameter and travels rostrally, following the curve of the jaw. The inferior alveolar branch continues to the rostral end of the mandible, terminating below the incisors (Figure 14a).

Entry point is on the medial surface of the dentary, posterior to the lower toothrow.

Number of mandibular foramina is 2, which are the mental foramina. Foramen 1 is a large, rostrolaterally oriented opening positioned just rostral to p1. Foramen 2 is much smaller, dorsorostrally oriented, and positioned within the diastema between the lower canine and premolars (Figure 14c).

3.4.14 | *Phocoena phocoena*

Maxillary canal forms a complex structure due to the telescoping of the anterior skull bones. The infraorbital canal is short, broad, and gives rise to four short

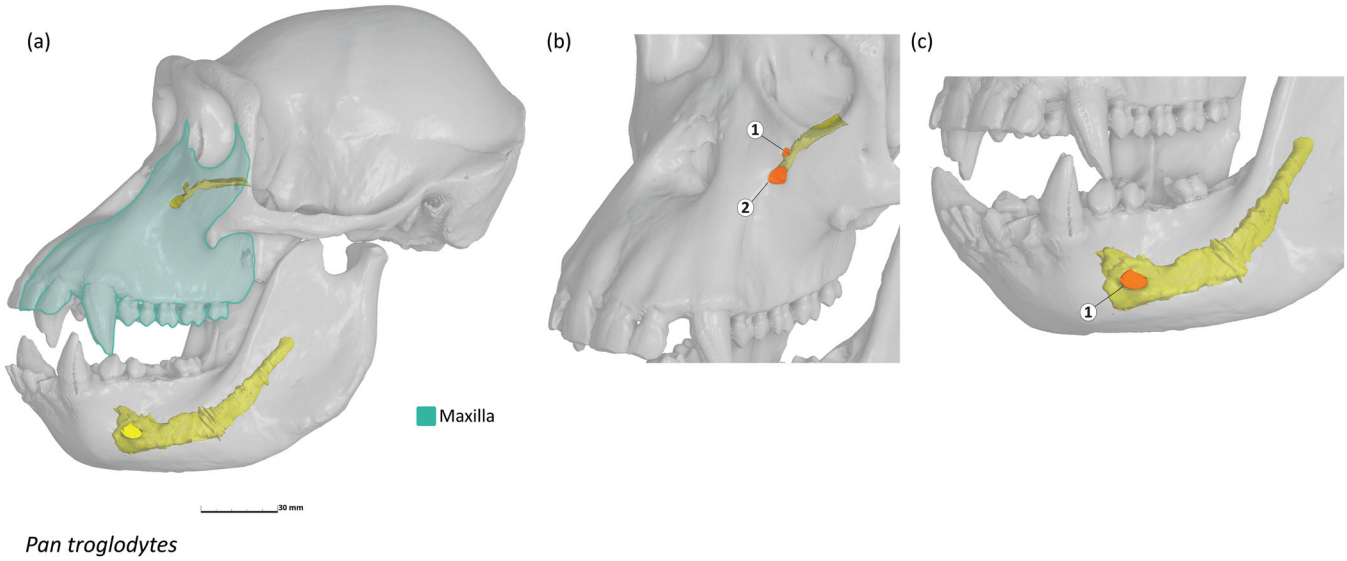

FIGURE 13 *Pan troglodytes* (AMNH: Mammals: M-167342) with maxillary and mandibular canals of the left side segmented in yellow. Foramina in red are numbered in an approximately caudal to rostral sequence. The skull is shown in (a) lateral view with the maxilla identified and color-coded, (b) maxillary canal in rostrolateral view, and (c) mandibular canal in lateral oblique view.

canals: four longer ones that run posteriorly, two longer and thin ones running medially inside the maxilla, and three long canals representing the rostral alveolar branches. One of the latter provides innervation for the posterior half of the toothrow, whereas two run inside the maxilla to the anterior teeth, one of which exits at the tip of the rostrum (Figure 15a).

Entry point consists of two foramina in the anterior wall of the orbit, far behind the toothrow.

Number of maxillary foramina is 8. Foramen 1–3 belong to the posteriorly oriented canals and are situated dorsal to the orbit. The largest one, foramen 1, may be identified as the dorsal IOF. Foramen 2 is oriented laterally, foramen 3 is very small and located anteromedially to 1 and 2. Anterior to this group, foramina 4 to 7 are arranged in an oblique row from posterolateral to anteromedial; foramina 4 to 6 are facing anteriorly. Foramen 7 is anteroposteriorly elongated and large; it is located in the nasal process of the premaxilla and can be identified as the premaxillary foramen although belonging to the infraorbital complex in odontocetes. Foramen 8 is the exit of the anteriormost alveolar branch, located at the rostral tip of the maxilla and premaxilla (Figure 15b).

Mandibular canal is a large structure that continues from the broad mandibular fossa on the medial surface of the dentary. The posterior portion of the canal behind the toothrow almost completely fills the lower jaw but tapers anteriorly, where short and thin branches lead to the external foramina (Figure 15c). Alveolar branches are not clearly visible, which might be due to the resolution of the scan. However, the proximal part of the inferior alveolar canal can be identified.

Entry point is the significantly enlarged mandibular foramen on the medial side of the dentary, posterior to the lower toothrow.

Number of mandibular foramina is 3. These mental foramina are in the anterior quarter of the lower jaw, while the anteriormost one reaches almost to the rostal tip of the dentary (Figure 15c).

The enlarged mandibular foramen and posterior portion of the mandibular canal also houses the mandibular fat body, which likely aids in conducting sound waves to the middle ear (Rauschmann et al., 2006; Sysueva & Popov, 2023).

3.4.15 | *Odobenus rosmarus*

Maxillary canal is short and great in diameter. At the anterior border of the IOF, the canal branches off into multiple smaller ramifications that run dorsally and anteriorly to the root of the upper canine (Figure 15d).

Entry point is a large foramen in the anteroventral wall of the orbit.

Number of maxillary foramina is 1. This enlarged IOF is oval in shape and located just posterior of the laterally projecting upper canine alveole (Figure 15e). This foramen opens out rostrolaterally.

Mandibular canal is thin, linear, and terminates as the inferior alveolar canal at the symphysis

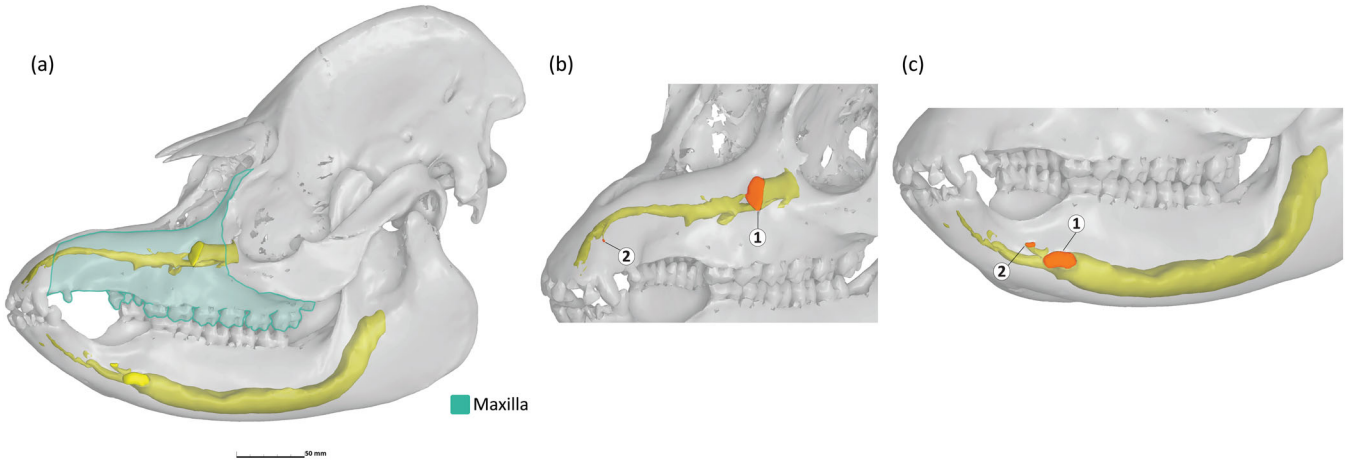

FIGURE 14 *Tapirus terrestris* (TMM-M16) with maxillary and mandibular canals of the left side segmented in yellow. Foramina in red are numbered in an approximately caudal to rostral sequence. The skull is shown in (a) lateral view with the maxilla identified and color-coded, (b) maxillary canal in rostrolateral view, and (c) mandibular canal in ventrorostral view.

(Figure 15d). At the large mental foramen, the canal shows a sigmoid bend. Multiple projections ascend into the alveolar space of the lower teeth, especially anterior to the mental foramen.

Entry point is the mandibular foramen which is located on the medial surface of the dentary at the level of the zygomatic postorbital process and thus far posterior to the cheek teeth.

Number of mandibular foramina is 6. Foramina 1 and 2 (which are very tiny) are located on the level of p2 in this individual, though the dental formula in this species shows high variation (Fay, 1985). Foramen 3, located on the level between c and p1, is by far the largest mandibular foramen and can be regarded as a mental foramen. In lateral view, it is hidden by the ventrally projecting enlarged upper canine. Three more foramina are visible on the anterior tip of the dentary. Foramen 4 opens anterodorsally on the anterior prominence of the dentary, foramen 5 is situated ventrally of the latter facing anteriorly, and foramen 6 opens medially on the medial surface of the prominence (Figure 15f).

3.4.16 | *Felis catus*

Maxillary canal is short and has the shape of a double-sided pestle, that is, both openings have a greater diameter than the middle section (Figure 16a). No further branches are detectable in the scan.

Entry point is a round foramen in the anteroventral wall of the orbit.

Number of maxillary foramina is 1. The IOF is triangular in cross-section and is located dorsally to P3 and facing anteriorly (Figure 16b).

Mandibular canal is an almost straight canal, running to the anterior tip of the dentary and giving off several smaller branches projecting dorsally toward the base of the teeth throughout the length of the lower toothrow (Figure 16a). The canal for the inferior alveolar nerve becomes greater in diameter and shows a complex web of small canals, especially below the lower incisors and canine. Posterior to the toothrow, the mandibular canal splits laterally into the primary canal that connects with the mandibular foramen and a larger diameter branch that runs parallel to the mandibular canal, but fades inside the bone without any outlet.

Entry point is the mandibular foramen located on the medial surface of the dentary at the level of the coronoid process and, thus, far posterior to the lower toothrow.

Number of mandibular foramina is 2, which both can be regarded as mental foramina. The small foramen 1 is on the level of p3. The much larger second foramen is on the level of the diastema between the lower canine and p3 (Figure 16c). Both foramina open out laterally.

3.4.17 | *Scalopus aquaticus*

Maxillary canal consists of a short infraorbital canal as well as the canal for the rostral alveolar nerve which continues anteriorly through the maxilla as a complex web-like structure surrounding the base of the upper teeth. The cheek teeth that are situated ventrally and posteriorly of the IOF are provided separate short canals (Figure 17a).

Entry point is the large foramen in the maxillary root of the zygomatic arch, and thus in the anteroventral wall of the orbit.

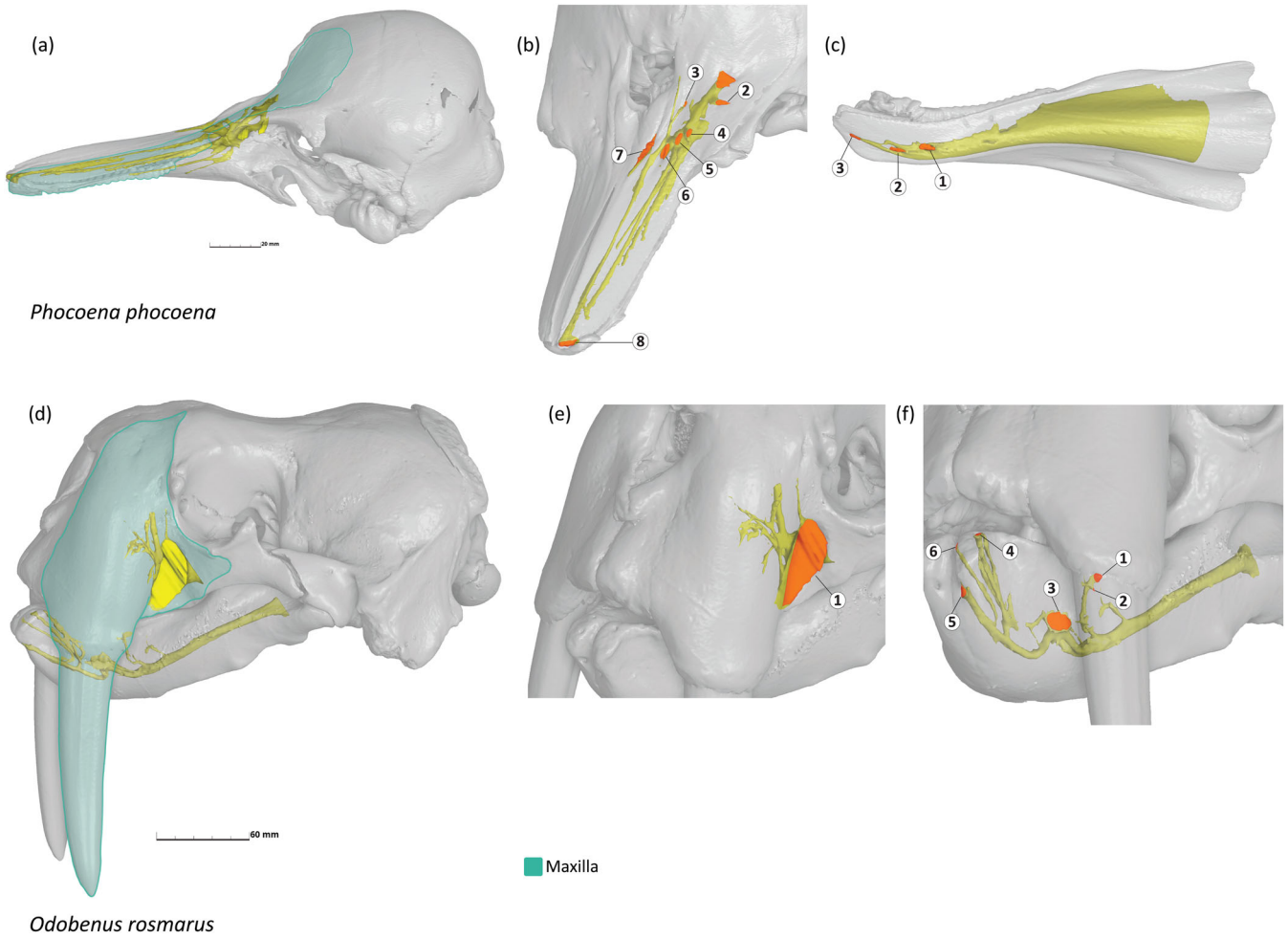

FIGURE 15 Marine mammals with maxillary and mandibular canals of the left side segmented in yellow. Foramina in red are numbered in an approximately caudal to rostral sequence. Relevant bones are identified and color-coded for each species in the whole skull view on the left. The echolocating cetacean *Phocoena phocoena* (MVZ: Mammal specimens: 172141) is shown in (a) lateral view of cranium only, (b) maxillary canals in dorsal oblique view, and (c) mandibular canal in ventrolateral view. *Odobenus rosmarus* (MVZ: Mammal specimens: 125566) is shown in (d) lateral view, (b) maxillary canals in dorsolateral oblique view, and (c) mandibular canals in rostrolateral view.

Number of maxillary foramina is 3. Foramen 1 is the large and horizontally elongated IOF that faces out laterally. Foramen 2 is located dorsally to 1 and forms a small, round, and dorsolaterally facing opening just anterior to the orbit. The third foramen is tiny and situated ventrally to the anterior portion of foramen 1, above M1 (Figure 17b).

Mandibular canal is a thin canal that follows the ventrally convex curvature of the dentary. Several small branches run to the teeth of the lower toothrow and the mandibular canal terminates anteriorly at the lower incisors (Figure 17a).

Entry point is the mandibular foramen situated in the center of the ramus of the dentary.

Number of mandibular foramina is 2. Foramen 1 is tiny, located on the level of the anterior root of m1, and opens out ventrolaterally. The larger and horizontally oval foramen 2, which can be confidently identified as a mental foramen, is situated ventrally to p2 and is oriented rostrolaterally (Figure 17c).

4 | DISCUSSION

The goal of this study is to test some of the assumptions that are made when interpreting the facial tactile sensory biology of extinct animals based on osteological correlates. In our examination of the maxillary and mandibular canals of 29 extant and 9 extinct species across major tetrapod groups, we found remarkable diversity in the morphology of these structures based on gross observations of the extent the canals travel

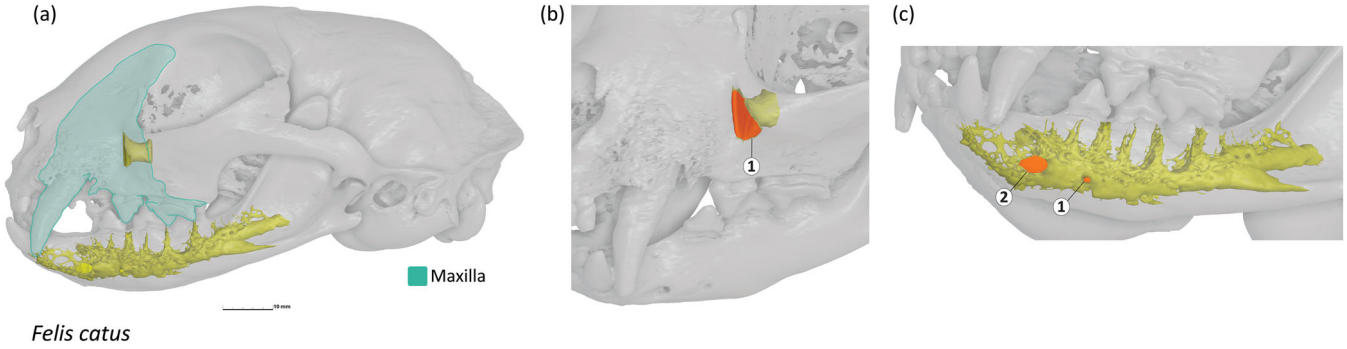

FIGURE 16 *Felis catus* (CET-018) with maxillary and mandibular canals of the left side segmented in yellow. Foramina in red are numbered in an approximately caudal to rostral sequence. The skull is shown in (a) lateral view 2with the maxilla identified and color-coded, (b) maxillary canal in dorsorostral view, and (c) mandibular canal in ventrolateral oblique view.

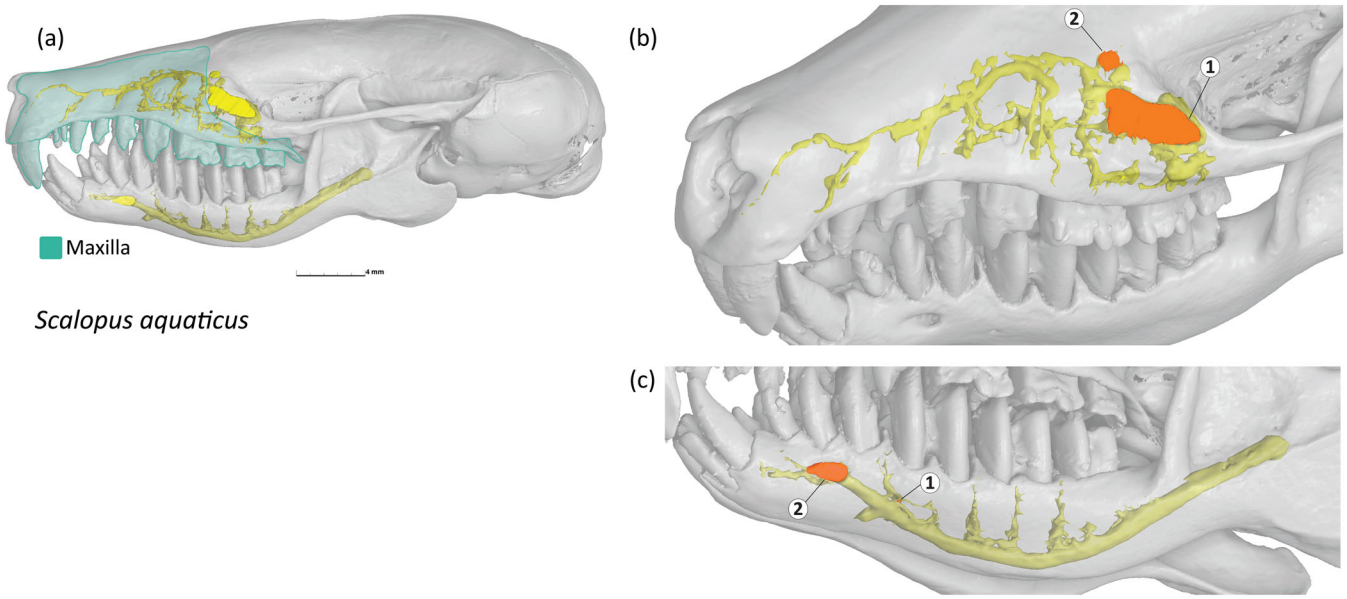

FIGURE 17 *Scalopus aquaticus* (CET-031) with maxillary and mandibular canals of the left side segmented in yellow. Foramina in red are numbered in an approximately caudal to rostral sequence. The skull is shown in (a) lateral view with the maxilla identified and color coded, (b) maxillary canal in lateral oblique view, and (c) mandibular canal in ventrolateral view.

through the length of the bones of the upper and lower jaws, canal branching patterns, the number of foramina representing points where nerve branches of V_2 and V_3 exit the bone, and the distribution of these foramina. The variety of configurations reflect not only phylogeny, but also likely adaptations to ontogenetic changes, different ecologies, and the development of specialized sensory systems (Figure 18). In the following sections, we discuss patterns in the diversity of maxillary and mandibular canal morphology for each major tetrapod group, explore how the evolution of novel sensory organs may impact canal morphology, test how our proposed form-function relationships can be applied to the case of extinct nonmammalian synapsids and extant mammals, and then venture into some of the caveats of using trigeminal canal morphology as an osteological correlate.

4.1 | Comparative sampling shows that each major tetrapod group has features that distinguish their maxillary and mandibular canal morphology

4.1.1 | Amphibians

A notable characteristic of this group is whether the maxillary or mandibular canals are present in the bones of the

jaws and if these canals actually serve as neurovascular passageways. Only in the extinct Lower Triassic temnospondyl *Lydekkerina* (Figure 1a) and extant giant salamander *Cryptobranchus* (Figure 1d), did we observe well-developed maxillary and mandibular canals that communicate with the overlying integument via foramina. We found *Ambystoma* (Figure 1g) lacks a maxillary canal completely. *Lithobates* (Figure 1i) has a maxillary canal, but it is uncertain how much, if any, of this space housed nerves. The mandibular canal in *Lithobates* is likewise clearly present, but

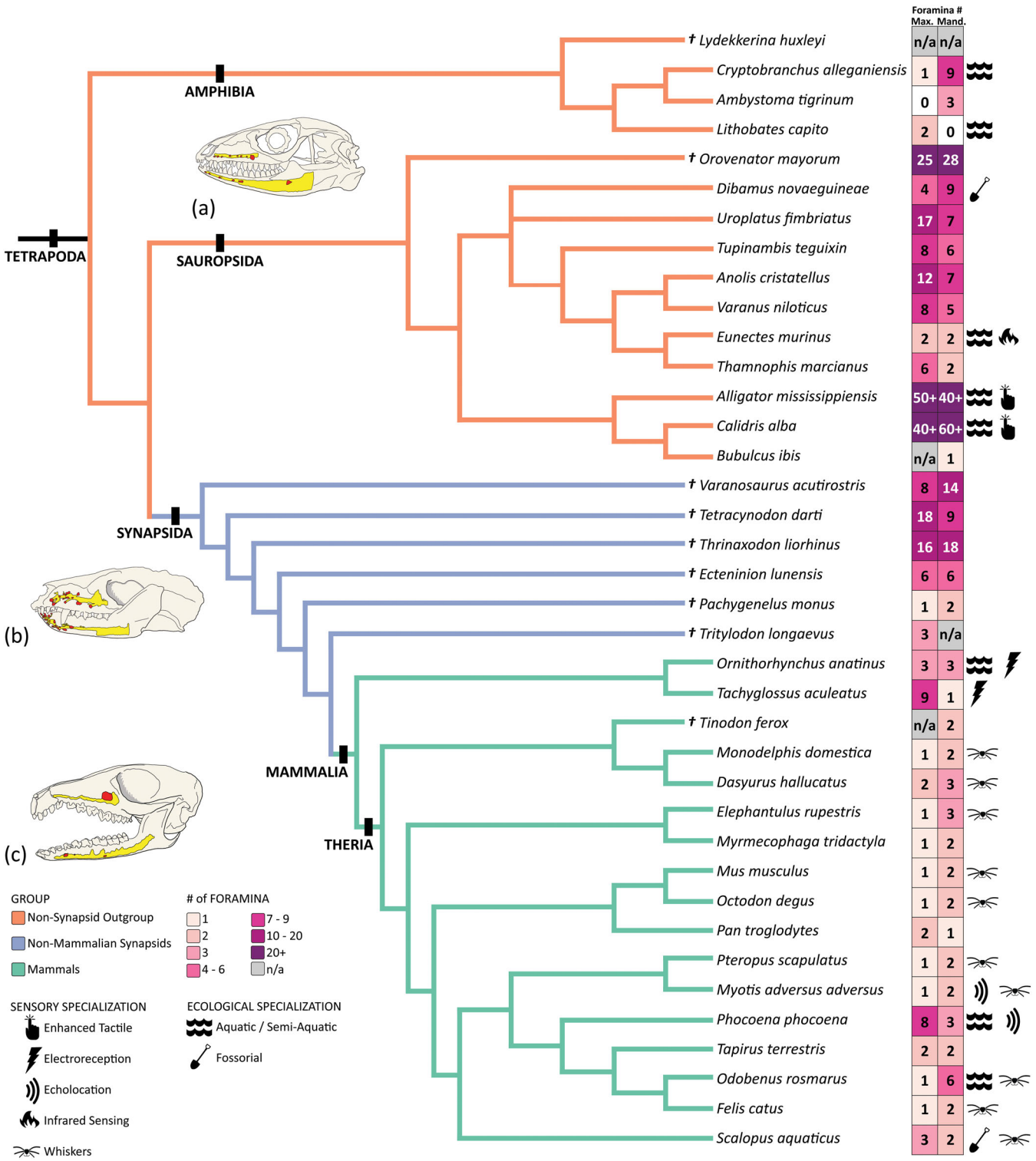

FIGURE 18 Legend on next page.

the absence of any foramina for the entrance or egress of neurovascular tracts suggests that the interior is solely occupied by Meckel's cartilage, which persists in many adult amphibians (Francis, 1934; McGregor, 1896; Rose, 2014). In *Cryptobranchus* and *Ambystoma*, the mandibular canal houses both Meckel's cartilage and a separate neurovascular passageway for branches of V_3 (we elected to only visualize the latter). The canal space was less separated in *Lydekkerina*, but we expect a similar arrangement. In addition, both *Cryptobranchus* and *Lydekkerina* possess prominent, dorsal-facing openings at the caudal end of the lower jaw that are contiguous with the mandibular canal. Dissection studies on giant salamanders show that this space is filled with a pad of articular cartilage that serves as the contact point for the jaw joint (Matsumoto et al., 2024) and that this cartilage is the exposed posterior portion of Meckel's cartilage (Francis, 1934; McGregor, 1896).

Instead of passing through the bones of the jaw, branches of V_2 and V_3 frequently travel through soft tissues in amphibians (Coghill, 1902; Ecker, 1889; Naumann & Olsson, 2018). In *Ambystoma*, branches of V_2 remain in the integument to ramify and innervate regions around the eye and upper lip (Coghill, 1902). Similarly, anatomical studies of *Lithobates pipiens* (Wyman, 1853), *Xenopus laevis* (Paterson, 1939), and *Lepidobatrachus llanensis* (Quinzio & Fabrezi, 2019) describe branches of V_3 traveling along the surface of the lower jaw, following the ventral edge. Wyman (1853) describes the nerves then terminating in the soft tissues near the midline symphysis in a "brush" shape.

The pathway of the maxillary and mandibular trigeminal nerve branches through soft tissues instead of bony canals may be related to the dramatic remodeling of the jaws and associated structures during ontogeny in lissamphibians, especially the metamorphosis from tadpole larvae to the adult form. The process of change characterized in both metamorphic and direct developing frogs includes shifting of the jaw articulation posteriorly, which forces the mandibular levator muscle complex to rotate. The V_2 and V_3 branches change course to follow these muscles, shifting from a horizontal to vertical orientation (Quinzio & Fabrezi, 2019; Schlosser & Roth, 1997a, 1997b). There is also elongation of the lower jaw that is accompanied by elongation of V_3 (Schlosser & Roth, 1997b). Instead of committing the path of the trigeminal nerves to canals within the bones of the jaws, the flexibility of the nerves to change course within the soft tissues may have been part of a suite of adaptations associated with amphibian metamorphosis. In comparison, *Lydekkerina* is projected to have experienced only minor morphological changes based on an ontogenetic study of temnospondyls (Schoch & Witzmann, 2024) and *Cryptobranchus* has been described as an obligate paedomorph that never undergoes metamorphosis (Naylor, 1981; Whiteman, 1994), which may account for their comparatively plesiomorphic morphologies among amphibians.

4.1.2 | Sauropsids

The maxillary and mandibular canals are generally long, extending anteroposteriorly through the length of the upper and lower jaws. Short branches diverge from the canals, usually as orthogonally directed offshoots at approximately regular intervals, resulting in a row of labial or nutrient foramina positioned near the toothrows. Examples of this simple configuration can be seen in both the maxillary and mandibular canals of *Dibamus* (Figure 3d), *Tupinambis* (Figure 3g), and *Varanus* (Figure 3m) as well as just the mandibular canals of *Uroplatus* (Figure 3c) and *Anolis* (Figure 3l).

In some of our sampled species, the single row of labial foramina is accompanied by additional foramina. In *Anolis* (Figure 3k), the maxillary canal widens dorsoventrally and more ramifications emerge from this region, resulting in a

FIGURE 18 Phylogeny consisting of the species sampled in this study with branches color-coded for the non-synapsid outgroup in orange, nonmammalian synapsids in purple, and Mammalia in green. Cartoon skulls on the left depict the maxilla and mandibular canals in yellow and associated foramina in red, and demonstrate key features of the (a) outgroup state with its long canals and several short branches terminating in labial foramina, (b) branched transitional state with its long canals and numerous ramifications terminating in rostral concentrations of foramina, and (c) simplified derived state with its reduced number of ramifications and shortening of the branch of the maxillary canal that bears the nerve that supplies the facial integument. The grid to the right of the phylogeny reports the color-coded number of foramina associated with the maxillary and mandibular canals. The icons represent any notable sensory specializations or ecologies within extant taxa. Legend key is at the bottom left of the figure. Tree topology is compiled from Benoit et al. (2020), Kumar et al. (2022), Ruta et al. (2013), and Schoch (2013). Within the synapsid clade, there is a crownward trend toward reducing the ramification of the maxillary and mandibular canals as indicated by the decreasing number of associated foramina, especially in the maxillary canal which is simplified into a rostral alveolar branch that remains internal to supply the upper teeth and a short infraorbital canal that typically terminates in a single infraorbital foramen. Among extant taxa with known sensory capabilities and ecologies, a higher number of foramina are often correlated with enhanced tactile ability or novel sensory organs that appear to compensate for vision-limited situations such as aquatic environments. One notable exception is among mammals that have developed and retained touch-sensitive mystacial vibrissae, which is innervated by the infraorbital nerve that exits via a single infraorbital foramen.

secondary row of foramina dorsal to the labial foramina. A similar doubling of the labial row can also be observed in the rostral end of the mandibular canal of the Early Permian diapsid *Orovenator* (Figure 2c). The maxillary canals of *Orovenator* (Figure 2b; also described in Benoit et al., 2021) and extant gecko *Uroplatus* (Figure 3b) widens rostrally into a conical-shaped expansion that sends out branches resulting in an irregular scatter of foramina over the dorsoventral height of the maxilla. Similar conical expansions have been reported in the basal archosauromorph *Prolacerta* (Bouabdellah et al., 2022) and the temnospondyl *Lydekkerina huxleyi* (Sibiya, 2021); however, it is not entirely clear what this structure signifies.

It is plausible that the distribution of maxillary and mandibular foramina reflects the distribution of microscopic cutaneous mechanoreceptors that protrude through the cornified skin. On the head, these mechanoreceptors are concentrated on the labial scales of the upper and lower jaw (Ananjeva et al., 1991; Crowe-Riddell & Lillywhite, 2023; Matveyeva & Ananjeva, 1995; Riedel & Schwarzkopf, 2022), in the regions generally coincident with the occurrence of foramina. The density of cutaneous mechanoreceptors does vary across different squamate groups, with iguanids and gekkonid lizards recorded as having 5–7 times the number of receptors as agamids (Ananjeva et al., 1991; Matveyeva & Ananjeva, 1995), which accords with observations of double rowed or scattered maxillary foramina in geckos and some members of Iguanidae (Miyamae, 2022). In addition, the density and morphology of cutaneous mechanoreceptors reflects changes in ecology, which will be discussed in the section below in terms of enhanced tactile sensing.

Snakes deviate from the maxillary and mandibular canal morphology described for the sauropsids above, primarily in greatly reducing the number of maxillary and mandibular foramina. Both canals still traverse the anteroposterior length of the maxilla and lower jawbones. The morphology of the maxillary canals are discussed in greater detail in the section below in terms of infrared sensing.

The canal morphology found in our sample of extant archosaurs—*Alligator*, *Bubulcus*, and *Calidris*—also deviate significantly from the general characteristics that distinguish other sauropsid maxillary and mandibular canals. *Alligator* retains the long canals that extend through the length of the upper and lower jaws, but they have extensive and irregular ramifications that are discussed in the section below. The remodeling of the upper jaw in birds, especially with the radical reduction of the maxilla and expansion of the premaxilla, has resulted in the maxillary canal passing through the premaxilla rostral of the narial opening. However, the contents of the maxillary canal are reported to vary from a branch of V_1 alone (Jones et al., 2019) to a branch of V_2 anastomosed with the nasal branch of V_1 (Ghetie et al., 1976). The mandibular canals are still long and extend through the length of the lower jaw. The distribution of foramina in these two bird species and the alligator are discussed in the section below on enhanced tactile sensing.

4.1.3 | Nonmammalian synapsids

The morphology of the maxillary and mandibular canals in nonmammalian synapsids follows an evolutionary trajectory of change from complex branching patterns to increasingly simplified morphologies with reduced branching and shortening of the maxillary canal (Benoit et al., 2020). The earliest synapsid in our sample, the Early Permian *Varanosaurus* (Figure 6a–c) shares some key features observed in the non-synapsid outgroup such as long maxillary and mandibular canals that extend through the anteroposterior length of the upper and lower jaws and relatively short ramifications. However, the orderly line of regularly spaced labial foramina found in several of our sampled amphibian and sauropsid species is replaced by more irregular positioning of a fewer number of foramina near the toothrows. What differentiates *Varanosaurus* is the greater concentration of foramina at the tip of the dentary near the symphysis and in the upper jaw, especially the premaxilla. A similar multiplicity of rostrally positioned foramina has been described in varanopid eupelycosaurs, that is, on the maxilla of *Archaeovenator hamiltonensis* from the Upper Pennsylvanian (Reisz & Dilkes, 2003) and the dentary of *Pyozia mesenensis* from the Middle Permian (Anderson & Reisz, 2004). These findings point toward a divergence in maxillary and mandibular canal morphology from non-synapsids appearing early in the evolutionary history of synapsids.

Later nonmammalian synapsids continue the trend of complex canal morphologies. Both *Tetracynodon* (Figure 6d–f) and *Thrinaxodon* (Figure 6g–i) from the Early Triassic display long maxillary and mandibular canals that have a multiplicity of ramifications that terminate in foramina concentrated on the rostral half of the snout. Foramina associated with the mandibular canal are densely clustered around the midline symphysis, while the maxillary foramina are spread in an irregular pattern over the dorsoventral height of the maxilla. The transition from a linear to a more branching maxillary canal is accompanied by the dorsoventral expansion of the maxilla in Permo-Triassic synapsids, which becomes the dominant bone forming the lateral surface of the snout (Duhamel et al., 2021).

A trajectory toward a more simplified morphology of the maxillary and mandibular canals is observed in the Late Triassic eucynodont *Ecteninion* (Figure 7a–c) and

Early Jurassic prozostrodont cynodonts *Pachygenelus* (Figure 7d–f) and *Tritylodon* (Figure 7g–h). *Thrinaxodon* possessed prolific maxillary canal branching with 16 associated foramina, whereas *Ecteninion* has 6, *Pachygenelus* has 1, and *Tritylodon* has 3 maxillary foramina. The number of mandibular foramina is similarly reduced and the position of these openings shifts away from the symphysis to the lateral aspect of the dentary. The simplification of the maxillary canal appears to be largely due to the gradual loss of the external nasal, internal nasal, and superior labial canals (Benoit et al., 2020). What remains is a shortened maxillary canal consisting of an infraorbital canal that terminates in the single large IOF and a rostral alveolar canal that remains internal of the maxilla to innervate the teeth. The first emergence of this derived simplified state that is shared with modern extant mammals is estimated to have appeared in the Mid-Triassic (~241 Ma) among basal probainognathians (Benoit et al., 2020).

It is worth noting that there is no current consensus in the literature on the identification of the IOF in nonmammalian synapsids, especially in taxa such as *Tritylodon*, where the number of maxillary foramina has reduced to three and their position in the infraorbital region above the postcanine teeth renders them all seemingly plausible candidates to be the IOF. In many descriptive works, all such openings are labeled as the IOF. For instance, the three maxillary foramina found on the Late Triassic to Mid-Jurassic mammaliaform *Morganucodon* spp. (Kermack et al., 1981; Kielan-Jaworowska et al., 2004); the two maxillary foramina found on Mesozoic multituberculates *Ctenacodon* and Paulchoffatidae (Kielan-Jaworowska et al., 1987); and the two maxillary foramina found on the Late Triassic traversodontid cynodont *Santagnathus mariensis* (Schmitt et al., 2024). The inclusion of the latter is particularly interesting because traversodontids represent a cynodont clade that diverged from Probainognathia and the lineage leading to mammals approximately at the Permo-Triassic boundary (Stefanello et al., 2023), suggesting that the simplification of the maxillary canal into branches terminating in one or two openings is possibly convergent. An attempt to homologize the maxillary canals and the IOF in nonmammalian prozostrodont cynodonts *Brasilitherium*, *Tritylodon*, *Ecteninion*, and *Lumkuia* are detailed in Benoit et al. (2020) and we have referred to those identifications in our anatomical descriptions of *Tritylodon* and *Ecteninion*.

4.1.4 | Mammals

The morphology of the maxillary and mandibular canals as observed in extant mammals has its emergence well before the origins of crown mammals, with the shift from a branched transitional state to the simplified derived state likely occurring among basal probainognathian cynodonts in the Mid-Triassic (Benoit et al., 2020). The maxillary canal is typically consolidated into two components. The infraorbital canal is a short, large-diameter passageway for the infraorbital branch of V_2 that terminates in a single large, forward-facing IOF. The rostral alveolar canal is typically more slender and extends rostrally through the maxilla to innervate the teeth; the canal remains internal and has no associated foramina. The mandibular canal still traverses the anteroposterior length of the lower jaw, but usually only bears a few ramifications resulting in one to few foramina on the lateral surface of the dentary. Though the overall morphology of the canals is simplified and the number of foramina reduced, the internal pathway can appear complex and netlike as the rostral alveolar and mandibular canals navigate around the roots of the teeth and send fine branches to supply the teeth with nerves and blood vessels. Such excursions into the dental alveoli are even retained in some, though not all, edentulous taxa such as anteaters (Vermilingua) and baleen whales (Mysticeti) (Ferreira-Cardoso et al., 2019). In addition, a few of our sampled mammal species such as *Pan troglodytes* have jawbones with a highly cancellous interior structure, making it difficult to disambiguate smaller neurovascular canal pathways from other open osseous spaces.

Despite the stunning morphological and functional diversity of mammalian heads (Figures 9–14; Figures 15d–f, 16, and 17), the overall morphology of the maxillary and mandibular canals remains remarkably consistent. There are notable exceptions, the monotremes (Figure 8) and cetaceans (Figure 15a–c). They will be discussed in more detail in the following section in relation to how specialized sensory systems may have impacted these unusual changes to canal morphology.

4.2 | Some variations in canal morphology are correlated with the development of specialized sensory systems

As a major sensory nerve of the head, the trigeminus has adopted a diversity of functions. The nerve primarily conveys mechanosensory information to the brain from specialized receptors or free nerve endings in the integument (Berg & Kleinfeld, 2003; Fox, 1999; Huber, 1930; Sperber et al., 2000; Williams et al., 1989; Wineski, 1985). However, trigeminal nerves have also proven capable of adapting to a wider range of sensory cues that have resulted in the evolution of novel sensory systems. We examine some

of these specializations in the sections below and how they may have reshaped maxillary and mandibular canal morphology away from their expected configurations.

4.2.1 | Infrared sensing in snakes

The ability to sense heat as infrared radiation (thermoreception) is present among species belonging to pythons (Pythonidae), boas (Boidae), and pit vipers (Viperidae) (Campbell et al., 2002; Goris, 2011; Molenaar, 1978; Noble & Schmidt, 1937). The complex sensory apparatus in pit vipers has been compared to a pinhole camera capable of producing thermal images (Goris, 2011). It consists of a large circular bony pit formed on the lateral surface of the maxilla positioned between the eye and the nostril (Hofstadler Deiques, 2002); within this capsule is a suspended membrane housing the terminal nerve masses that detect infrared radiation (Goris, 2011; Noble & Schmidt, 1937). In contrast, boids such as *Boa constrictor* and *Eunectes murinus* (Figure 4a–c), these pits are simplified to a series of more or less distinct invaginations between adjacent labial scales and the infrared sensors are located in patches around the rim of these depressions (Campbell et al., 2002; Goris, 2011). Alongside the infrared receptors in *Eunectes*, are also tactile mechanoreceptors, suggesting a multimodal labial sensory organ (Barrett, 1970; Campbell et al., 2002), Pythonids show a series of wide pits between their labial scales with the infrared sensors located at the fundus (Goris, 2011). The heat sensing pits are innervated by branches of V_1 and/or V_2, as well as V_3 in boids (Goris, 2011; Molenaar, 1978). Behavioral experiments demonstrate that infrared sensing snakes are capable of detecting and tracking heat sources even when vision is obscured, supporting the role of the pit organ as a substitute for vision when hunting at night or within dark burrows (Campbell et al., 2002; Ebert et al., 2007; Noble & Schmidt, 1937). In comparison, colubrids such as *Thamnophis marcianus* (Figure 4d–f) possess neither infrared sensors nor any behavioral response to infrared stimuli (Barrett, 1970).

Osteologically, the presence of a crotaline pit viper-like pit organ would be fairly evident as it appears as a large bony cup or capsule-shaped structure on the lateral surface of the maxilla between the eye and narial opening (Hofstadler Deiques, 2002). The large maxillary and mandibular foramina in *Eunectes* positioned in the region of the labial scales may indicate a large neurovascular tract to supply the infrared sensors. This is especially striking in comparison to *Thamnophis*, which bears relatively small foramina. An anatomical study of the cranial nerves in a different species of *Thamnophis* found that most branches of V_2 and V_3 within the canals were directed toward innervating the teeth or surrounding muscles, with no particular mention of sensory innervation (Auen & Langebartel, 1977). However, the lack of data on infrared sensing in a pit-less snake like *Eunectes* leaves unresolved questions about the morphological relationship between the distribution of the infrared sensors with the pathways of the trigeminal nerves.

4.2.2 | Enhanced tactile sensing via cutaneous mechanoreceptors in sauropsids

Despite a skin hardened with scales and osteoderms, extant reptiles can sense tactile cues through microscopic cutaneous (or integumentary) mechanoreceptors that occur as either minute bristles or dome-shaped protrusions through the skin. Direct contact of these sensors with the substrate can provide tactile information such as vibration, texture, and stimuli duration and intensity (Crowe-Riddell & Lillywhite, 2023). The density and distribution of these mechanoreceptors on the labial and surrounding scales are known to vary between lizard clades (Ananjeva et al., 1991; Matveyeva & Ananjeva, 1995), but also with ecology. In geckos such as *Uroplatus*, the high number of mechanoreceptors surrounding the mouth may be adaptive for these nocturnal predators to capture and handle prey when visual cues are limited (Riedel & Schwarzkopf, 2022). The presence of an expanded maxillary canal in *Uroplatus* (Figure 3b) with foramina occurring as both a supralabial row and scattered over the rostral end of the maxilla may indicate abundant local supplying of overlying cutaneous mechanoreceptors. Another instance where tactile sensation supersedes vision is in fossorial species such as *Dibamus*, which has vestigial scale-covered eyes (Das & Lim, 2009; Kliukin et al., 2023; Rieppel, 1984). In general, burrowing squamates tend to have more cutaneous mechanoreceptors concentrated on the head region than non-burrowers (Crowe-Riddell & Lillywhite, 2023). Species within the *Dibamus* genus have a rostral pad that envelops the entire snout and is populated by a large number of sensory papillae (Das & Lim, 2009; Kliukin et al., 2023). This coverage seems to coincide with the distribution of both maxillary canal foramina and foramina from short unconnected canals present on the maxilla and nasal bones that is suggestive of increasing innervation to this site (Figure 3e).

Transitioning from a terrestrial to aquatic habitat also has demonstrated impacts on cutaneous mechanoreceptors. A study on fully aquatic sea snakes in comparison with semiaquatic sea kraits and fully terrestrial relatives found that sea snakes have larger sensory receptors (i.e., sensilla), resulting in "exceptionally high" overall sensory coverage over the same postocular

scale area (Crowe-Riddell et al., 2016). In the alligator (Figure 5a–c), thousands of dome-shaped integumentary sensory organs are distributed over the facial scales and especially highly concentrated along the margins of the upper and lower jaws near the teeth (Leitch & Catania, 2012), where most of the maxillary and mandibular foramina are located. Soares (2002) reported hexagonal arrangements of foramina which were not apparent from our segmentation. Tissue staining has revealed an extensive and complex network of branching of V_1, V_2, and V_3 over the alligator face (Leitch & Catania, 2012), which suggests that the resolution of the scan used in our study may not have been sufficient to capture all the minute ramifications supplying the sensory receptors. But the overall morphological pattern remains distinctive. This dense innervation of the integumentary sensory organs allows alligators to not only detect tactile information from direct contact or the slightest disturbances in the water, but also a whole range of environmental stimuli including temperature, pH, salinity, and low frequency sounds (Bowman et al., 2022; Di-Poï & Milinkovitch, 2013; Leitch & Catania, 2012; Soares, 2002).

Bird beaks are also capable of a range of tactile sensitivity depending on ecology and feeding strategies, and a number of taxa have evolved specialized bill-tip organs or similar concentrations of tactile sensors (Du Toit et al., 2024). The sensory information gathered by mechanoreceptors in the beak are processed in a region of the brain called the principal sensory nucleus of the trigeminal nerve. The relative volume of that brain region in probing shorebirds such as *Calidris* is nearly 16 times that of a non-specialist bird species. When foraging in soft sediments, probing shorebirds introduce the tip of the beak to sense vibrations and changes in pressure to locate hidden prey (Du Toit et al., 2024; Gutiérrez-Ibáñez et al., 2009). *Calidris* features an incredibly dense array of maxillary and mandibular foramina pitting the entire tip of the beak (Figure 5h–i). This morphology is very similar to that observed in kiwis (*Apteryx* spp.), another probe forager, albeit a distantly related one with terrestrial habits (Cunningham et al., 2013). In contrast, the cattle egret *Bubulcus* is another bird that frequents shorelines, but is a diurnal hunter that relies upon vision (Rojas et al., 1999). The relative volume of the trigeminal sensory nucleus for this group of birds is lower than average (Gutiérrez-Ibáñez et al., 2009) and this is reflected in the nearly nonexistent presence of maxillary or mandibular foramina we found in *Bubulcus* (Figure 5e,f).

From our sample of sauropsid maxillary and mandibular canals, there is a strong correlation between higher number and density of foramina with enhanced tactile sensitivity either through direct skin contact or contact with pressure waves. In addition, the localization of these foramina at the rostral tip can indicate the function of a touch sensitive probe.

4.2.3 | Mammalian electroreception in monotremes

As the most basal lineage of crown mammals, monotremes occupy a distinguished position of representing deeply ancestral characters while simultaneously manifesting highly derived features. This mélange of characters requires careful consideration of how monotremes could be used in a comparative study. We have posited in a previous publication (Benoit et al., 2020) that the key features of the simplified derived state of the maxillary canal first appeared approximately 241 Ma. This significantly predates estimates for the evolutionary origin of monotremes, which are hypothesized to have evolved in the Late Jurassic (~150 Ma) based on genomic estimates (Musser, 2013; Phillips et al., 2009; Zhou et al., 2021) and fossil evidence of the oldest known monotreme, *Teinolophus trusleri*, which dates to the Early Cretaceous (~126 Ma) (Flannery et al., 2022). The branching patterns of the maxillary and mandibular canals in extant platypus and echidna (Figure 8) are different from the simplified derived morphology we described for the other mammals in our sample, but are mostly likely the result of secondary changes instead of being plesiomorphic.

The maxillary foramina and their homology in monotremes were missing in Benoit et al. (2016, 2020), with the reasoning that their condition was too derived for comparison. The monotreme maxillary canals may in fact represent a highly derived condition, but it is notable that the platypus (*Ornithorhynchus anatinus*, Figure 8b) shares features with nonmammalian prozostrodonts that are consistent with the interpretation of the homology of the maxillary canals established in our previously published work, Benoit et al. (2020). In the platypus, foramen 3 is associated with a long canal that passages the rostral alveolar ramus of V_2 (Kesteven & Furst, 1929; Manger & Pettigrew, 1996), which is likely equivalent with the "Raf"the (foramen for the rostral alveolar canal) in Benoit et al. (2020). In addition, the short, laterally oriented canal that terminates in foramen 1, that is, the platypus IOF, (Kesteven & Furst, 1929; Manger & Pettigrew, 1996) is likely homologous to the nonmammalian prozostrodont IOF (Benoit et al., 2020). The zygomaticofacial canal is absent in the platypus. The condition in the echidna (Figure 8e) appears to be unique and the homology of the canals could neither be addressed here nor the identity of the IOF resolved in previous publications (Andres et al., 1991; Manger et al., 1997).

Behavioral and neurobiological research on monotremes have demonstrated the presence of a specialized sensory system of mechano- and electroreceptors concentrated in the integument of the platypus bill and echidna beak (Andres et al., 1991; Asahara et al., 2016; Bino et al., 2019; Manger et al., 1997; Manger & Pettigrew, 1995, 1996; Musser, 2013; Pettigrew, 1999; Proske et al., 1998). Platypus are nearly exclusive underwater foragers and have approximately 40,000 electroreceptors scattered over the entire surface of the bill and oral cavity (Pettigrew, 1999). Combined with highly sensitive "push-rod" mechanoreceptors, platypus are capable of detecting and capturing hidden benthic invertebrate prey as they swim about in waters with their eyes, ears, and nostrils closed (Manger & Pettigrew, 1995, 1996; Proske et al., 1998). As biologically relevant electrical signals only conduct through water, electroreception suggests an ecological origin tied to aquatic or moist environments. The terrestrial echidna is also equipped with electroreceptors capable of detecting weak electrical signals (Gregory et al., 1989; Manger et al., 1997; Manger & Pettigrew, 1996), but it is less certain how much utility these electroreceptors have. *Zaglossus bruijnii* inhabits wet tropical forests where damp soils may be able to convey electrical signals from buried invertebrate prey (Manger et al., 1997; Pettigrew, 1999). *Tachyglossus aculeatus* lives in more arid environments and possesses far fewer electroreceptors compared to *Zaglossus* (about 400 vs. 2000) (Pettigrew, 1999), but is frequently seen keeping the tip of the snout moist with nasal secretions or even by blowing bubbles of mucus into a wet froth which may aid in generating an electroconductive zone while probing the substrate to forage (Augee et al., 2006; Gregory et al., 1989).

The maxillary and mandibular canals of the platypus (Figure 8a–c) and the echidna (Figure 8d–f) both differ from the simplified canal morphology distinctive of most extant mammals. However, they also differ from each other. The platypus maxillary and mandibular canals are exceptionally wide in diameter and possess three large foramina that are directed not only rostrally, but also toward the oral cavity. The maxillary canal houses massive branches of V_2 that innervate the electroreceptors covering the dorsal surface of the bill and the palatal surface of the oral cavity. Likewise, the mandibular canal houses branches of V_3 that innervate the ventral surface of the bill and lingual surface of the oral cavity (Manger & Pettigrew, 1996). In contrast, the maxillary canal in the echidna is slender with numerous branches of different relative lengths, resulting in an irregular distribution of foramina on the lateral surface of the rostral half of the snout. There are no comparable studies showing the pathway of the V_2 nerve branches in echidnas, but a map of the electroreceptors in both *Tachyglossus* and *Zaglossus* showed the sensors are concentrated at the rostral tip of the snout (Pettigrew, 1999).

Monotremes share some key similarities with the sauropsids discussed in the previous section on enhanced tactile sensing via cutaneous mechanoreceptors. Compared to the simplified derived morphology of most mammalian canals, monotremes do exhibit more branching and, thus, more foramina. This accords with the relationship that a higher number of foramina correlate to greater sensory sensitivity. However, the diameter of the canals or foramina can sometimes override this pattern, as demonstrated by the platypus. Based on osteology alone, the echidna with its more numerous foramina could be read as having a better developed trigeminal sensory system compared to a generalist; however, if the echidna is compared with the platypus, this interpretation will not be supported by microanatomical, physiological, and experimental behavior studies (Gregory et al., 1989;Pettigrew, 1999; Phillips et al., 2009).

The presence of electroreceptors in the terrestrial echidna has been seen as a vestigial retention of a sensory system inherited from aquatic ancestors (Pettigrew, 1999; Phillips et al., 2009). The oldest known monotreme fossil *Teinolophus trusleri* consists of a partial lower jaw that preserves an enlarged mandibular canal that was used as evidence for the presence of electroreceptive (or at the very least, highly mechanoreceptive) snout in a platypus-like ancestor. Environmental reconstruction of the fossil site reveals a dense polar forest where probing for food underneath leaf litter and snow with an electro- and/or mechanosensitive beak-like rostrum could be a successful adaptive strategy (Flannery et al., 2022). Given that the comparatively simple branching pattern of the maxillary and mandibular canals, as well as the presence of an identifiable IOF, in extant platypus are closer in morphology to the general mammalian morphological configuration than the echidna, this provides some evidence of polarity to support a more platypus-like ancestral form for monotremes. However, with new monotreme fossils being discovered, described, and placed within a diverse ecosystem populated by other ancient monotremes (Flannery et al., 2022, 2024), the evolutionary history of this group and its distinctive sensory system in relation to its ecology may soon come into greater focus.

4.2.4 | Cetacean trigeminal sensory complex and echolocation

The maxillary canal of the harbor porpoise *Phocoena phocoena* (Figure 15a–c) is a network of multiple branching canals that terminate in several large foramina clustered around the narial opening and one foramen located at the very tip of the rostrum. This unusual configuration suggests intense trigeminal innervation of the facial region which

supports a complex of different sensory systems in cetaceans that includes enhanced facial touch, vibrissal sensing, and nasal sound production feedback (De Vreese et al., 2023). Both toothed (odontocete) and baleen (mysticete) whales exhibit highly sensitive facial skin, with concentrations of integumentary mechanoreceptors surrounding the eye, angle of the mouth, lips, and blowhole. Enhanced sensitivity of those regions are hypothesized to contribute toward benthic foraging, social touch, sensing the water-air interface, and contributing to an overall sense of hydrodynamic flow (Bauer et al., 2018; De Vreese et al., 2023). Despite being hairless marine mammals, cetaceans still exhibit short vibrissae. Mysticetes have vibrissal hairs distributed over the upper and lower jaws and surrounding the blowhole, likely serving similar functions of sensing hydrodynamic flow and changes at the water-air interface (De Vreese et al., 2023). Most odontocetes will lose their vibrissae as adults, leaving behind the mechanoreceptor-rich follicle-sinus complexes that had encircled the hair root (Czech-Damal et al., 2013; De Vreese et al., 2023; Hüttner et al., 2023). These latent vibrissal pits or crypts are not vestigial structures, but sensory organs that are innervated by the same infraorbital nerve branch of V_2 at a density similar to or exceeding that of rodent whiskers (Hüttner et al., 2023). South American river dolphin species *Sotalia fluviatilis* and *S. guianensis*, as well as bottlenose dolphins *Tursiops truncatus*, have modified their follicle-sinus complexes into gel-filled ampullae capable of electoreception (Bauer et al., 2018; Czech-Damal et al., 2013; De Vreese et al., 2023; Hüttner et al., 2023).

What is perhaps the most distinctive part of the cetacean trigeminal sensory system pertains to control and feedback of the nasal vocal organ which produces the clicks used in odontocete echolocation. Since mysticetes do not echolocate, they do not have a nasal vocal organ, but rather make vocalizations using novel modifications of the larynx (Elemans et al., 2024). The production of 130–140 kHz high-frequency clicks in *Phocoena* is generated by pneumatic bursts passing through the valve-like phonic lips, which is part of an intricate nasal vocal organ consisting of air sacs, fat bodies, melon, and other soft tissue structures surrounding the nasal passage (Huggenberger et al., 2009). The entire nasal vocal organ appears to be populated by a high density of mechanoreceptors innervated by the infraorbital nerve (V_2), but the phonic lips and fat bodies surrounding it are especially well supplied (De Vreese et al., 2023; Prahl et al., 2009). The abundance of pressure-sensitive receptors in the nasal vocal organ is probably important in perceiving rapid movements or vibrations that are integrated into a neural feedback loop for fine motor control of sound production (De Vreese et al., 2023).

The unique morphology of the maxillary canal in *Phocoena* is reflected in the development of both enhanced tactile sensation of the skin and the nasal vocal organ used in echolocation. The latter seems especially well-represented by the cluster of branching and large foramina in the proximity of the nasal opening which is retracted posteriorly toward the forehead and the concave depression where the melon sits (Huggenberger et al., 2009). We have not sampled a mysticete whale to see how canal morphology may differ in species lacking a nasal vocal organ; however, mysticetes do possess multiple large foramina distributed over the maxilla and this feature emerged very early in the divergence of this clade (Bisconti & Carnevale, 2022). This would suggest that significant change in maxillary canal morphology is characteristic of cetaceans as a whole.

The maxillary canal in bats (Figure 12) does not appear notably different between an echolocating (*Myotis adversus adversus*) versus non-echolocating (*Pteropus scapulatus*) species, except that the snout of *Myotis* appears more anteroposteriorly compressed and the maxillary canal is lattice-like in appearance as it navigates through an upper jaw crowded with tooth roots. Sounds used in bat echolocation are produced either in the larynx or through tongue clicks, so there is no indication that the trigeminal nerves are recruited into this sensory system (Jones et al., 2013).

4.3 | Interpreting the sensory biology of nonmammalian synapsids using modern analogues suggest enhanced tactile sensitivity of the facial integument via direct touch

The potential functional implications of the highly branched transitional state of the maxillary and mandibular canals observed in early nonmammalian synapsids are obviously lost to time, but there are sufficient modern analogues to help make a reasoned interpretation of this morphology. The key feature of the transitional synapsid state is the abundant ramification of both the maxillary and mandibular canals that result in an irregular scattering of foramina located on the rostral half of the jaws. In previous sections, we have argued that higher numbers and density of foramina are generally correlated with increased sensitivity of the overlying facial skin. This relationship also seems to be strongly associated with species where visual cues may be periodically limited or vision is supplanted altogether as the primary sensory modality: the nocturnal predator gecko (*Uroplatus fimbriatus*), fossorial blind skink (*Dibamus novaeguineae*), semiaquatic alligator (*Alligator mississippiensis*) and platypus (*Ornithorhynchus anatinus*), substrate-probing sanderling (*Calidris alba*) and echidna (*Tachyglossus aculeatus*), and the

aquatic/benthic foraging/echolocating harbor porpoise (*Phocoena phocoena*). Based on these modern analogues, we suggest that nonmammalian synapsids such as *Varanosaurus*, *Tetracynodon*, *Thrinaxodon*, and *Ecteninion* possessed greater tactile sensitivity in the skin of the snout, especially compared to a non-synapsid outgroup.

The tendency for the maxillary and mandibular foramina to be primarily distributed on the rostral half of the snout is suggestive of touch sensitive skin functioning as a sensory probe. In particular, the densely clustered mandibular foramina on the forward-facing surface of the mandibular symphysis are positioned on a hypothetical nonmammalian synapsid snout to provide the greatest tactile sensitivity when making first exploratory contact with an object or sweeping near the ground for obstacles or food items during foraging. The maxillary foramina are also localized to the rostral end of the snout, especially on the lateral surface of the maxilla just above and anterior to the caniniform/canine tooth. These openings are usually not tightly clustered in one area, but cover the dorsoventral height of the maxilla. In our hypothetical nonmammalian synapsid, these areas of touch sensitive skin are most likely to encounter objects during sweeping, side-to-side motions of the head or while probing into narrow spaces.

We find that there is a general overlap in the timing of when nonmammalian synapsids have the branching transitional canal morphology with earliest evidence of behaviors that involve tactile sensing. A survey of the orbital morphology based on sclerotic ring dimensions of nonmammalian synapsids from the Carboniferous to Jurassic found data supporting a wider diversity in diel activity patterns than expected, especially a greater incidence of nocturnality (Angielczyk & Schmitz, 2014). The enhancement of other sensory systems such as touch, smell, and hearing compensate for the reduced utility of vision or supplant it entirely as the primary sensory modality (Adriaens & Verraes, 1997; Ahl, 1986; Billo & Wake, 1987; Catania, 2012; Dehnhardt et al., 1999; Delaunay et al., 2020; Hall et al., 2012; Huber, 1930; Sarko et al., 2011; Wake, 1985). Possession of tactile sensitive snouts, including the rhinarium, to locate objects and navigate the immediate surrounding environment is one possible strategy or part of a larger suite of adaptations to life in low-light conditions. Another low-light situation are burrows, whether as dwellings or hunting grounds for fossorial prey. A partial skeleton of *Thrinaxodon* has been discovered in a burrow cast dated to around the Permo-Triassic boundary (Damiani et al., 2003; Fernandez et al., 2013). A number of fossilized early synapsids captured in their burrows have been found, the oldest one dating from the Mid-Permian and containing the remains of the dicynodont *Diictodon* (Abdala et al., 2006; Damiani et al., 2003; Fernandez et al., 2013; Jasinoski & Abdala, 2017; Krapovickas et al., 2013; Marchetti et al., 2024).

4.4 | Synapsid maxillary canal morphology indicates an evolutionary trajectory from enhanced facial integument sensitivity to a novel, specialized sensory organ: Mobilized whiskers

The gradual transformation of canal morphology, especially of the maxillary canal, from complex and abundant branching to simplified and few branches is a pattern of change that appears unique to the synapsid lineage. The synapsid evolutionary trajectory is distinct from our amphibian and sauropsid outgroup, which typically manifest features such as long maxillary and/or mandibular canals that extend anteroposteriorly through the length of the jaws and the presence of labial foramina. This outgroup morphology may be plesiomorphic for tetrapods, but a dedicated investigation into basal tetrapods and stem tetrapods with a larger fossil taxon sample size would be necessary to better establish this hypothesis.

A functional interpretation for the transitional branched canal morphology in nonmammalian synapsids based on comparisons with modern analogues identifies the rostral areas densely populated by foramina as regions of enhanced tactile sensitivity of the integument. It is important to emphasize here that this tactile sensitivity is based on either direct contact with the skin or stimuli communicated through an environmental substrate, such as pressure waves through water. It may not be completely coincidental to see that the area of the maxilla that frequently sees the most foramina broadly corresponds to the region that will later host the mystacial whiskers in extant mammals.

Most extant mammals possess an array of specialized sensory hairs called mystacial whiskers or mystacial vibrissae sprouting from either side of the nose and upper lips. Mystacial whiskers are innervated by the infraorbital nerve branch of V_2 which passes through the infraorbital canal and then exits via the IOF. Once released from the osseous confines of the maxillary bone, the infraorbital nerve travels rostrally through the soft tissues of the face (Benoit et al., 2020; Dörfl, 1985; Miyamae, 2022) to reach the mystacial whiskers where they ramify into vibrissal nerves that innervate the follicle-sinus complex at the base of each whisker (Dörfl, 1985; Kim et al., 2012; Maklad et al., 2010).

Despite the simplification of the maxillary canal into this short, unbranched infraorbital canal and a long rostral alveolar canal that serves the roots of the upper teeth, this does not equate to a simplification of the sensory system. On the contrary, by exiting the bone, the infraorbital nerve is free to be incorporated into a sensory apparatus that utilizes two key mammalian characters—hair and facial muscles—a combination that expands the sensory

range from direct skin contact to a whisker's length in multiple directions and the ability to actively gather tactile sensory information by mobilizing the mystacial whiskers. Deflection of the whiskers as they encounter objects or air/water currents activate the mechanoreceptors and free nerve endings in the follicle-sinus complex. Gathering and processing of tactile information from the whiskers can be very sophisticated, providing the animal with data for spatial navigation, detecting moving prey, evaluating an object's properties such as texture and shape, handling of objects, and social interactions (Ahl, 1986; Berg & Kleinfeld, 2003; Brecht et al., 1997; Dehnhardt et al., 1999; Grant et al., 2018; Haidarliu et al., 2010; Luo et al., 2021; Prescott et al., 2016; Wineski, 1985).

In our sample of extant mammals, there is a remarkable consistency in the presence of a shortened infraorbital canal, usually terminating in one large, forward-facing foramen. This feature is shared across marsupial (Figure 9) and placental mammals, the fossorial mole (Figure 17a–c), aerial bats (Figure 12), small rodents (Figure 11), massive marine walrus (Figure 15d–f), anteaters with highly modified skulls (Figure 10d–f), whiskerless chimpanzees (Figure 13), and sengis (Figure 10a–c) and tapirs (Figure 14) that have mobile nasal probosces. We discussed in a previous section how the monotreme and odontocete maxillary canals have been secondarily modified from the simplified derived morphology as part of novel sensory systems of electroreception and echolocation, respectively. Another significant component in shaping this morphology is the radical reduction of the facial muscles. The platypus and echidna both appear to have very limited, if at any, facial muscles present on the electrosensitive beak (Ashwell & Musser, 2013). Dolphin vibrissal crypts lack any remnant of the muscles that would mobilize the whiskers in other mammal species (Mynett et al., 2022) and their facial muscles are absent in the superficial layers of the skin, but have been modified and repurposed as part of the nasal vocal organ to change the shape of the melon during echolocation (Huggenberger et al., 2009).

The appearance of mobile mystacial whiskers as a novel and unique trigeminal sensory system among tetrapods is accompanied by the appearance of a correspondingly unique cranial morphology: the simplified derived form of the maxillary and mandibular canals. The Early Jurassic tritheledontid *Pachygenelus* is the oldest species in our sample to show the derived state morphology. However, Benoit et al. (2020) suggests that the derived state appeared as early as the Mid-Triassic (~241 Ma) among basal probainognathians. This timing is based on their inclusion of the older *Probainognathus*, a probainognathian with a fossil range from the Mid to Late Triassic, that manifests key characteristics of the derived state. The position of *Probainognathus* was compared against a cynodont phylogeny erected by Ruta et al. (2013) to estimate that the origins of the derived state occurred in the last common ancestor of *Probainognathus* and crown Mammalia. The fossil record indicates that this evolutionary transition occurred in a gradual, stepwise fashion (Benoit et al., 2020).

We might speculate that from bare, tactile sensitive skin there was an intermediate state involving stationary, passive whiskers. Such hypothetical "protovibrissae" could have functioned akin to bristle-like rictal or elongated head feathers often found in birds that are nocturnal and/or navigate through burrows or holes to reach their nests (Cunningham et al., 2011; Delaunay et al., 2020; Seneviratne & Jones, 2008). Measurements of the cross-sectional area of the IOF in *Pachygenelus* and *Tritylodon* were reported by Benoit et al. (2016) and assessed by Muchlinski et al. (2020) in a study of IOF size and the occurrence of whisking, a specialized form of vibrissal sensing that involves cyclic oscillations of the mystacial whiskers like those seen in mice and rats (Deschênes et al., 2012; Muchlinski et al., 2020; Wineski, 1985). The large size of the infraorbital foramina in *Pachygenelus* and *Tritylodon* plotted in a regression model suggests the presence of mystacial whiskers, though they were not likely engaged in whisking; however, mystacial whiskers are still highly mobile even if they do not engage in whisking (Ahl, 1986; Grant & Goss, 2022; Milne et al., 2020).

The diversification of vertebrates into novel habitats, functions, and behaviors often evolve in concert with their nervous systems. We have explored some of these possibilities, that enhancing the sense of facial tactile sensitivity through highly innervated skin or whiskers is important for close-range detection and investigation of objects, especially in low-light conditions resulting from a temporal shift into nocturnal activity patterns, going into burrows, entering the water, or searching for items hidden in the substrate. But facial touch also has important behavioral and social uses in fostering social bonds, communicating social dominance/submission, and developing the neural and behavioral pathways for parental care and normal social behavior (Ahl, 1986; Brecht et al., 1997; Gromov, 2013; Wolfe et al., 2011). Intriguingly, the early and extensive development of the trigeminal nerve and consequent sensory innervation of the perioral region and snout (including incipient vibrissae) appears critical for neonates in locating milk sources, attaching to the teat, and coordinating critical reflexes (Ahl, 1986; Ashwell, 2015; Finan & Barlow, 1998; Kenyon et al., 1982; Larson & Stein, 1984; Smith & Keyte, 2020; Sperber et al., 2000). Newborn kittens (*Felis catus*) were demonstrated to rely upon tactile sensation of the snout for locating and attaching to a nipple (Larson & Stein, 1984). Rat neonates (*Rattus norvegicus*) placed into

artificially large litters compensated for the intensified competition for milk with faster mystacial whisker growth (Park, 1970). The expansion of the trigeminal sensory field over the face and concomitant evolution of facial muscles may thus have a role in mammalian life history traits and maternal provisioning of offspring with milk. Though the integration of these data into our understanding of nonmammalian synapsid and mammal evolution is still speculative, the deep history and legacy of sensory innovations in shaping the identity of mammals can be appreciated.

4.5 | Caveats and nuances to the interpretation of sensory biology from trigeminal canals

We have used maxillary and mandibular canal morphology to infer the pathways of the sensory branches of the trigeminal nerve and, thus, the evolution of facial tactile sensing in synapsids. This interpretation was supported by comparisons with modern analogues for which we have some data about their sensory capabilities. The general relationship we found is that a greater number of foramina correlates to greater sensory sensitivity, as more openings in the surface of the bone we assumed to mean more nerve branches were diverging from the main trunks of V_2 and V_3 housed inside the respective maxillary and mandibular canals to innervate the surrounding soft tissue and integument. However, accessing a broad phylogenetic sampling has been helpful in introducing some nuance to this correlative relationship. For instance, in our own evaluation of synapsids, strict adhesion to the number of maxillary and mandibular foramina alone as indicators of tactile sensitivity would result in misinterpreting the simplification of canal morphology is a diminishment rather than an indicator for the novel emergence of mystacial whiskers, which neurophysiological and behavioral studies with extant mammals reveals to be a surprisingly sophisticated sensory organ.

Even if the correlation between foramina number and tactile sensitivity holds, using such data may not always be appropriate within a given context. Bowman et al. (2022) made the initial assumption that as excellent semi-aquatic predators, the trigeminal canal morphology of modern crocodylians would be a good indicator of the terrestrial-to-aquatic ecological shift in the evolutionary history of metriorhynchoid thalattosuchians, a marine clade of crocodylomorphs from the Jurassic. However, an investigation of the maxillary canals preserved in metriorhynchoid skulls found a lack of extensive and complex trigeminal innervation. The integumentary sensory organs that are so important and prominent in extant crocodylians were neither ancestral nor a necessity for metriorhynchoids to enter the marine realm. However, integrating information about the presence of scleral rings in the eye provided support for the hypothesis that metriorhynchoids employed an alternate sensory strategy by investing in greater visual acuity as their dominant sensory modality (Bowman et al., 2022).

In a comparison between extant monotremes, the number of maxillary foramina in platypus is considerably fewer than in echidnas, but supports approximately 100 times more electroreceptors (Pettigrew, 1999). The maxillary canal of the platypus houses massive nerves consisting of nearly 400,000 axons bundled together to support the array of electroreceptors and mechanoreceptors in the bill (Manger & Pettigrew, 1996). Taking this into account, canal or foramina size is another metric for estimating sensory abilities based on canal morphology. Cross-sectional area of the IOF has been explored as a proxy for nerve size to predict the relative abundance of whiskers, tactile sensitivity, and ecology and has been found to have only broad predictive power (Muchlinski, 2008, 2010; Muchlinski et al., 2020; Sánchez-Villagra & Asher, 2002). Muchlinski (2008) provided the essential groundwork in assessing the contents of the infraorbital canal, which consists primarily of the infraorbital nerve and an artery that occupied a very small portion of the IOF cross-sectional area. Examining the contents of the maxillary and mandibular canals, especially of the finer ramifications, through histology or dissection is important for confirming that the nerve canals identified osteologically are, in fact, conveying nerves or if they only carry blood vessels or other structures. The IOF of rodents can be especially misleading if the size of the opening is assumed to represent the size of the infraorbital nerve alone. The IOF size in the rodents *Mus* (Figure 11a,b) and *Octodon* (Figure 11d,e) are both substantial, but part of that space is occupied by a jaw adductor muscle, the infraorbital zygomaticomandibularis, which threads through the IOF (Baverstock et al., 2013; Cox & Jeffery, 2011; Ginot et al., 2018). However, as a hystricomorph rodent, the opening in *Octodon* is characteristically massive because the infraorbital zygomaticomandibularis is a larger muscle in this group of rodents compared to either myomorph or sciuromorph rodent groups (Cox & Jeffery, 2011).

While a few selected species have been well-studied as model organisms, there remains a significant paucity of data on the gross and cellular anatomy, physiology, ecology, and behavior for many species. The remarkable diversity of maxillary and mandibular canal morphology across extant tetrapods deserves to be investigated by integrating data from these various methodological approaches so that we may come to a closer approximation in reconstructing the sensory world of extinct taxa.

5 | CONCLUSION

The morphology of the maxillary and mandibular canals that serve as passageways for trigeminal nerve branches of V_2 and V_3, respectively, have frequently been used as osteological correlates to interpret the sensory capabilities of extinct fossil taxa. In order to support our own investigation into the evolution of the mammalian facial sensory systems, we have described the maxillary and mandibular canal morphologies of 38 extinct and extant tetrapod species (amphibians, sauropsids, synapsids) to both reveal a pattern of evolutionary change that is specific to synapsids and to test these form-function relationships using a variety of modern analogues with known ecologies and sensory biology. We have found that compared to an amphibian and sauropsid outgroup, the maxillary and mandibular canal morphology of synapsids records a unique evolutionary history of change from a branched transitional to a simplified derived morphological form. In nonmammalian synapsids with the transitional state morphology, we interpreted the heavy concentration of maxillary and mandibular foramina at the rostral ends of the snout as an indicator for touch-sensitive skin that could be used as a rostral probe based on modern analogues such as alligators, probing shorebirds, and monotremes. A gradual shift toward more simplified canals with reduced branching and the emergence of a single large IOF is correlated with the presence of facial muscle mobilized mystacial whiskers, a specialized sensory organ unique to mammals.

There are necessary caveats and nuances to interpreting sensory functionalities based on trigeminal canal morphology that can be addressed through integrating anatomical, paleontological, physiological, behavioral, ecological, and other contextual data to establish robust, clade-specific form-function relationships.

AUTHOR CONTRIBUTIONS

Juri A. Miyamae: Conceptualization; investigation; visualization; writing – original draft; methodology; data curation; writing – review and editing. **Julien Benoit:** Conceptualization; investigation; writing – review and editing. **Irina Ruf:** Conceptualization; investigation; writing – review and editing. **Zoleka Sibiya:** Writing – review and editing; investigation. **Bhart-Anjan S. Bhullar:** Funding acquisition; resources.

ACKNOWLEDGMENTS

For access to specimens scanned for this study, we thank the Yale Peabody Museum's Division of Vertebrate Paleontology (C. Norris, V. Rhue, D. Brinkman, and M. Fox), the Wagner Lab at Yale University's Department of Ecology and Evolutionary Biology (G.P. Wagner, J. Maziarz), and the California Academy of Sciences' Ornithology and Mammalogy Department (M. Flannery). Scans were performed with the help of staff at Harvard University Center of Nanoscale Systems and Chemical and Biophysical Instrumentation Center at Yale University. Scans of *Pachygenelus* and *Tritylodon* were performed on beamline ID19 by Vincent Fernandez and Paul Tafforeau at the European Synchrotron Radiation Facility (ESRF), Grenoble, France. Additional scans were made available through the significant help of DigiMorph and MorphoSource. The authors thank the following for their financial support: J.A.M. was funded by the Department of Earth and Planetary Sciences at Yale University, the Yale Institute for Biospheric Studies, and Robotics at the University of Michigan; J.B. was funded by the DSI-NRF African Origins Platform (AOP210218587003; UID: 136505); Z.S. was funded by the Genus-Centre of Excellence in Palaeosciences; and B.-A.S.B. was funded by NSF CAREER DEB 2046868. T.Y. Moore (University of Michigan) is appreciated for providing feedback and advice on the preparation of this manuscript. Finally, the authors thank T.D. Smith, L.C. Pusch, and an anonymous reviewer who helped to improve the manuscript.

DATA AVAILABILITY STATEMENT

The microCT and synchrotron data obtained through online data repositories MorphoSource and DigiMorph can be accessed with the media data provided in Table 1 of Materials and Methods as well as in Supplemental Materials. Scan of *Varanosaurus acutirostris* are available on request from the Field Museum of Natural History Department of Geology. Scans of *Tetracynodon darti*, *Thrinaxodon liorhinus*, and *Ecteninion lunensis* are available upon request from the High-Resolution X-ray Computed Tomography Facility at The University of Texas at Austin. All other scans can be received through the corresponding author upon reasonable request. Scan of *Ornithorhynchus anatinus* is only available as a surface mesh. Surface meshes of segmented scans used in this study (PLY, STL, and 3D PDF formats) are available upon reasonable request from the corresponding author.

ORCID

Juri A. Miyamae https://orcid.org/0009-0007-9461-727X
Julien Benoit https://orcid.org/0000-0001-5378-3940
Irina Ruf https://orcid.org/0000-0002-9728-1210
Zoleka Sibiya https://orcid.org/0000-0003-3800-7614
Bhart-Anjan S. Bhullar https://orcid.org/0000-0002-0838-8068

REFERENCES

Abdala, F., Cisneros, J. C., & Smith, R. M. H. (2006). Faunal aggregation in the Early Triassic Karoo Basin: Earliest evidence of

shelter-sharing behavior among tetrapods? *PALAIOS*, *21*(5), 507–512. https://doi.org/10.2110/palo.2005.P06-001R

Adriaens, D., & Verraes, W. (1997). Ontogeny of the maxillary barbel muscles in Clarias gariepinus (Siluroidei: Clariidae), with some notes on the palatine-maxillary mechanism. *Journal of Zoology*, *241*, 117–133.

Ahl, A. S. (1986). The role of vibrissae in behavior: A status review. *Veterinary Research Communications*, *10*, 245–268.

Ananjeva, N. B., Dilmuchamedov, M. E., & Matveyeva, T. N. (1991). The skin sense organs of some Iguanian lizards. *Journal of Herpetology*, *25*(2), 186. https://doi.org/10.2307/1564647

Anderson, J. S., & Reisz, R. R. (2004). *Pyozia mesenensis*, a new, small varanopid (Synapsida, Eupelycosauria) from Russia: "Pelycosaur" diversity in the middle Permian. *Journal of Vertebrate Paleontology*, *24*(1), 173–179. https://doi.org/10.1671/1940-13

Andres, K. H., von Düring, M., Iggo, A., & Proske, U. (1991). The anatomy and fine structure of the echidna Tachyglossus aculeatus snout with respect to its different trigeminal sensory receptors including the electroreceptors. *Anatomy and Embryology*, *184*(4), 371–393. https://doi.org/10.1007/BF00957899

Angielczyk, K. D., & Schmitz, L. (2014). Nocturnality in synapsids predates the origin of mammals by over 100 million years. *Proceedings of the Royal Society B: Biological Sciences*, *281*(1793), 20141642. https://doi.org/10.1098/rspb.2014.1642

Aria, C., Vannier, J., Park, T. S., & Gaines, R. R. (2023). Interpreting fossilized nervous tissues. *BioEssays*, *45*(3), 2200167. https://doi.org/10.1002/bies.202200167

Asahara, M., Koizumi, M., Macrini, T. E., Hand, S. J., & Archer, M. (2016). Comparative cranial morphology in living and extinct platypuses: Feeding behavior, electroreception, and loss of teeth. *Science Advances*, *2*(10), e1601329. https://doi.org/10.1126/sciadv.1601329

Ashwell, K. W. S. (2015). Timing of mammalian peripheral trigeminal system development relative to body size: A comparison of metatherians with rodents and monotremes. *Somatosensory and Motor Research*, *32*(3), 187–199.

Ashwell, K. W. S., & Musser, A. M. (2013). Atlas and tables of peripheral nervous system anatomy. In K. W. S. Ashwell (Ed.), *Neurobiology of the Monotremes: Brain evolution in our distant mammalian cousins* (pp. 299–313). CSIRO Publishing.

Auen, E. L., & Langebartel, D. A. (1977). The cranial nerves of the colubrid snakes *Elaphe* and *Thamnophis*. *Journal of Morphology*, *154*(2), 205–222. https://doi.org/10.1002/jmor.1051540203

Augee, M. L., Gooden, B., & Musser, A. CSIRO (Australia) (Ed.). (2006). *Echidna: Extraordinary egg-laying mammal*. CSIRO Publishing.

Barrett, R. (1970). The pit organs of snakes. In C. Gans & T. S. Parsons (Eds.), *Biology of the Reptilia* (Vol. 2, pp. 277–314). Academic Press.

Bauer, G. B., Reep, R. L., & Marshall, C. D. (2018). The tactile senses of marine mammals. *International Journal of Comparative Psychology*, *31*. https://doi.org/10.46867/ijcp.2018.31.02.01

Baverstock, H., Jeffery, N. S., & Cobb, S. N. (2013). The morphology of the mouse masticatory musculature. *Journal of Anatomy*, *223*(1), 46–60. https://doi.org/10.1111/joa.12059

Benoit, J., Angielczyk, K. D., Miyamae, J. A., Manger, P., Fernandez, V., & Rubidge, B. (2018). Evolution of facial innervation in anomodont therapsids (Synapsida): Insights from X-ray computerized microtomography. *Journal of Morphology*, *279*(5), 673–701. https://doi.org/10.1002/jmor.20804

Benoit, J., Ford, D. P., Miyamae, J. A., & Ruf, I. (2021). Can maxillary canal morphology inform varanopid phylogenetic affinities? *Acta Palaeontologica Polonica*, *66*(2), 389–393. https://doi.org/10.4202/app.00816.2020

Benoit, J., Manger, P. R., & Rubidge, B. S. (2016). Palaeoneurological clues to the evolution of defining mammalian soft tissue traits. *Scientific Reports*, *6*(1), 25604. https://doi.org/10.1038/srep25604

Benoit, J., Ruf, I., Miyamae, J. A., Fernandez, V., Rodrigues, P. G., & Rubidge, B. S. (2020). The evolution of the Maxillary Canal in Probainognathia (Cynodontia, Synapsida): Reassessment of the homology of the infraorbital foramen in mammalian ancestors. *Journal of Mammalian Evolution*, *27*, 329–348. https://doi.org/10.1007/s10914-019-09467-8

Berg, R. W., & Kleinfeld, D. (2003). Rhythmic whisking by rat: Retraction as well as protraction of the vibrissae is under active muscular control. *Journal of Neurophysiology*, *89*(1), 104–117. https://doi.org/10.1152/jn.00600.2002

Berman, D. S., Reisz, R. R., Bolt, J. R. & Scott, D. (1995). The cranial anatomy and relationships of the synapsid Varanosaurus (Eupelycosauria: Ophiacodontidae) from the early Permian of Texas and Oklahoma. *Annals of the Carnegie Museum 64*(2), 99–133.

Bertrand, O. C., Amador-Mughal, F., Lang, M. M., & Silcox, M. T. (2019). New virtual endocasts of Eocene Ischyromyidae and their relevance in evaluating neurological changes occurring through time in Rodentia. *Journal of Mammalian Evolution*, *26*(3), 345–371. https://doi.org/10.1007/s10914-017-9425-6

Billo, R., & Wake, M. H. (1987). Tentacle development in Dermophis mexicanus (Amphibia, Gymnophiona) with an hypothesis of tentacle origin. *Journal of Morphology*, *192*(2), 101–111. https://doi.org/10.1002/jmor.1051920203

Bino, G., Kingsford, R. T., Archer, M., Connolly, J. H., Day, J., Dias, K., Goldney, D., Gongora, J., Grant, T., Griffiths, J., Hawke, T., Klamt, M., Lunney, D., Mijangos, L., Munks, S., Sherwin, W., Serena, M., Temple-Smith, P., Thomas, J., … Whittington, C. (2019). The platypus: Evolutionary history, biology, and an uncertain future. *Journal of Mammalogy*, *100*(2), 308–327. https://doi.org/10.1093/jmammal/gyz058

Bisconti, M., & Carnevale, G. (2022). Skeletal transformations and the origin of baleen whales (Mammalia, Cetacea, Mysticeti): A study on evolutionary patterns. *Diversity*, *14*(3), 221. https://doi.org/10.3390/d14030221

Bisconti, M., Damarco, P., Tartarelli, G., Pavia, M., & Carnevale, G. (2021). A natural endocast of an early Miocene odontocete and its implications in cetacean brain evolution. *Journal of Comparative Neurology*, *529*(6), 1198–1227. https://doi.org/10.1002/cne.25015

Bouabdellah, F., Lessner, E., & Benoit, J. (2022). The rostral neurovascular system of tyrannosaurus rex. *Palaeontologia Electronica*, *25*(1), a3. https://doi.org/10.26879/1178

Bowman, C. I. W., Young, M. T., Schwab, J. A., Walsh, S., Witmer, L. M., Herrera, Y., Choiniere, J., Dollman, K. N., & Brusatte, S. L. (2022). Rostral neurovasculature indicates sensory trade-offs in Mesozoic pelagic crocodylomorphs. *The*

Anatomical Record, *305*(10), 2654–2669. https://doi.org/10.1002/ar.24733

Brecht, M., Preilowski, B., & Merzenich, M. M. (1997). Functional architecture of the mystacial vibrissae. *Behavioural Brain Research*, *84*(1–2), 81–97. https://doi.org/10.1016/S0166-4328(97)83328-1

Brink, A. S. (1956). Speculations on some advanced mammalian characteristics in the higher mammal-like reptiles. *Palaeontologia Africana*, *4*, 77–96.

Buchholtz, E. A., & Seyfarth, E.-A. (2001). The study of "fossil brains": Tilly Edinger (1897–1967) and the beginnings of Paleoneurology. *Bioscience*, *51*(8), 674. https://doi.org/10.1641/0006-3568(2001)051[0674:TSOFBT]2.0.CO;2

Campbell, A. L., Naik, R. R., Sowards, L., & Stone, M. O. (2002). Biological infrared imaging and sensing. *Micron*, *33*(2), 211–225. https://doi.org/10.1016/S0968-4328(01)00010-5

Carr, T. D., Varricchio, D. J., Sedlmayr, J. C., Roberts, E. M., & Moore, J. R. (2017). A new tyrannosaur with evidence for anagenesis and crocodile-like facial sensory system. *Scientific Reports*, *7*(1), 44942. https://doi.org/10.1038/srep44942

Catania, K. C. (2012). Tactile sensing in specialized predators—From behavior to the brain. *Current Opinion in Neurobiology*, *22*(2), 251–258. https://doi.org/10.1016/j.conb.2011.11.014

Clements, T., Dolocan, A., Martin, P., Purnell, M. A., Vinther, J., & Gabbott, S. E. (2016). The eyes of Tullimonstrum reveal a vertebrate affinity. *Nature*, *532*(7600), 500–503. https://doi.org/10.1038/nature17647

Cofran, Z., Hurst, S., Beaudet, A., & Zipfel, B. (2023). An overlooked Australopithecus brain endocast from Makapansgat, South Africa. *Journal of Human Evolution*, *178*, 103346. https://doi.org/10.1016/j.jhevol.2023.103346

Coghill, G. E. (1902). The cranial nerves of Amblystoma tigrinum. *Journal of Comparative Neurology*, *12*(3), 205–289. https://doi.org/10.1002/cne.910120302

Cox, P. G., & Jeffery, N. (2011). Reviewing the morphology of the jaw-closing musculature in squirrels, rats, and Guinea pigs with contrast-enhanced MicroCt. *The Anatomical Record*, *294*(6), 915–928. https://doi.org/10.1002/ar.21381

Crompton, A. W., Musinsky, C., Rougier, G. W., Bhullar, B.-A. S., & Miyamae, J. A. (2017). Origin of the lateral Wall of the mammalian skull: Fossils, Monotremes and therians revisited. *Journal of Mammalian Evolution*, 25, 301−313. https://doi.org/10.1007/s10914-017-9388-7

Crowe-Riddell, J. M., & Lillywhite, H. B. (2023). Sensory systems. In C. Warwick, P. C. Arena, & G. M. Burghardt (Eds.), *Health and welfare of captive reptiles* (pp. 45–91). Springer International Publishing. https://doi.org/10.1007/978-3-030-86012-7

Crowe-Riddell, J. M., Snelling, E. P., Watson, A. P., Suh, A. K., Partridge, J. C., & Sanders, K. L. (2016). The evolution of scale sensilla in the transition from land to sea in elapid snakes. *Open Biology*, *6*(6), 160054. https://doi.org/10.1098/rsob.160054

Cunningham, S. J., Alley, M. R., & Castro, I. (2011). Facial bristle feather histology and morphology in New Zealand birds: Implications for function. *Journal of Morphology*, *272*(1), 118–128. https://doi.org/10.1002/jmor.10908

Cunningham, S. J., Corfield, J. R., Iwaniuk, A. N., Castro, I., Alley, M. R., Birkhead, T. R., & Parsons, S. (2013). The anatomy of the bill tip of kiwi and associated somatosensory regions of the brain: Comparisons with shorebirds. *PLoS One*, *8*(11), e80036. https://doi.org/10.1371/journal.pone.0080036

Czech-Damal, N. U., Dehnhardt, G., Manger, P., & Hanke, W. (2013). Passive electroreception in aquatic mammals. *Journal of Comparative Physiology A*, *199*(6), 555–563. https://doi.org/10.1007/s00359-012-0780-8

Damiani, R., Modesto, S., Yates, A., & Neveling, J. (2003). Earliest evidence of cynodont burrowing. *Proceedings of the Royal Society of London. Series B: Biological Sciences*, *270*(1525), 1747–1751. https://doi.org/10.1098/rspb.2003.2427

Dart, R. A. (1925). Australopithecus africanus the man-ape of South Africa. *Nature*, *115*(2884), 195–199. https://doi.org/10.1038/115195a0

Das, I., & Lim, K. K. P. (2009). A new species of Dibamus (Squamata: Dibamidae) from Pulau Simeuleu, Mentawai archipelago, Indonesia. *Zootaxa*, *2088*(1), 15−23. https://doi.org/10.11646/zootaxa.2088.1.2

De Vreese, S., Orekhova, K., Morell, M., Gerussi, T., & Graïc, J.-M. (2023). Neuroanatomy of the cetacean sensory systems. *Animals*, *14*(1), 66. https://doi.org/10.3390/ani14010066

Dehnhardt, G., Hyvarinen, H., Palviainen, A., & Klauer, G. (1999). Structure and innervation of the vibrissal follicle-sinus complex in the Australian water rat, Hydromys chrysogaster. *The Journal of Comparative Neurology*, *411*(4), 550–562. https://doi.org/10.1002/(SICI)1096-9861(19990906)411:4<550::AID-CNE2>3.0.CO;2-G

Delaunay, M. G., Larsen, C., Lloyd, H., Sullivan, M., & Grant, R. A. (2020). Anatomy of avian rictal bristles in Caprimulgiformes reveals reduced tactile function in open-habitat, partially diurnal foraging species. *Journal of Anatomy*, *237*, 355–366. https://doi.org/10.1111/joa.13188

Deschênes, M., Moore, J., & Kleinfeld, D. (2012). Sniffing and whisking in rodents. *Current Opinion in Neurobiology*, *22*(2), 243–250. https://doi.org/10.1016/j.conb.2011.11.013

Di-Poï, N., & Milinkovitch, M. C. (2013). Crocodylians evolved scattered multi-sensory micro-organs. *EvoDevo*, *4*(1), 19. https://doi.org/10.1186/2041-9139-4-19

Dörfl, J. (1985). The innervation of the mystacial region of the white mouse: A topographical study. *Journal of Anatomy*, *142*, 173–184.

Druzinsky, R. E., Doherty, A. H., & De Vree, F. L. (2011). Mammalian masticatory muscles: Homology, nomenclature, and diversification. *Integrative and Comparative Biology*, *51*(2), 224–234. https://doi.org/10.1093/icb/icr067

Du Toit, C. J., Bond, A. L., Cunningham, S. J., Field, D. J., & Portugal, S. J. (2024). Tactile bill-tip organs in seabirds suggest conservation of a deep avian symplesiomorphy. *Biology Letters*, *20*(9), 20240259. https://doi.org/10.1098/rsbl.2024.0259

Duhamel, A., Benoit, J., Rubidge, B. S., & Liu, J. (2021). A reassessment of the oldest therapsid Raranimus confirms its status as a basal member of the clade and fills Olson's gap. *Science of Nature*, *108*(4), 26. https://doi.org/10.1007/s00114-021-01736-y

Dyce, K. M., Sack, W. O., & Wensing, C. J. G. (2010). *Textbook of veterinary anatomy* (4th ed.). Saunders Elsevier.

Early, C. M., Ridgely, R. C., & Witmer, L. M. (2020). Beyond endocasts: Using predicted brain-structure volumes of extinct birds to assess neuroanatomical and behavioral inferences. *Diversity*, *12*(1), 34. https://doi.org/10.3390/d12010034

Ebert, J., Müller, S., & Westhoff, G. (2007). Behavioural examination of the infrared sensitivity of ball pythons. *Journal of Zoology*, *272*(3), 340–347. https://doi.org/10.1111/j.1469-7998.2006.00275.x

Ecker, A. (1889). In G. Haslam (Ed.), *The anatomy of the frog*. Clarendon Press.

Elemans, C. P. H., Jiang, W., Jensen, M. H., Pichler, H., Mussman, B. R., Nattestad, J., Wahlberg, M., Zheng, X., Xue, Q., & Fitch, W. T. (2024). Evolutionary novelties underlie sound production in baleen whales. *Nature*, *627*(8002), 123–129. https://doi.org/10.1038/s41586-024-07080-1

Elwood, J. R. L., & Cundall, D. (1994). Morphology and behavior of the feeding apparatus in *Cryptobranchus alleganiensis* (Amphibia: Caudata). *Journal of Morphology*, *220*(1), 47–70. https://doi.org/10.1002/jmor.1052200106

Fay, F. H. (1985). Odobenus rosmarus. *Mammalian Species*, *238*, 1–7.

Fernandez, V., Abdala, F., Carlson, K. J., Cook, D. C., Rubidge, B. S., Yates, A., & Tafforeau, P. (2013). Synchrotron reveals Early Triassic odd couple: Injured amphibian and aestivating therapsid share burrow. *PLoS One*, *8*(6), e64978. https://doi.org/10.1371/journal.pone.0064978

Ferreira-Cardoso, S., Delsuc, F., & Hautier, L. (2019). Evolutionary tinkering of the mandibular canal linked to convergent regression of teeth in placental mammals. *Current Biology*, *29*(3), 468–475.e3. https://doi.org/10.1016/j.cub.2018.12.023

Figueroa, R. T., Goodvin, D., Kolmann, M. A., Coates, M. I., Caron, A. M., Friedman, M., & Giles, S. (2023). Exceptional fossil preservation and evolution of the ray-finned fish brain. *Nature*, *614*(7948), 486–491. https://doi.org/10.1038/s41586-022-05666-1

Finan, D. S., & Barlow, S. M. (1998). Intrinsic dynamics and mechanosensory modulation of non-nutritive sucking in human infants. *Early Human Development*, *52*(2), 181–197. https://doi.org/10.1016/S0378-3782(98)00029-2

Findlay, G. H. (1968). On the scaloposaurid skull of Olivieria parringtoni, Brink with a note on the origin of hair. *Palaeontologia Africana*, *11*, 47–59.

Flannery, T. F., McCurry, M. R., Rich, T. H., Vickers-Rich, P., Smith, E. T., & Helgen, K. M. (2024). A diverse assemblage of monotremes (Monotremata) from the Cenomanian lightning ridge fauna of New South Wales, Australia. *Alcheringa: An Australasian Journal of Palaeontology*, *48*(2), 319–337. https://doi.org/10.1080/03115518.2024.2348753

Flannery, T. F., Rich, T. H., Vickers-Rich, P., Ziegler, T., Veatch, E. G., & Helgen, K. M. (2022). A review of monotreme (Monotremata) evolution. *Alcheringa: An Australasian Journal of Palaeontology*, *46*(1), 3–20. https://doi.org/10.1080/03115518.2022.2025900

Ford, D. P., & Benson, R. B. J. (2019). A redescription of *Orovenator mayorum* (Sauropsida, Diapsida) using high-resolution μ CT, and the consequences for early amniote phylogeny. *Papers in Palaeontology*, *5*(2), 197–239. https://doi.org/10.1002/spp2.1236

Fox, H. (1999). Barbels and barbel-like tentacular structures in submammalian vertebrates: A review. *Hydrobiologia*, *403*, 153–193.

Francis, E. T. B. (1934). *The anatomy of the salamander*. The Clarendon Press.

Ghetie, V., Chitescu, S., & Hillebrand, A. (1976). *Anatomical atlas of domestic birds*. Editura Academiei Republicii Socialiste Romania.

Ginot, S., Claude, J., & Hautier, L. (2018). One skull to rule them all? Descriptive and comparative anatomy of the masticatory apparatus in five mouse species. *Journal of Morphology*, *279*(9), 1234–1255. https://doi.org/10.1002/jmor.20845

Goris, R. C. (2011). Infrared organs of snakes: An integral part of vision. *Journal of Herpetology*, *45*(1), 2–14. https://doi.org/10.1670/10-238.1

Grant, R. A., Breakell, V., & Prescott, T. J. (2018). Whisker touch sensing guides locomotion in small, quadrupedal mammals. *Proceedings of the Royal Society B: Biological Sciences*, *285*(1880), 20180592. https://doi.org/10.1098/rspb.2018.0592

Grant, R. A., & Goss, V. G. A. (2022). What can whiskers tell us about mammalian evolution, behaviour, and ecology? *Mammal Review*, *52*(1), 148–163. https://doi.org/10.1111/mam.12253

Gregory, J. E., Iggo, A., McIntyre, A. K., & Proske, U. (1989). Responses of electroreceptors in the snout of the echidna. *The Journal of Physiology*, *414*(1), 521–538. https://doi.org/10.1113/jphysiol.1989.sp017701

Gromov, V. S. (2013). The Early experience of tactile stimulation and its behavioral consequences related to socialization in mammals. In E. L. Anderson & S. Thomas (Eds.), *Socialization: Theories, processes and impact* (pp. 1–28). Nova Science Publisher's.

Gutiérrez-Ibáñez, C., Iwaniuk, A. N., & Wylie, D. R. (2009). The independent evolution of the enlargement of the principal sensory nucleus of the trigeminal nerve in three different groups of birds. *Brain, Behavior and Evolution*, *74*(4), 280–294. https://doi.org/10.1159/000270904

Haidarliu, S., Simony, E., Golomb, D., & Ahissar, E. (2010). Muscle architecture in the Mystacial pad of the rat. *The Anatomical Record: Advances in Integrative Anatomy and Evolutionary Biology*, *293*(7), 1192–1206. https://doi.org/10.1002/ar.21156

Hall, M. I., Kamilar, J. M., & Kirk, E. C. (2012). Eye shape and the nocturnal bottleneck of mammals. *Proceedings of the Royal Society B: Biological Sciences*, *279*(1749), 4962–4968. https://doi.org/10.1098/rspb.2012.2258

Herrick, C. J. (1894). The cranial nerves of amblystoma punctatum. With plates XIX and XX. *Journal of Comparative Neurology*, *4*(4), 193–207. https://doi.org/10.1002/cne.910040402

Hofstadler Deiques, C. (2002). The development of the pit organ of *Bothrops jararaca* and *Crotalus durissus terrificus* (Serpentes, Viperidae): Support for the monophyly of the subfamily Crotalinae. *Acta Zoologica*, *83*(3), 175–182. https://doi.org/10.1046/j.1463-6395.2002.00110.x

Holliday, C. M., Tsai, H. P., Skiljan, R. J., George, I. D., & Pathan, S. (2013). A 3D interactive model and atlas of the jaw musculature of Alligator mississippiensis. *PLoS One*, *8*(6), e62806. https://doi.org/10.1371/journal.pone.0062806

Huber, E. (1930). Evolution of facial musculature and cutaneous field of trigeminus. Part I. *The Quarterly Review of Biology*, *5*(2), 133–188. https://doi.org/10.1086/394355

Huggenberger, S., Rauschmann, M. A., Vogl, T. J., & Oelschläger, H. H. A. (2009). Functional morphology of the nasal complex in the harbor porpoise (*Phocoena phocoena* L.). *The Anatomical Record*, *292*(6), 902–920. https://doi.org/10.1002/ar.20854

Hüttner, T., Von Fersen, L., Miersch, L., & Dehnhardt, G. (2023). Passive electroreception in bottlenose dolphins (*Tursiops truncatus*): Implication for micro- and large-scale orientation.

Journal of Experimental Biology, *226*(22), jeb245845. https://doi.org/10.1242/jeb.245845

Jasinoski, S. C., & Abdala, F. (2017). Aggregations and parental care in the Early Triassic basal cynodonts *Galesaurus planiceps* and *Thrinaxodon liorhinus*. *PeerJ*, *5*, e2875. https://doi.org/10.7717/peerj.2875

Jeannot, A. M., Damiani, R., & Rubidge, B. S. (2006). Cranial anatomy of the Early Triassic stereospondyl *Lydekkerina huxleyi* (Tetrapoda: Temnospondyli) and the taxonomy of south African lydekkerinids. *Journal of Vertebrate Paleontology*, *26*(4), 822–838. https://doi.org/10.1671/0272-4634(2006)26[822:CAOTET]2.0.CO;2

Jones, G., Teeling, E. C., & Rossiter, S. J. (2013). From the ultrasonic to the infrared: Molecular evolution and the sensory biology of bats. *Frontiers in Physiology*, *4*, 117. https://doi.org/10.3389/fphys.2013.00117

Jones, M. E. H., Button, D. J., Barrett, P. M., & Porro, L. B. (2019). Digital dissection of the head of the rock dove (Columba livia) using contrast-enhanced computed tomography. *Zoological Letters*, *5*(1), 17. https://doi.org/10.1186/s40851-019-0129-z

Kenyon, C. A. P., Keeble, S., & Cronin, P. (1982). The role of perioral sensation in nipple attachment by weanling rat pups. *Developmental Psychobiology*, *15*(5), 409–421. https://doi.org/10.1002/dev.420150503

Kermack, K. A., Mussett, F., & Rigney, H. W. (1981). The skull of Morganucodon. *Zoological Journal of the Linnean Society*, *71*(1), 1–158. https://doi.org/10.1111/j.1096-3642.1981.tb01127.x

Kesteven, H. L., & Furst, H. C. (1929). The skull of Ornithorhynchus, its later development and adult features. *Journal of Anatomy*, *63*(Pt 4), 447–472.

Kielan-Jaworowska, Z., Cifelli, R. L., & Luo, Z.-X. (2004). *Mammals from the age of dinosaurs: Origins, evolution, and structure*. Columbia University Press.

Kielan-Jaworowska, Z., Dashzeveg, D., & Trofimov, B. A. (1987). Early cretaceous multituberculates from Monglia and a comparison with late Jurassic forms. *Acta Palaeontologica Polonica*, *32*(1–2), 3–47.

Kim, J.-N., Yoo, J.-Y., Lee, J.-Y., Koh, K.-S., & Song, W.-C. (2012). A mechanism of rat vibrissal movement based on actual morphology of the intrinsic muscle using three-dimensional reconstruction. *Cells, Tissues, Organs*, *196*(6), 565–569. https://doi.org/10.1159/000338332

Kliukin, N. S., Nguyen, T. V., Le, S. X., Bragin, A. M., Tran, T. T. V., Gorin, V. A., & Poyarkov, N. A. (2023). A new species of the genus Dibamus Duméril & Bibron, 1839 (Squamata: Dibamidae) from the driest and hottest place of Vietnam. *Zootaxa*, *5380*(4), 301–320. https://doi.org/10.11646/zootaxa.5380.4.1

Krapovickas, V., Mancuso, A., Marsicano, C. A., Domnanovich, N. S., & Schultz, C. L. (2013). Large tetrapod burrows from the middle Triassic of Argentina: A behavioural adaptation to seasonal semi-arid climate? *Lethaia*, *46*(2), 154–169. https://doi.org/10.1111/j.1502-3931.2012.00329.x

Kumar, S., Suleski, M., Craig, J. M., Kasprowicz, A. E., Sanderford, M., Li, M., Stecher, G., & Hedges, S. B. (2022). TimeTree 5: An expanded resource for species divergence times. *Molecular Biology and Evolution*, *39*(8), msac174. https://doi.org/10.1093/molbev/msac174

Larson, M. A., & Stein, B. E. (1984). The use of tactile and olfactory cues in neonatal orientation and localization of the nipple. *Developmental Psychobiology*, *17*(4), 423–436. https://doi.org/10.1002/dev.420170408

Leitch, D. B., & Catania, K. C. (2012). Structure, innervation and response properties of integumentary sensory organs in crocodilians. *Journal of Experimental Biology*, *215*(23), 4217–4230. https://doi.org/10.1242/jeb.076836

Lessner, E. J., & Holliday, C. M. (2022). 3D ontogenetic atlas of *Alligator mississippiensis* cranial nerves and their significance for comparative neurology of reptiles. *The Anatomical Record*, *305*(10), 2854–2882. https://doi.org/10.1002/ar.24550

Liem, K. F., Bemis, W. E., Walker, W. F., Jr., & Grande, L. (2001). *Functional anatomy of the vertebrates: An evolutionary perspective* (3rd ed.). Brooks/Cole.

Lingham-Soliar, T. (2014). *The vertebrate integument: Origin and evolution* (Vol. 1). Springer. https://doi.org/10.1007/978-3-642-53748-6

Luo, Y., Bresee, C. S., Rudnicki, J. W., & Hartmann, M. J. Z. (2021). Constraints on the deformation of the vibrissa within the follicle. *PLoS Computational Biology*, *17*(4), e1007887. https://doi.org/10.1371/journal.pcbi.1007887

Maier, W. (1993). Cranial morphology of the therian common ancestor, as suggested by the adaptations of neonate marsupials. In F. S. Szalay, M. J. Novacek, & M. C. McKenna (Eds.), *Mammal phylogeny* (pp. 165–181). Springer. https://doi.org/10.1007/978-1-4613-9249-1

Maklad, A., Conway, M., Hodges, C., & Hansen, L. A. (2010). Development of innervation to maxillary whiskers in mice. *The Anatomical Record: Advances in Integrative Anatomy and Evolutionary Biology*, *293*(9), 1553–1567. https://doi.org/10.1002/ar.21194

Manger, P. R., Collins, R., & Pettigrew, J. D. (1997). Histological observations on presumed electroreceptors and mechanoreceptors in the beak skin of the long-beaked echidna, *Zaglossus bruijnii*. *Proceedings of the Royal Society of London. Series B: Biological Sciences*, *264*(1379), 165–172. https://doi.org/10.1098/rspb.1997.0024

Manger, P. R., & Pettigrew, J. D. (1995). Electroreception and the feeding behaviour of platypus (*Ornithorhynchus anatinus*: Monotremata: Mammalia). *Philosophical Transactions of the Royal Society of London. Series B: Biological Sciences*, *347*(1322), 359–381. https://doi.org/10.1098/rstb.1995.0030

Manger, P. R., & Pettigrew, J. D. (1996). Ultrastructure, number, distribution and innervation of electroreceptors and mechanoreceptors in the bill skin of the platypus, *Ornithorhynchus anatinus*. *Brain, Behavior and Evolution*, *48*(1), 27–54. https://doi.org/10.1159/000113185

Marchetti, L., MacDougall, M. J., Buchwitz, M., Canoville, A., Herde, M., Kammerer, C. F., & Fröbisch, J. (2024). Origin and early evolution of vertebrate burrowing behaviour. *Earth-Science Reviews*, *250*, 104702. https://doi.org/10.1016/j.earscirev.2024.104702

Martinez, R. N., May, C. L., & Forster, C. A. (1996). A new carnivorous cynodont from the Ischigualasto Formation (Late Triassic, Argentina), with comments on eucynodont phylogeny. *Journal of Vertebrate Paleontology*, *16*(2), 271–284. https://doi.org/10.1080/02724634.1996.10011314

Matsumoto, R., Fujiwara, S., & Evans, S. E. (2024). The anatomy and feeding mechanism of the Japanese giant salamander (*Andrias japonicus*). *Journal of Anatomy*, *244*(5), 679–707. https://doi.org/10.1111/joa.14004

Matveyeva, T. N., & Ananjeva, N. B. (1995). The distribution and number of the skin sense organs of agamid, iguanid and gekkonid lizards. *Journal of Zoology*, *235*(2), 253–268. https://doi.org/10.1111/j.1469-7998.1995.tb05142.x

McGregor, J. H. (1896). Preliminary notes on the cranial nerves of Cryptobranchus alleghaniensis. *The Journal of Comparative Neurology*, *6*(1), 45–53.

Milne, A. O., Smith, C., Orton, L. D., Sullivan, M. S., & Grant, R. A. (2020). Pinnipeds orient and control their whiskers: A study on Pacific walrus, California sea lion and harbor seal. *Journal of Comparative Physiology A*, *206*(3), 441–451. https://doi.org/10.1007/s00359-020-01408-8

Miyamae, J. A. (2022). *Mammalian facial muscles: Their evolution, function, diversity, and study through comparative methods*. Yale University.

Molenaar, G. J. (1978). The sensory trigeminal system of a snake in the possession of infrared receptors. I. The sensory trigeminal nuclei. *The Journal of Comparative Neurology*, *179*(1), 123–135. https://doi.org/10.1002/cne.901790108

Msuya, C. P., & Harrison, T. (1994). The circumorbital foramina in primates. *Primates*, *35*(2), 231–240. https://doi.org/10.1007/BF02382059

Muchlinski, M. N. (2008). The relationship between the infraorbital foramen, infraorbital nerve, and maxillary Mechanoreception: Implications for interpreting the paleoecology of fossil mammals based on infraorbital foramen size. *The Anatomical Record: Advances in Integrative Anatomy and Evolutionary Biology*, *291*(10), 1221–1226. https://doi.org/10.1002/ar.20742

Muchlinski, M. N. (2010). A comparative analysis of vibrissa count and infraorbital foramen area in primates and other mammals. *Journal of Human Evolution*, *58*(6), 447–473. https://doi.org/10.1016/j.jhevol.2010.01.012

Muchlinski, M. N., Wible, J. R., Corfe, I., Sullivan, M., & Grant, R. A. (2020). Good vibrations: The evolution of whisking in small mammals. *The Anatomical Record*, *303*(1), 89–99. https://doi.org/10.1002/ar.23989

Musser, A. M. (2013). Classification and evolution of the monotremes. In K. W. S. Ashwell (Ed.), *Neurobiology of the Monotremes: Brain evolution in our distant mammalian cousins* (pp. 1–16). CSIRO Publishing.

Mynett, N., Mossman, H. L., Huettner, T., & Grant, R. A. (2022). Diversity of vibrissal follicle anatomy in cetaceans. *The Anatomical Record*, *305*(3), 609–621. https://doi.org/10.1002/ar.24714

Naumann, B., & Olsson, L. (2018). Three-dimensional reconstruction of the cranial and anterior spinal nerves in early tadpoles of *Xenopus laevis* (Pipidae, Anura). *Journal of Comparative Neurology*, *526*(5), 836–857. https://doi.org/10.1002/cne.24370

Naylor, B. G. (1981). Cryptobranchid salamanders from the Paleocene and Miocene of Saskatchewan. *Copeia*, *1981*(1), 76. https://doi.org/10.2307/1444042

Noble, G. K., & Schmidt, A. (1937). The structure and function of the facial and labial pits of snakes. *Proceedings of the American Philosophical Society*, *77*(3), 263–288.

Norris, H. W., & Hughes, S. P. (1918). The cranial and anterior spinal nerves of the caecilian amphibians. *Journal of Morphology*, *31*(3), 489–560. https://doi.org/10.1002/jmor.1050310304

Park, W. (1970). Morphological adaptation in developing vibrissae of rats. *Cells, Tissues, Organs*, *75*(1), 67–78. https://doi.org/10.1159/000143441

Paterson, N. F. (1939). The head of Xenopus laevis. *Journal of Cell Science*, *S2-81*(322), 161–232. https://doi.org/10.1242/jcs.s2-81.322.161

Pettigrew, J. D. (1999). Electroreception in monotremes. *Journal of Experimental Biology*, *202*, 1447–1454.

Phillips, M. J., Bennett, T. H., & Lee, M. S. Y. (2009). Molecules, morphology, and ecology indicate a recent, amphibious ancestry for echidnas. *Proceedings of the National Academy of Sciences*, *106*(40), 17089–17094. https://doi.org/10.1073/pnas.0904649106

Prahl, S., Huggenberger, S., & Schliemann, H. (2009). Histological and ultrastructural aspects of the nasal complex in the harbour porpoise, *Phocoena phocoena*. *Journal of Morphology*, *270*(11), 1320–1337. https://doi.org/10.1002/jmor.10760

Prescott, T. J., Mitchinson, B., & Grant, R. A. (2016). Vibrissal behavior and function. In T. J. Prescott, E. Ahissar, & E. Izhikevich (Eds.), *Scholarpedia of touch* (pp. 103–116). Atlantis Press. https://doi.org/10.2991/978-94-6239-133-8

Proske, U., Gregory, J. E., & Iggo, A. (1998). A review of recent developments in the study of electroreception in the platypus. *Australian Mammalogy*, *20*(2), 163. https://doi.org/10.1071/AM98163

Pusch, L. C., Kammerer, C. F., & Fröbisch, J. (2019). Cranial anatomy of the early cynodont *Galesaurus planiceps* and the origin of mammalian endocranial characters. *Journal of Anatomy*, *234*(5), 592–621. https://doi.org/10.1111/joa.12958

Pusch, L. C., Kammerer, C. F., & Fröbisch, J. (2024). The origin and evolution of Cynodontia (Synapsida, Therapsida): Reassessment of the phylogeny and systematics of the earliest members of this clade using 3D -imaging technologies. *The Anatomical Record*, *307*(4), 1634–1730. https://doi.org/10.1002/ar.25394

Pusch, L. C., Ponstein, J., Kammerer, C. F., & Fröbisch, J. (2020). Novel Endocranial data on the Early therocephalian Lycosuchus vanderrieti underpin high character variability in Early Theriodont evolution. *Frontiers in Ecology and Evolution*, *7*, 464. https://doi.org/10.3389/fevo.2019.00464

Quinzio, S. I., & Fabrezi, M. (2019). The peripheral nerves of *Lepidobatrachus* tadpoles (Anura, Ceratophryidae). *Journal of Morphology*, *280*(1), 4–19. https://doi.org/10.1002/jmor.20849

Rauschmann, M. A., Huggenberger, S., Kossatz, L. S., & Oelschläger, H. H. A. (2006). Head morphology in perinatal dolphins: A window into phylogeny and ontogeny. *Journal of Morphology*, *267*(11), 1295–1315. https://doi.org/10.1002/jmor.10477

Reese, A. M. (1906). Anatomy of Cryptobranchus allegheniensis. *The American Naturalist*, *40*(472), 287–326. https://doi.org/10.1086/278619

Reisz, R. R., & Dilkes, D. W. (2003). *Archaeovenator hamiltonensis*, a new varanopid (Synapsida: Eupelycosauria) from the Upper Carboniferous of Kansas. *Canadian Journal of Earth Sciences*, *40*(4), 667–678. https://doi.org/10.1139/e02-063

Riedel, J., & Schwarzkopf, L. (2022). Variation in density, but not morphology, of cutaneous sensilla among body regions in nine species of Australian geckos. *Journal of Morphology*, *283*(5), 637–652. https://doi.org/10.1002/jmor.21462

Rieppel, O. (1984). The cranial morphology of the fossorial lizard genus Dibamus with a consideration of its phylogenetic relationships*. *Journal of Zoology*, *204*(3), 289–327. https://doi.org/10.1111/j.1469-7998.1984.tb02376.x

Rojas, L. M., McNeil, R., Cabana, T., & Lachapelle, P. (1999). Behavioral, morphological and physiological correlates of diurnal and nocturnal vision in selected wading bird species. *Brain, Behavior and Evolution*, *53*(5–6), 227–242. https://doi.org/10.1159/000006596

Romer, A. S., & Parsons, T. S. (1986). *The vertebrate body* (6th ed.). Saunders College Publishing.

Rose, C. S. (2014). The importance of cartilage to amphibian development and evolution. *The International Journal of Developmental Biology*, *58*(10–11–12), 917–927. https://doi.org/10.1387/ijdb.150053cr

Rowe, T. B., Macrini, T. E., & Luo, Z.-X. (2011). Fossil evidence on origin of the mammalian brain. *Science*, *332*(6032), 955–957.

Ruta, M., Botha-Brink, J., Mitchell, S. A., & Benton, M. J. (2013). The radiation of cynodonts and the ground plan of mammalian morphological diversity. *Proceedings of the Royal Society B: Biological Sciences*, *280*(1769), 20131865. https://doi.org/10.1098/rspb.2013.1865

Sánchez-Villagra, M. R., & Asher, R. J. (2002). Cranio-sensory adaptations in small faunivorous semiaquatic mammals, with special reference to olfaction and the trigeminal system. *Mamm*, *66*(1), 93–110. https://doi.org/10.1515/mamm.2002.66.1.93

Sarko, D. K., Rice, F. L., & Reep, R. L. (2011). Mammalian tactile hair: Divergence from a limited distribution. *Annals of the New York Academy of Sciences*, *1225*(1), 90–100. https://doi.org/10.1111/j.1749-6632.2011.05979.x

Schlosser, G., & Roth, G. (1997a). Evolution of nerve development in frogs: I. The development of the peripheral nervous system in Discoglossus pictus (Discoglossidae). *Brain, Behavior and Evolution*, *50*, 61–93.

Schlosser, G., & Roth, G. (1997b). Evolution of nerve development in frogs: II. Modified development of the peripheral nervous system in the direct-developing frog Eleutherodactylus coqui (Leptodactylidae). *Brain, Behavior and Evolution*, *50*, 94–128.

Schmitt, M. R., Martinelli, A. G., Kaiuca, J. F. L., Schultz, C. L., & Soares, M. B. (2024). Old fossil findings in the Upper Triassic rocks of southern Brazil improve diversity of traversodontid cynodonts (Therapsida, Cynodontia). *The Anatomical Record*, *307*(4), 1474–1514. https://doi.org/10.1002/ar.25244

Schoch, R. R. (2013). The evolution of major temnospondyl clades: An inclusive phylogenetic analysis. *Journal of Systematic Palaeontology*, *11*(6), 673–705. https://doi.org/10.1080/14772019.2012.699006

Schoch, R. R., & Witzmann, F. (2024). The evolution of larvae in temnospondyls and the stepwise origin of amphibian metamorphosis. *Biological Reviews*, *99*, brv.13084. https://doi.org/10.1111/brv.13084

Seneviratne, S. S., & Jones, I. L. (2008). Mechanosensory function for facial ornamentation in the whiskered auklet, a crevice-dwelling seabird. *Behavioral Ecology*, *19*(4), 784–790. https://doi.org/10.1093/beheco/arn029

Sibiya, Z. (2021). *Is the pattern of the maxillary canal apomorphic to synapsids?* University of the Witwatersrand.

Smith, K. K., & Keyte, A. L. (2020). Adaptations of the marsupial newborn: Birth as an extreme environment. *The Anatomical Record*, *303*(2), 235–249. https://doi.org/10.1002/ar.24049

Soares, D. (2002). An ancient sensory organ in crocodilians. *Nature*, *417*(6886), 241–242. https://doi.org/10.1038/417241a

Sperber, G. H., Sperber, S. M., & Guttmann, G. D. (2000). Muscle development. In *Craniofacial embryogenetics and development* (2nd ed., pp. 191–202). People's Medical Publishing House USA.

Stefanello, M., Martinelli, A. G., Müller, R. T., Dias-da-Silva, S., & Kerber, L. (2023). A complete skull of a stem mammal from the late Triassic of Brazil illuminates the early evolution of prozostrodontian cynodonts. *Journal of Mammalian Evolution*, *30*(2), 299–317. https://doi.org/10.1007/s10914-022-09648-y

Stensiö, E. A. (1927). *The Downtonian and Devonian vertebrates of Spitsbergen. Part I. Family Cephalaspidae*. Skrifter øm Svalbard og Ishavet.

Strausfeld, N. J., Ma, X., & Edgecombe, G. D. (2016). Fossils and the evolution of the arthropod brain. *Current Biology*, *26*(20), R989–R1000. https://doi.org/10.1016/j.cub.2016.09.012

Sysueva, E. V., & Popov, V. V. (2023). The acoustic window in the lower jaw of the dolphin: Assessment of bone thickness. *Neuroscience and Behavioral Physiology*, *53*(6), 1056–1060. https://doi.org/10.1007/s11055-023-01498-2

Trinajstic, K., Marshall, C., Long, J., & Bifield, K. (2007). Exceptional preservation of nerve and muscle tissues in late Devonian placoderm fish and their evolutionary implications. *Biology Letters*, *3*(2), 197–200. https://doi.org/10.1098/rsbl.2006.0604

Van Valen, L. (1960). Therapsids as mammals. *Evolution*, *14*(3), 304–313.

Wake, M. H. (1985). The comparative morphology and evolution of the eyes of caecilians (Amphibia, Gymnophiona). *Zoomorphology*, *105*(5), 277–295. https://doi.org/10.1007/BF00312059

Watkinson, G. B. (1906). The cranial nerves of Varanus bivittatus. In *Morphologisches Jahrbuch* (Vol. 35, pp. 450–472). Wilhelm Engelmann.

Watson, D. M. S. (1931). On the skeleton of a bauriamorph reptile. *Proceedings of the Zoological Society of London*, *101*(3), 1163–1205. https://doi.org/10.1111/j.1096-3642.1931.tb01056.x

Whiteman, H. H. (1994). Evolution of facultative Paedomorphosis in salamanders. *The Quarterly Review of Biology*, *69*(2), 205–221. https://doi.org/10.1086/418540

Williams, P. L., Warwick, R., Dyson, M., & Bannister, L. H. (Eds.). (1989). *Gray's Anatomy* (37th ed.). Churchill Livingstone.

Wineski, L. E. (1985). Facial morphology and vibrissal movement in the golden hamster. *Journal of Morphology*, *183*(2), 199–217. https://doi.org/10.1002/jmor.1051830208

Wolfe, J., Mende, C., & Brecht, M. (2011). Social facial touch in rats. *Behavioral Neuroscience*, *125*(6), 900–910. https://doi.org/10.1037/a0026165

Wyman, J. (1853). *Anatomy of the nervous system of Rana pipiens*. Smithsonian Institution. https://doi.org/10.5962/bhl.title.31475

Zhou, Y., Shearwin-Whyatt, L., Li, J., Song, Z., Hayakawa, T., Stevens, D., Fenelon, J. C., Peel, E., Cheng, Y., Pajpach, F., Bradley, N., Suzuki, H., Nikaido, M., Damas, J., Daish, T., Perry, T., Zhu, Z., Geng, Y., Rhie, A., … Zhang, G. (2021). Platypus and echidna genomes reveal mammalian biology and evolution. *Nature*, *592*(7856), 756–762. https://doi.org/10.1038/s41586-020-03039-0

SUPPORTING INFORMATION

Additional supporting information can be found online in the Supporting Information section at the end of this article.

How to cite this article: Miyamae, J. A., Benoit, J., Ruf, I., Sibiya, Z., & Bhullar, B.-A. S. (2025). Synapsids and sensitivity: Broad survey of tetrapod trigeminal canal morphology supports an evolutionary trend of increasing facial tactile specialization in the mammal lineage. *The Anatomical Record*, 1–48. https://doi.org/10.1002/ar.25604